

NAG 2-228

DAA/AMES

**PURDUE UNIVERSITY**  
**SCHOOL OF AERONAUTICS AND ASTRONAUTICS**

**OPTIMAL COOPERATIVE CONTROL SYNTHESIS  
OF ACTIVE DISPLAYS**

by

**SANJAY GARG and DAVID K. SCHMIDT**

{NASA-177102) OPTIMAL COOPERATIVE CONTROL  
SYNTHESIS OF ACTIVE DISPLAYS Final Report  
{Purdue Univ.) 160 p CSCI 20F

N86-29651

Unclas  
43235

G3/74

22nd October, 1985



**West Lafayette, Indiana 47907**

OPTIMAL COOPERATIVE CONTROL SYNTHESIS  
OF ACTIVE DISPLAYS

by

SANJAY GARG and DAVID K. SCHMIDT  
School of Aeronautics and Astronautics  
Purdue University  
West Lafayette, IN 47907

Submitted to:

NASA Dryden Flight Research Facility

Ames Research Center

Final Report for grant NAG2-228

22<sup>nd</sup> October, 1985

ACKNOWLEDGMENT

This research was supported by NASA Dryden Research Facility, Ames Research Center under grant NAG2-228. Mr. E. L. Duke is the technical monitor.

TABLE OF CONTENTS

	Page
LIST OF TABLES.....	v
LIST OF FIGURES.....	vi
LIST OF SYMBOLS.....	xi
ABSTRACT.....	xiv
CHAPTER 1 INTRODUCTION.....	1
CHAPTER 2 ANALYSIS OF DISPLAYS FOR A $K/s^2$ PLANT.....	8
2.1 $K/s^2$ Plant and Task Description.....	8
2.2 Display Quickening For $K/s^2$ Plant.....	12
CHAPTER 3 OPTIMAL COOPERATIVE CONTROL/DISPLAY DESIGN METHODOLOGY.....	19
3.1 Problem Formulation.....	19
3.2 Design Objectives.....	20
3.3 Solution for $\bar{u}_1$ .....	23
3.4 Solution for $\bar{u}_2$ and $\bar{u}_d$ .....	24
3.5 Application to Pilot-in-the-Loop Synthesis....	26
3.6 Numerical Solution Algorithm.....	29
CHAPTER 4 APPLICATION OF DISPLAY DESIGN METHODOLOGY TO $K/s^2$ PLANT.....	34
4.1 Problem Formulation and Synthesis Results.....	34
4.2 Evaluation of the Display Quickening Control Laws.....	38
4.2.1 Mean-Square Analysis.....	38
4.2.2 Power Spectrum Analysis.....	42
4.2.3 Frequency Domain Analysis.....	44
CHAPTER 5 APPLICATION OF COOPERATIVE METHODOLOGY TO A MORE COMPLEX DISPLAY DESIGN.....	52
5.1 System Dynamics.....	52
5.2 Task modeling.....	54
5.3 Optimal Display Synthesis for F-15 Model.....	65

5.4	Comparison of the Displays.....	68
5.4.1	Time Histories.....	68
5.4.2	Frequency Domain Analysis.....	73
5.4.3	RMS Analysis.....	76
5.4.4	Spectral Analysis.....	78
CHAPTER 6 SUMMARY.....		83
REFERENCES.....		86
APPENDICES		
APPENDIX A	DERIVATION OF NECESSARY CONDITIONS FOR CONTROLLER 2 ( $\bar{u}_2$ ).....	89
APPENDIX B	THE OPTIMAL CONTROL PILOT MODEL.....	94
APPENDIX C	ANALYSIS RESULTS FOR $K/s^2$ PLANT.....	102
APPENDIX D	DATA AND ANALYSIS RESULTS FOR F-15 AIRCRAFT.....	120

# LIST OF TABLES

Table	Page
2.1 OCM RESULTS FOR VARYING DISPLAY BANDWIDTH.....	13
2.2 OCM RESULTS FOR VARYING DISPLAY CONTROL GAINS.....	17
4.1 OPTIMAL DISPLAY DESIGNS FOR $K/s^2$ PLANT.....	37
4.2 OCM ANALYSIS RESULTS FOR VARIOUS CASES.....	39
5.1 PILOT PERCEPTION THRESHOLDS.....	64
5.2 OCM ANALYSIS RESULTS.....	77
APPENDIX TABLES	
D.1 TRIM CONDITIONS FOR F-15 MODEL.....	121
D.2 MATRICES $A_v$ AND $B_v$ FOR F-15 MODEL.....	122
D.3 PILOT OBSERVATION MATRICES FOR STATUS DISPLAY....	123

LIST OF FIGURES

Figure	Page
1.1 Simplified Block Diagrams for Control/Display Augmentation.....	3
1.2 Control vs. Display Augmentation.....	4
2.1 Display for $K/s^2$ Plant.....	10
2.2 Parametric Performance - Manual Control Rate.....	14
2.3 Parametric Performance - Manual Control Activity..	15
3.1 Block Diagram for Control and Display Augmentation.....	21
3.2 Simplified Pilot Model Block Diagram.....	28
3.3 Flowchart for Numerical Procedure.....	31
4.1 Error vs. Manual Control Rate for Various Displays.....	40
4.2 Error vs. Manual Control Activity for Various Displays.....	41
4.3 Comparison of Human Operator's Control Spectrum, $\Delta(\omega)$ .....	43
4.4 Block Diagram for Display Augmented Plant.....	45
4.5 Comparison of Display Augmented Plants, $G(s)$ .....	47
4.6 Comparison of Human Describing Functions, $P(s)$ ....	48
4.7 Comparison of Human's Phase Compensation (adjusted phase).....	49
4.8 Comparison of Closed-Loop Frequency Response for Displays 1,3 and 5.....	51

5.1(a)	$a_z$ Response to Step Elevator Input ( $\delta_{ec} = 0.01$ rads, +ve down).....	55
5.1(b)	Mach Response to Step Elevator Input.....	56
5.1(c)	$\theta$ Response to Step Elevator Input.....	57
5.2(a)	$a_z$ Response to Step Throttle Input ( $\delta T_c = 1$ ft/sec <sup>2</sup> , +ve thrust).....	58
5.2(b)	Mach Response to Step Throttle Input.....	59
5.2(c)	$\theta$ Response to Step Throttle Input.....	60
5.3	Conceptual Display Format for Status Display.....	61
5.4	Conceptual Display Format for Augmented Display...	63
5.5(a)	$x_{d1}$ Response to Step Elevator Input ( $\delta_{ec} = 0.01$ rads, +ve down).....	69
5.5(b)	$x_{d2}$ Response to Step Elevator Input.....	70
5.6(a)	$x_{d1}$ Response to Step Throttle Input ( $\delta T_c = 1$ ft/sec <sup>2</sup> , +ve thrust).....	71
5.6(b)	$x_{d2}$ Response to Step Throttle Input.....	72
5.7	Block Diagram for Status Display.....	74
5.8	Block Diagram for Augmented Display.....	75
5.9	Comparison of $e_{az}$ Power Spectrum.....	79
5.10	Comparison of Pilot Commanded Elevator Spectrum...	80
5.11	Comparison of Pilot Commanded Throttle Spectrum...	81
APPENDIX FIGURES		
B.1	OCM Block Diagram.....	95
C.1	Control Spectrum for Limiting Case - A.....	103
C.2	Control Spectrum for Display 1.....	104
C.3	Control Spectrum for Display 2.....	105



C.4	Control Spectrum for Display 3.....	106
C.5	Control Spectrum for Display 4.....	107
C.6	Control Spectrum for Display 5.....	108
C.7	Bode-plots of $K/s^2$ Plant Plus Display 1.....	109
C.8	Bode-plots of $K/s^2$ Plant Plus Display 2.....	110
C.9	Bode-plots of $K/s^2$ Plant Plus Display 3.....	111
C.10	Bode-plots of $K/s^2$ Plant Plus Display 4.....	112
C.11	Bode-plots of $K/s^2$ Plant Plus Display 5.....	113
C.12	Pilot Describing Function for Limiting Case-A....	114
C.13	Pilot Describing Function for Display 1.....	115
C.14	Pilot Describing Function for Display 2.....	116
C.15	Pilot Describing Function for Display 3.....	117
C.16	Pilot Describing Function for Display 4.....	118
C.17	Pilot Describing Function for Display 5.....	119
D.1	Pilot Describing Function $P \frac{\delta e}{a_{zc}}$ for Status Display.....	124
D.2	Pilot Describing Function $P \frac{\delta e}{e_{az}}$ for Status Display.....	125
D.3	Pilot Describing Function $P \frac{\delta e}{M}$ for Status Display.....	126
D.4	Pilot Describing Function $P \frac{\delta e}{\theta}$ for Status Display.....	127
D.5	Pilot Describing Function $P \frac{\delta T}{a_{zc}}$	

for Status Display.....	128
D.6 Pilot Describing Function $P \frac{\delta T}{e_{az}}$	
for Status Display.....	129
D.7 Pilot Describing Function $P \frac{\delta T}{M}$	
for Status Display.....	130
D.8 Pilot Describing Function $P \frac{\delta T}{\theta}$	
for Status Display.....	131
D.9 Pilot Describing Function $P \frac{\delta e}{a_{zc}}$	
for Augmented Display.....	132
D.10 Pilot Describing Function $P \frac{\delta e}{x_{d1}}$	
for Augmented Display.....	133
D.11 Pilot Describing Function $P \frac{\delta e}{x_{d2}}$	
for Augmented Display.....	134
D.12 Pilot Describing Function $P \frac{\delta e}{\theta}$	
for Augmented Display.....	135
D.13 Pilot Describing Function $P \frac{\delta T}{a_{zc}}$	
for Augmented Display.....	136
D.14 Pilot Describing Function $P \frac{\delta T}{x_{d1}}$	
for Augmented Display.....	137
D.15 Pilot Describing Function $P \frac{\delta T}{x_{d2}}$	
for Augmented Display.....	138
D.16 Pilot Describing Function $P \frac{\delta T}{\theta}$	

for Augmented Display.....	139
D.17 $e_{az}$ Power Spectrum for status Display.....	140
D.18 Pilot Commanded Elevator Spectrum for Status Display.....	141
D.19 Pilot Commanded Throttle Spectrum for Status Display.....	142
D.20 $e_{az}$ Power Spectrum for Augmented Display.....	143
D.21 Pilot Commanded Elevator Spectrum for Augmented Display.....	144
D.22 Pilot Commanded Throttle Spectrum for Augmented Display.....	145

LIST OF SYMBOLS

Symbol	Meaning
$a_z$ .....	normal acceleration (ft/sec <sup>2</sup> )
$A$ .....	plant matrix
$B$ .....	system control distribution matrix
$C$ .....	output state distribution matrix
$D$ .....	system noise distribution matrix
$D(s)$ .....	display system transfer function
$e$ .....	plant position error
$e_{az}$ .....	normal acceleration tracking error (ft/sec <sup>2</sup> )
$E$ .....	output control distribution matrix
$f_i$ .....	fractional attention allocation for $i^{\text{th}}$ observation
$g$ .....	control rate weighting
$g_d$ .....	display control gain
$G$ .....	gain matrices
$G(s)$ .....	plant transfer function/matrix
$I$ .....	identity matrix
$J$ .....	cost functional
$K$ .....	plant gain
$K_1$ .....	control gain matrix
$M$ .....	Mach error (.001 Mach)
$M_1$ .....	Kalman filter gain matrix
$P$ .....	solution to Ricatti equation
$P(s)$ .....	human operator transfer function/matrix
$q$ .....	pitch rate (.01 rads/sec)
$q$ .....	augmented system state vector
$q_e$ .....	error weighting

## Symbol

## Meaning

$Q$	state weighting matrix
$r$	control weighting
$R, F$	control weighting matrices
$T(s)$	closed-loop transfer function
$u$	control vector
$v_m$	motor noise vector
$v_y$	observation noise vector
$V$	perturbed forward velocity (ft/sec)
$v_y$	measurment noise intensity
$w$	system noise input vector
$W$	system noise intensity
$x$	$K/s^2$ plant position
$x$	state vector
$x_d$	display variable
$y$	system output vector, measurment vector
$\alpha$	angle of attack (.01 rads)
$\alpha_i$	perception threshold value for $i^{\text{th}}$ observation
$\chi$	augmented system state vector
$\hat{\chi}$	augmented system state estimate vector
$\delta$	human operator's control input vector
$\delta_e$	elevator control input (.01 rads)
$\delta T$	throttle control input (ft/sec <sup>2</sup> )
$\mu$	pilot input
$\mu^*$	optimal pilot input
$\rho_u$	motor noise ratio
$\rho_{y1}$	observation noise ratio for $i^{\text{th}}$ observation
$\sigma_x$	root mean square value of $x$
$\Sigma$	state error covariance matrix
$\Sigma_x(\omega)$	power spectral density of $x$
$\tau$	time delay
$\tau_d$	display lag time constant

## Symbol

## Meaning

$\tau_n$ .....neuromotor lag time constant  
 $\theta$ .....pitch rate (.01 rads)

## operations

$\dot{(\cdot)}$ .....time derivative of  $(\cdot)$   
 $E\{.\}$ .....expected value operator  
 $(\cdot)^T$ .....transpose of  $(\cdot)$   
 $(\cdot)^{-1}$ .....inverse of  $(\cdot)$

## subscripts

1.....refers to Controller 1  
 2.....refers to Controller 2  
 aug.....augmented system  
 A.....augmented system  
 c.....closed loop system, command  
 d.....display augmentation system  
 o.....nominal values, unaugmented system matrices  
 p.....human operator/pilot  
 v.....vehicle

ABSTRACT

A technique is developed that is intended to provide a systematic approach to synthesizing display augmentation for optimal manual control in complex, closed-loop tasks. A cooperative control synthesis technique, previously developed to design pilot-optimal control augmentation for the plant, is extended to incorporate the simultaneous design of performance enhancing displays. The technique utilizes an optimal control model of the man in the loop. It is applied to the design of a quickening control law for a display and a simple  $K/s^2$  plant, and then to an F-15 type aircraft in a multi-channel task. Utilizing the closed loop modeling and analysis procedures, the results from the display design algorithm are evaluated and an analytical validation is performed. Experimental validation is recommended for future efforts.

CHAPTER 1INTRODUCTION

The utility of providing augmented displays to the human operator as an aid in the closed-loop control of high order dynamical systems is well known, and discussion of some of the early work done in evaluating various types of augmented displays can be found in [1]. With the advent of high performance aircraft, the amount of information to be processed by the pilot to successfully accomplish the assigned task has continued to increase. It has, therefore, become more critical to determine the best informational set and display dynamics needed by the pilot so as to reduce the pilot's workload and improve performance. For example, the use of flight directors to achieve this objective has been analytically evaluated in [2] using closed loop or "pilot - modeling" techniques, and validated through man-in-the-loop simulation in [3].

Ongoing research in the area of automatic flight test trajectory controllers [4,5] has demonstrated the usefulness of such controllers, rather than manual control, for accurately following specified complex trajectories. These controllers, however, take the pilot out of the control loop, and it is desirable to avoid this. The possibility of doing so while aiding the pilot with an appropriate display is worth exploring, and that is the subject of this work.

In general, the design of active displays for the human controller requires extensive real time man-in-the-loop simulation to evaluate various candidate designs. Although simulator validation is always appropriate, the objective of this study is to develop an analytical technique to aid in the design of pilot-optimal display augmentation

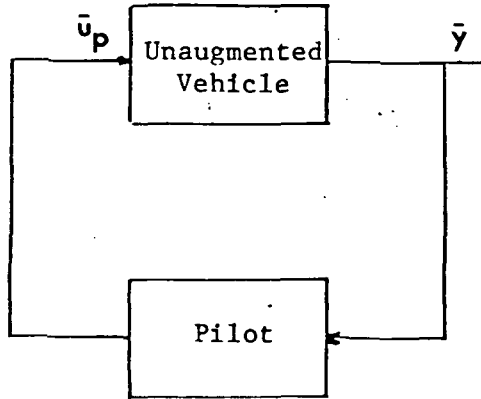


systems.

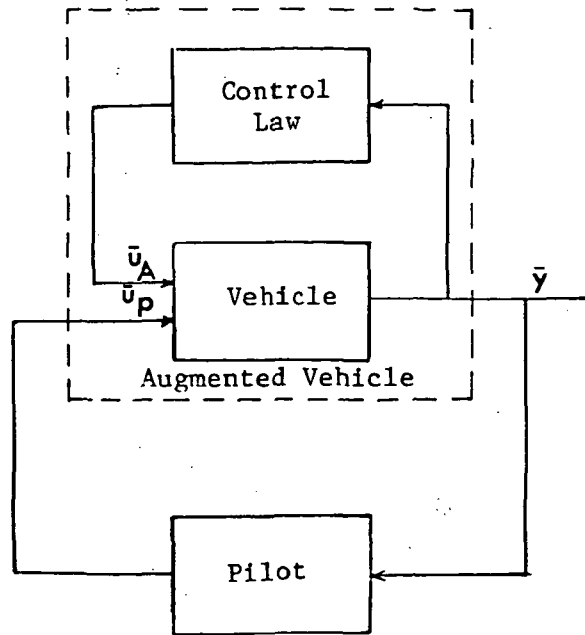
In the past, analytical methods have been proposed in which models of human behaviour were used to identify, investigate and evaluate the properties of augmented aircraft dynamics. In all these methods, however, the "pilot model analysis" was added a posteriori. The idea that the augmentation system works in cooperation with the pilot and a technique which considers the augmentation system and the pilot to be two controllers working in "parallel" was first suggested by Schmidt [7]. This technique was later modified and its application to synthesize control augmentation that directly optimizes pilot opinion rating was demonstrated for a modern control configured aircraft [8,9]. The cooperative control synthesis technique has the advantage that it incorporates a mathematical model of the pilot behaviour and uses optimal control theory to synthesize control gains that are pilot-optimal as modeled.

Since display augmentation, like control augmentation, has to be in harmony with the pilot's abilities and limitations in order to be acceptable to him as an aid in accomplishing his task, the cooperative synthesis technique is considered to provide an appropriate framework for synthesizing pilot-optimal display augmentation.

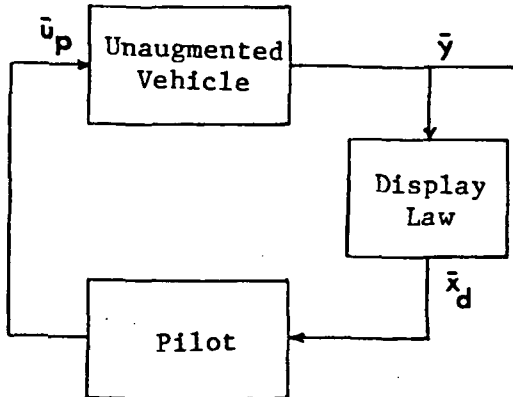
Even though the objective of both the control augmentation and the display augmentation is to aid the pilot, the way this is achieved is fundamentally different for the two types of augmentation. The differences between these two types of augmentation are best understood by considering the simplified block diagrams of Figures (1.1) and (1.2). Figure (1.1(a)) depicts the pilot controlling an unaugmented vehicle. For this case, the responses ( $\bar{y}$ ) observed by the pilot are those being



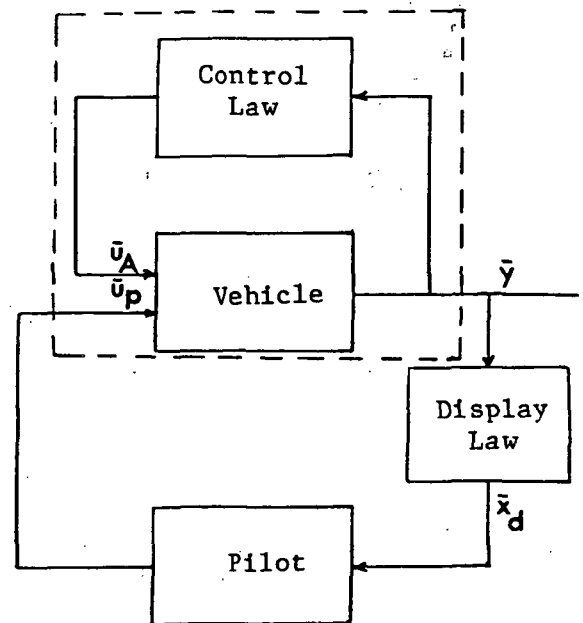
(a) Unaugmented Vehicle



(b) Control Augmentation

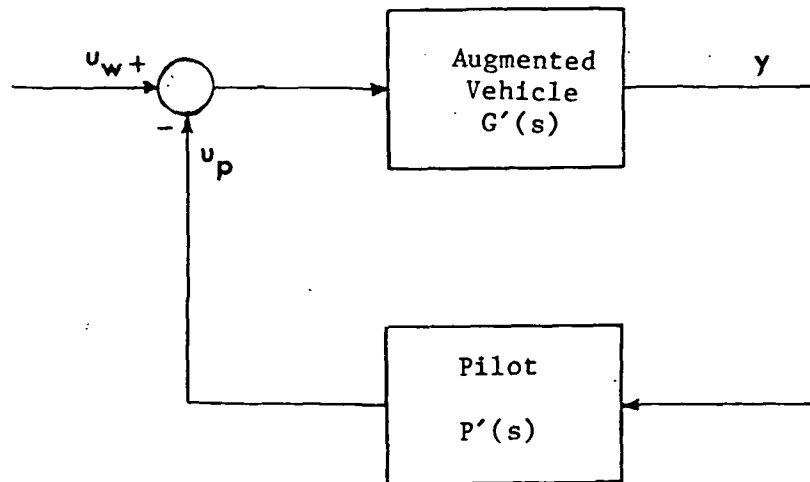


(c) Display Augmentation

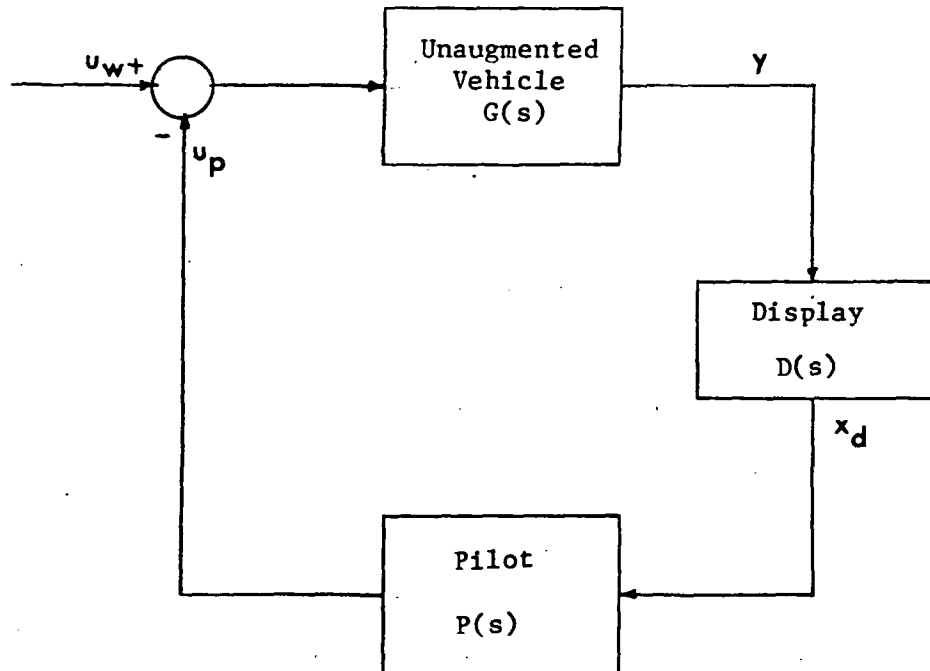


(d) Control and Display Augmentation

Figure 1.1 Simplified Block Diagrams for Control/Display Augmentation



(a) Control Augmented Vehicle



(b) Display Augmented Vehicle

Figure 1.2 Control vs. Display Augmentation

controlled by the pilot.

Figure (1.1(b)) shows the case of a pilot controlling an augmented vehicle. Note that the control augmentation changes the effective plant dynamics being controlled by the pilot, and may be designed so as to aid the pilot in accomplishing his task and to achieve desired dynamics for improved handling qualities. Here again, however, the responses ( $\bar{y}$ ) observed by the pilot are still those he is directly controlling.

Figure (1.1(c)) shows a simplified case of display augmentation, wherein the vehicle responses drive a display observed by the pilot. Note that any display dynamic augmentation does not change the characteristics of the vehicle dynamics being controlled (i.e.  $y/u_p$  is unchanged). It only modifies the dynamics being observed by the pilot (or  $x_d/u_p$ ). Here, clearly, though the pilot observes and controls  $\bar{x}_d$  (the displayed signal), the controlled variables of interest are still the vehicle responses  $\bar{y}$ . The case of combined control and display augmentation is shown in Figure (1.1(d)).

Consider the manual control of a vehicle  $G(s)$ , with control augmentation such that the augmented vehicle is  $G'(s)$ , as in Fig. (1.2(a)). The closed-loop transfer function, including the pilot, from some disturbance  $u_w$  to the vehicle output  $y$  is

$$y(s) = \frac{G'(s)}{1 + G'(s) P'(s)} u_w(s) \quad (1.1)$$

where  $P'(s)$  represents the pilot describing function. Next consider the pilot controlling the vehicle without control augmentation but with display augmentation, as in Fig. (1.2(b)). The closed-loop transfer function for this case is

$$y(s) = \frac{G(s)}{1 + G(s) D(s) P(s)} u_w(s) \quad (1.2)$$

Now if the display dynamics  $D(s)$  are chosen, for example, such that  $G(s)D(s)=G'(s)$ , then the pilot describing function  $P(s)$  of the display augmentation case (Fig. (1.2(b))) is approximately the same as  $P'(s)$  for the control augmentation case. Then Eqn. (1.2) becomes

$$y(s) = \frac{G(s)}{1 + G'(s) P'(s)} u_w(s) \quad (1.3)$$

Comparing Eqn. (1.3) to Eqn. (1.1), it is apparent that though the stability characteristics in terms of the closed-loop characteristic polynomial are the same for the two cases of augmentation, the closed loop transfer functions are not. The point here is that the closed-loop system dynamics obtained through control augmentation may be quite different from that obtained through display augmentation.

Chapter 2 of this report provides motivation for display augmentation through analytical evaluation of various display "quickenings" control laws, synthesized essentially through trial and error, for a simple  $K/s^2$  plant. A compensatory tracking task is analyzed using an Optimal Control Model (OCM) [6] of human behavior.

In Chapter 3 a methodology to synthesize pilot-optimal display/control laws which is sensitive to the control and information processing limitations of the human controller is proposed. This methodology is an extension of the cooperative control synthesis technique previously developed to design pilot-optimal control augmentation [7,8,9]. Though the proposed methodology has been developed so as to be applicable to simultaneous synthesis of pilot-optimal control augmentation and display augmentation, the present discussion focuses on the application of the technique to display design only.

The application of the cooperative display design technique to

again synthesize display laws for the  $K/s^2$  plant in the tracking task is discussed in Chapter 4. When compared to the results of Chapter 2, the results of this application tend to analytically validate the synthesis procedure. The displays lead to predicted reduction in pilot workload when evaluated using the OCM. Also the ability of the methodology to provide task tailoring of the displays is demonstrated.

In Chapter 5 the application of the methodology to high order dynamical systems in a multi-control task scenario is demonstrated for a modern aircraft. The chosen model closely represents the unaugmented longitudinal dynamics of the F-15 aircraft, and the task is that of tracking a normal acceleration command while regulating Mach number. The control inputs available to the pilot are the elevator stick and throttle. Model-based evaluation of the synthesized display again indicates reduction in pilot workload in accomplishing the task.

Finally a summary of the work is presented in Chapter 6 and recommendations made for future research.

CHAPTER 2ANALYSIS OF DISPLAYS FOR A  $K/s^2$  PLANT

Motivation for providing the human controller with augmented displays is explored through analytical evaluation of various empirically-derived display "quickening" control laws for a simple  $K/s^2$  plant. The results of this evaluation agree with the known fact that the human operator's workload can be significantly reduced and his performance improved by a proper design of the signal being displayed to him.

2.1  $K/s^2$  Plant and Task Description

Consider the  $K/s^2$  plant dynamics as discussed, for example, by Kleinman et al. in [6]. The system state equations are

$$\begin{bmatrix} \dot{x} \\ \ddot{x} \end{bmatrix} = \begin{bmatrix} 0 & 1 \\ 0 & 0 \end{bmatrix} \begin{bmatrix} x \\ \dot{x} \end{bmatrix} + \begin{bmatrix} 0 \\ K \end{bmatrix} \delta(t) \quad (2.1.1)$$

where  $x(t)$  is the plant position and  $\delta(t)$  is the input from the human controller.

A velocity disturbance is applied to the plant. It is modeled as a first order Markov process having a break frequency of 2 rads/sec and is given by

$$\dot{x}_1(t) = -2x_1(t) + w(t) \quad (2.1.2)$$

where  $w(t)$  has intensity  $W = 0.217$  to give  $E\{x_1^2\} = 0.054 \text{ in.}^2$ . Defining the plant position error ( $e$ ) and the error rate ( $\dot{e}$ ) as

$$e(t) \triangleq x_2(t) \quad ; \quad \dot{e}(t) \triangleq x_1(t) + x_3(t) \quad (2.1.3)$$

and letting  $K = 1 \text{ in./in.}$ , the plant equations (2.1.1) can be combined

with the disturbance equation (2.1.2) to get

$$\begin{bmatrix} \dot{x}_1 \\ \dot{x}_2 \\ \dot{x}_3 \end{bmatrix} = \begin{bmatrix} -2 & 0 & 0 \\ 1 & 0 & 1 \\ 0 & 0 & 0 \end{bmatrix} \begin{bmatrix} x_1 \\ x_2 \\ x_3 \end{bmatrix} + \begin{bmatrix} 0 \\ 0 \\ 1 \end{bmatrix} \delta(t) + \begin{bmatrix} 1 \\ 0 \\ 0 \end{bmatrix} w(t)$$

or in concise form

$$\dot{\bar{x}} = A_o \bar{x} + B_o u + D_o w \quad (2.1.4)$$

The human operator's task is to minimize the position error  $x_2(t)$  in the presence of the disturbance.

Next consider a display exhibiting some transport lag modeled in the form

$$x_d(s) = \frac{1}{\tau_d s + 1} e(s) \quad (2.1.5)$$

The dynamics of the disturbance, plant, and display can then be written as

$$\begin{bmatrix} \dot{\bar{x}} \\ \dot{x}_d \end{bmatrix} = \begin{bmatrix} A_o & 0 \\ -\frac{1}{\tau_d} & -\frac{1}{\tau_d} \end{bmatrix} \begin{bmatrix} \bar{x} \\ x_d \end{bmatrix} + \begin{bmatrix} B_o \\ 0 \end{bmatrix} \delta + \begin{bmatrix} D_o \\ 0 \end{bmatrix} w \quad (2.1.6)$$

The human operator's observations for this system are

$$\begin{aligned} y_1 &= x_d \\ y_2 &= \dot{x}_d \end{aligned} \quad (2.1.7)$$

where it is assumed, in accordance with the known abilities of the human controller, that he is able to reconstruct the displayed-variable rate by observing the displayed variable itself.

As shown in Fig. (2.1), the human operator's task with the display is to keep the needle on the display centered to the best of his



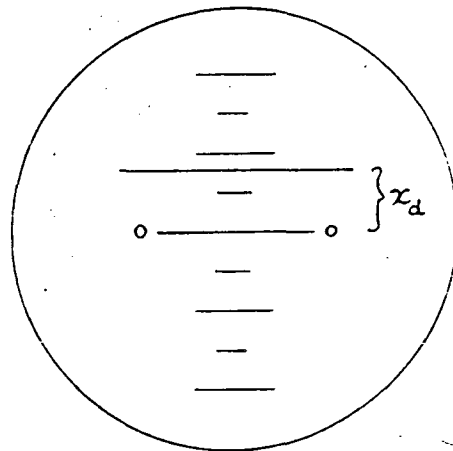


Figure 2.1 Display for  $K/s^2$  Plant

abilities, subject to reasonable workload. This performance objective can be reflected in terms of minimizing the cost

$$J_p(\delta) = E\left\{\lim_{T \rightarrow \infty} \frac{1}{T} \int_0^T (x_d^2 + g\dot{\delta}^2) dt\right\} \quad (2.1.8)$$

With the above formulation in mind, the performance of the manually controlled system is evaluated using the OCM model for various values of  $\tau_d$ . A brief description of the OCM modeling technique is given in Appendix B. For all the analysis carried out in this section, the parameters that define the OCM model were set to the following values:

- (i) Human operator's observation time delay,  $\tau$ , set to 0.2 seconds
- (ii) Observation noise ratio set at -20 dB for both observations
- (iii) Motor noise ratio was set at -25 dB
- (iv) The weighting,  $g$ , on the control rate in the human controller's objective function was always adjusted to yield a neuromotor lag time constant,  $\tau_n$ , of 0.1 secs.
- (v) Very low values of thresholds were used for the observations available to the human, and he was assumed to devote full attention to the displayed signal.

The OCM model obtained for the above values of the parameters has been shown to correlate very well with the experimentally observed behaviour of the human controller [6], especially in single-axis tasks such as the one being discussed here. The significance of these parameters in modeling the human operator dynamics is explained in Appendix B.

The results for various values of display lag  $\tau_d$  are presented in Table 2.1, in terms of the mean square values of the variables of interest. These results are also plotted in Figures (2.2) and (2.3) (to be discussed later) and correspond to the curve marked ① in these figures. From these results it is clear that with only error  $e$  driving the display, the pilot's performance improves as the display bandwidth is increased. As  $\frac{1}{\tau_d} \rightarrow \infty$  the pilot's performance approaches a limiting case where the error is displayed instantaneously to the human, or the limiting case where there is no display lag. This limiting idealized case (labeled A in the figures) assumes that the error can be sensed and displayed without any computational delay or lag, and may not be achievable. The question now is whether the performance (or pilot's workload situation) can be improved by augmenting the display dynamics.

## 2.2 Display Quickening For $K/s^2$ Plant

Consider the augmented display dynamics of the form

$$\dot{x}_d = \frac{-1}{\tau_d} x_d + \frac{1}{\tau_d} x_2 + g_d x_3 \quad (2.1.9)$$

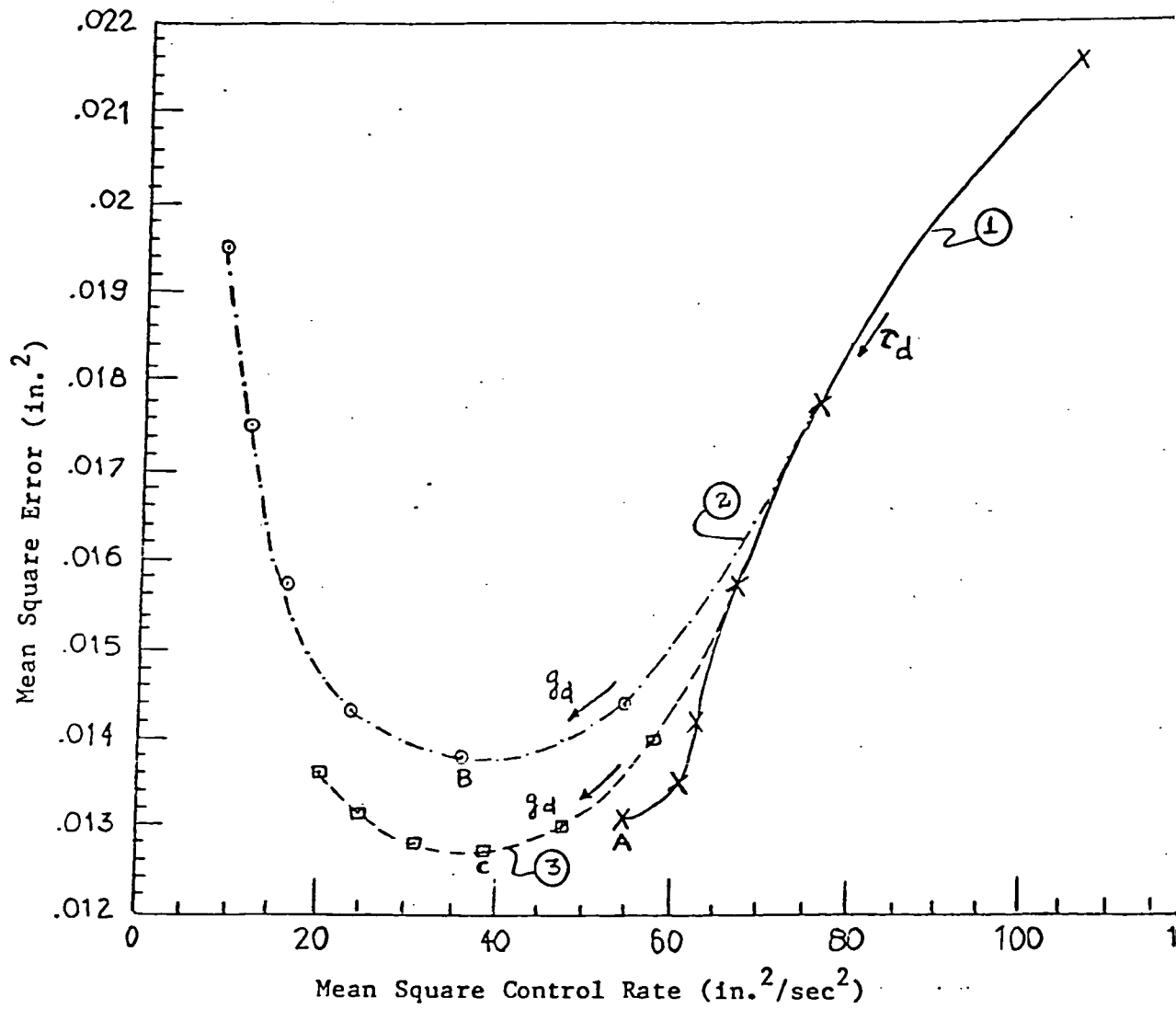
where  $g_d$  is a gain to be adjusted. Since  $x_3(t)$  is the plant velocity state, the above form of display will provide some lead information to the human. Note that this form of display dynamics can be written in general as

$$\begin{aligned} \dot{x}_d &= a_d x_d + u_d \\ u_d &= G_d \bar{y}_d \end{aligned} \quad (2.2.1)$$

where  $\bar{y}_d = C_d \bar{x}$  is the vector of plant responses available for driving the display, and  $u_d$  is the display control law to be determined. In the formulation of display dynamics as above, the choice of  $a_d$  determines

TABLE 2.1: OCM RESULTS FOR VARYING DISPLAY BANDWIDTH

$\tau_d$ (sec)	M.S. Error (e) (in. <sup>2</sup> )	M.S. Input ( $\delta$ ) (in. <sup>2</sup> )	M.S. Control Rate ( $\dot{\delta}$ ) (in. <sup>2</sup> /sec <sup>2</sup> )
0.20	0.0215	2.176	106.91
0.10	0.0177	1.543	76.47
0.05	0.0157	1.353	67.44
0.02	0.0142	1.261	62.9
0.01	0.0135	1.223	60.98
$\rightarrow 0$	0.0131	1.141	54.73

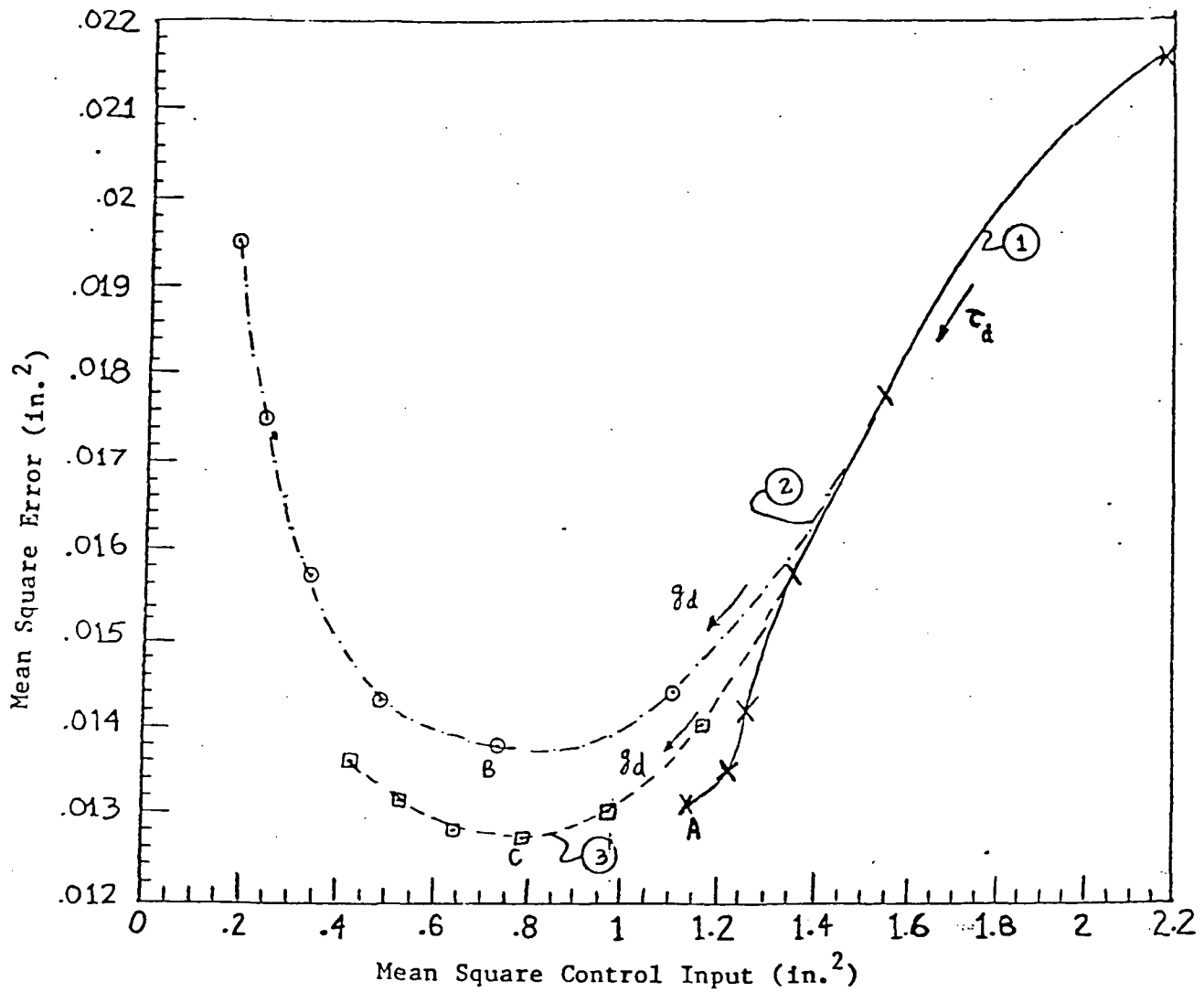


#### Nomenclature

- ① Only e driving display,  $\tau_d = .20 \rightarrow 0$
- ②  $\tau_d = .10$ ,  $g_d = 1, 2, 3, 4, 5, 6$ ; B :  $g_d = 2$
- ③  $\tau_d = .05$ ,  $g_d = 1, 2, 3, 4, 5, 6$ ; C :  $g_d = 3$

$\tau_d$  in seconds

Figure 2.2 Parametric Performance - Manual Control Rate



#### Nomenclature

- ① Only e driving display,  $\tau_d = .20 \rightarrow 0$
  - ②  $\tau_d = .10$ ,  $g_d = 1, 2, 3, 4, 5, 6$ ; B :  $g_d = 2$
  - ③  $\tau_d = .05$ ,  $g_d = 1, 2, 3, 4, 5, 6$ ; C :  $g_d = 3$
- $\tau_d$  in seconds

Figure 2.3 Parametric Performance - Manual Control Activity

the bandwidth of the display.

With the same OCM parameters as above, an analysis was performed for two values of  $\tau_d$ : .10 and .05 secs. These values were chosen so that the display dynamics are near the bandwidth of the human controller as modeled. For each of these values,  $g_d$  is varied from 1 to 6. The results are presented in Table 2.2 and are also plotted in Figures (2.2) and (2.3) so as to compare them with the previous results. In the two figures, the curve marked (2) corresponds to  $\tau_d = .10$  secs and that marked (3) to  $\tau_d = .05$  secs.

Fig. (2.2) is a plot of mean square error (e) vs. mean square manual control rate ( $\dot{\delta}$ ) for the various display cases discussed above. Fig. (2.3) is a plot of mean square error vs. the mean square manual control input ( $\delta$ ). From these two figures it is clear that the mean square control input and control rate both decrease as the display control gain  $g_d$  is increased. The mean square error initially decreases as  $g_d$  is increased, and then increases beyond a certain value of  $g_d$  that depends on the choice of display bandwidth.

Note that earlier work [10,11] has shown that the human operator's workload is directly related to his mean-square control rate. This means that it should be possible in this case to improve performance (of which mean square error is a measure), while at the same time decreasing workload. Moreover, the results indicate that for a given display bandwidth there is an optimal choice of display control gains. For example, point C in Figures (2.2) and (2.3) is such an optimal display for  $\tau_d = .05$  secs, and for this case the performance is slightly better than even the idealized limiting case at point A.

TABLE 2.2: OCM RESULTS FOR VARYING DISPLAY CONTROL GAINS

(a)  $\tau_d = .10$  secs

$g_d$	M.S. Error (e) (in. <sup>2</sup> )	M.S. Input ( $\delta$ ) (in. <sup>2</sup> )	M.S. Control Rate ( $\dot{\delta}$ ) (in. <sup>2</sup> /sec <sup>2</sup> )
1	0.0144	1.113	54.75
2	0.0138	0.733	35.92
3	0.0143	0.486	23.71
4	0.0157	0.339	16.52
5	0.0175	0.248	12.05
6	0.0195	0.187	9.01

(b)  $\tau_d = .05$  secs

$g_d$	M.S. Error (e) (in. <sup>2</sup> )	M.S. Input ( $\delta$ ) (in. <sup>2</sup> )	M.S. Control Rate ( $\dot{\delta}$ ) (in. <sup>2</sup> /sec <sup>2</sup> )
1	0.014	1.175	58.06
2	0.013	0.968	47.47
3	0.0127	0.789	38.49
4	0.0128	0.639	30.97
5	0.0131	0.521	25.15
6	0.0136	0.427	20.46



It would then appear desirable to develop a systematic approach to display augmentation which will make it possible to directly synthesize the optimal display gains without having to resort to trial and error. In the following chapter an extension of the optimal cooperative control synthesis technique [7-9] is proposed as a methodology to accomplish this.

## CHAPTER 3

### OPTIMAL COOPERATIVE CONTROL/DISPLAY DESIGN METHODOLOGY

The problem formulation for the cooperative control/display design methodology is presented and the necessary conditions for optimality are derived in detail. Application of the methodology to pilot-in-the-loop synthesis is demonstrated and various special cases of augmentation are discussed.

#### 3.1 Problem Formulation

In this section the mathematical formulation of the cooperative control synthesis technique is presented. Necessary conditions for the simultaneous optimality of the display and control augmentation systems are developed in the sections that follow. The procedure followed here is very similar to that of [8,9].

Consider a dynamic system acted upon by two controllers, and described by the linear time invariant set of first order differential equations

$$\dot{\bar{x}} = A_o \bar{x} + B_{1o} \bar{u}_1 + B_{2o} \bar{u}_2 + D_o \bar{w} \quad (3.1.1)$$

with  $\bar{x} \in \mathbb{R}^n$ ,  $\bar{u}_1 \in \mathbb{R}^{m_1}$ ,  $\bar{u}_2 \in \mathbb{R}^{m_2}$  and  $\bar{w}$  a zero-mean Gaussian white noise process with intensity  $W$ . The two controls represent two physically independent controllers, and in section (3.5) it is shown how the controller 1 ( $\bar{u}_1$ ) can be made to closely approximate the OCM model of human behaviour.

The display dynamics are assumed to be of the form

$$\dot{\bar{x}}_d = A_d \bar{x}_d + B_{do} \bar{u}_d \quad (3.1.2)$$

with  $\bar{x}_d \in \mathbb{R}^d$ ,  $\bar{u}_d \in \mathbb{R}^{m_d}$ , and  $\bar{u}_d$  is the display quickening controller. The

objective is to find the optimal cooperative controllers 1 and 2 ( $\bar{u}_1$  and  $\bar{u}_2$ ) along with the optimal display control law  $\bar{u}_d$ .

Controller 1 ( $\bar{u}_1$ ) is assumed to have noisy observations available for feedback given by

$$\bar{y}_1 = C_{10}\bar{x} + C_{d1}\bar{x}_d + C_u\bar{u}_d + \bar{v}_y \quad (3.1.3)$$

where  $\bar{v}_y$  is also a zero-mean Gaussian white noise process with intensity  $V_y$ . This controller will be shown to include state estimation.

The augmentation controller  $\bar{u}_2$  and the display control law  $\bar{u}_d$  are assumed to have noise-free system outputs  $\bar{y}_2$  and  $\bar{y}_d$ , respectively, available for feedback, where

$$\bar{y}_2 = C_{20}\bar{x}; \quad \bar{y}_d = C_d \begin{bmatrix} \bar{x} \\ \bar{x}_d \end{bmatrix} \quad (3.1.4)$$

Note that the above formulation does not allow feedback of the display states  $\bar{x}_d$  to the augmentation controller  $\bar{u}_2$ . Finally, these two latter controllers are constrained to have the direct output feedback form

$$\begin{aligned} \bar{u}_2 &= G_2\bar{y}_2 = G_2C_{20}\bar{x} \\ \bar{u}_d &= G_d\bar{y}_d = G_dC_d \begin{bmatrix} \bar{x} \\ \bar{x}_d \end{bmatrix} \end{aligned} \quad (3.1.5)$$

The interaction between the different controllers is shown in the block diagram of Figure (3.1).

### 3.2 Design Objectives

Controller 1 is to be optimal with respect to the cost

$$J_1 = E\left\{\lim_{T \rightarrow \infty} \frac{1}{T} \int_0^T (\bar{x}^T Q_{10} \bar{x} + \bar{x}_d^T Q_{1d} \bar{x}_d + \bar{u}_1^T R_1 \bar{u}_1 + \bar{u}_2^T F_1 \bar{u}_2) dt\right\} \quad (3.2.1)$$

in the presence of the action of control inputs  $\bar{u}_2$  and  $\bar{u}_d$ . Here  $E\{\cdot\}$

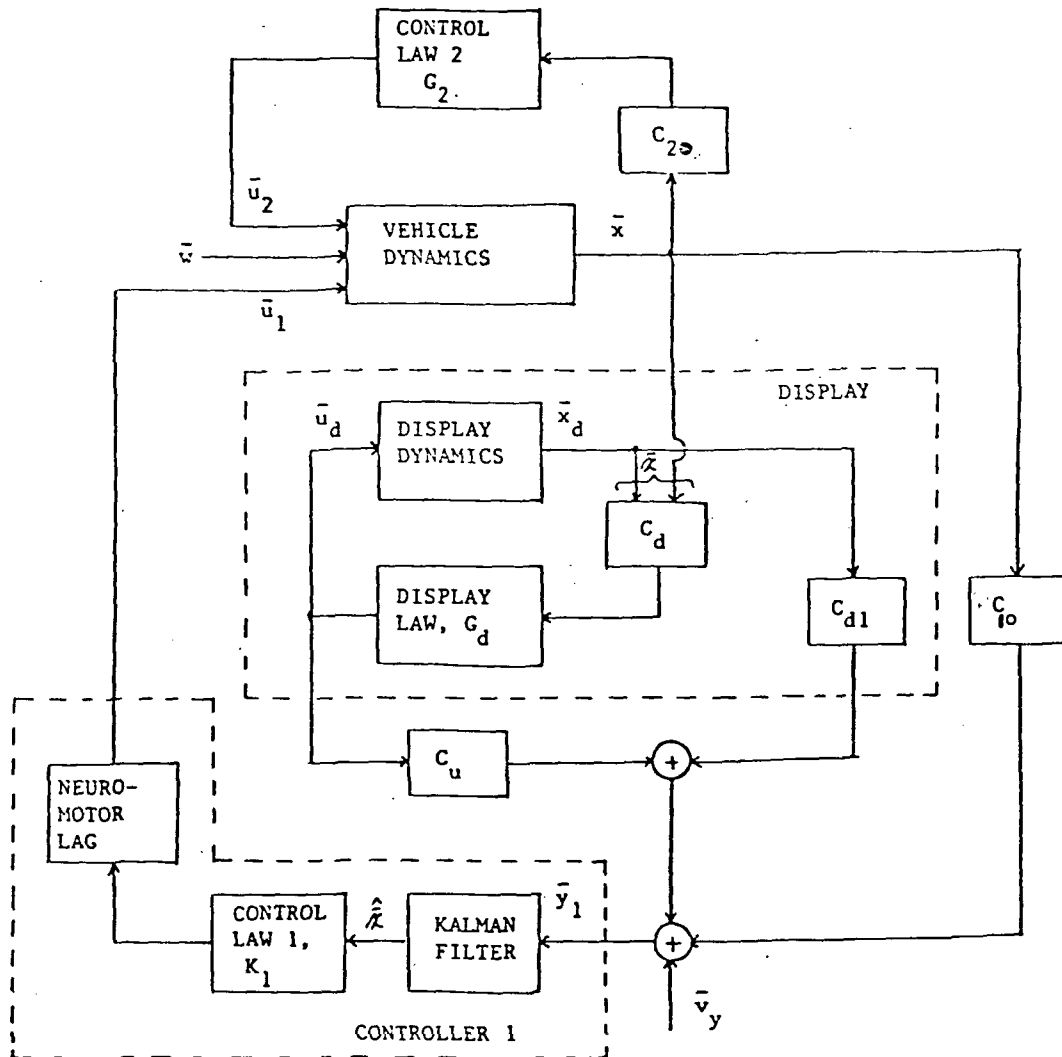


Figure 3.1 Block Diagram for Control and Display Augmentation

indicates the expected value operator and the weighting matrices are  $Q_{1o} > 0$ ,  $Q_{1d} > 0$ ,  $R_1 > 0$ ,  $F_1 > 0$ . Conversely, Controller 2 ( $\bar{u}_2$ ) and the display control law  $\bar{u}_d$  are to be optimal with respect to the cost

$$J_2 = E\left\{\lim_{T \rightarrow \infty} \frac{1}{T} \int_0^T (\bar{x}^T Q_{2o} \bar{x} + \bar{x}_d^T Q_{2d} \bar{x}_d + \bar{u}_1^T R_2 \bar{u}_1 + \bar{u}_2^T F_2 \bar{u}_2 + \bar{u}_d^T F_{2d} \bar{u}_d) dt\right\} \quad (3.2.2)$$

in the presence of the control action  $\bar{u}_1$ . The weighting matrices are  $Q_{2o} > 0$ ,  $Q_{2d} > 0$ ,  $R_2 > 0$ ,  $F_2 > 0$ ,  $F_{2d} > 0$ .

Augmenting the system dynamics (3.1.1) with the display dynamics (3.1.2), the state-space description of this augmented system is

$$\begin{bmatrix} \dot{\bar{x}} \\ \bar{x} \\ \dot{\bar{x}}_d \\ \bar{x}_d \end{bmatrix} = \begin{bmatrix} A_o & 0 \\ 0 & A_d \end{bmatrix} \begin{bmatrix} \bar{x} \\ \bar{x}_d \end{bmatrix} + \begin{bmatrix} B_{1o} \\ 0 \end{bmatrix} \bar{u}_1 + \begin{bmatrix} B_{2o} \\ 0 \end{bmatrix} \bar{u}_2 + \begin{bmatrix} 0 \\ B_{do} \end{bmatrix} \bar{u}_d + \begin{bmatrix} D_o \\ 0 \end{bmatrix} \bar{w} \quad (3.2.3)$$

Defining  $\bar{X} = \text{COL}(\bar{x}, \bar{x}_d)$ , (3.2.3) can be written in a compact form with appropriate definitions for the matrices as

$$\dot{\bar{X}} = A\bar{X} + B_1 \bar{u}_1 + B_2 \bar{u}_2 + B_d \bar{u}_d + D\bar{w} \quad (3.2.4)$$

The measurements can similarly be written as

$$\begin{aligned} \bar{y}_1 &= C_1 \bar{X} + C_u \bar{u}_d + \bar{v}_y \\ \bar{y}_2 &= C_2 \bar{X} \\ \bar{y}_d &= C_d \bar{X} \end{aligned} \quad (3.2.5)$$

The two cost functions can then be expressed in terms of the augmented state vector  $\bar{X}$  as

$$\begin{aligned} J_1 &= E\left\{\lim_{T \rightarrow \infty} \frac{1}{T} \int_0^T (\bar{X}^T Q_1 \bar{X} + \bar{u}_1^T R_1 \bar{u}_1 + \bar{u}_2^T F_1 \bar{u}_2) dt\right\} \\ J_2 &= E\left\{\lim_{T \rightarrow \infty} \frac{1}{T} \int_0^T (\bar{X}^T Q_2 \bar{X} + \bar{u}_1^T R_2 \bar{u}_1 + \bar{u}_2^T F_2 \bar{u}_2 + \bar{u}_d^T F_{2d} \bar{u}_d) dt\right\} \end{aligned} \quad (3.2.6)$$

where the weighting matrices  $Q_1$  and  $Q_2$  are appropriately defined. (Note that this formulation is formally that for a multi-player non-zero sum game, and we seek a Nash solution [22]).

### 3.3 Solution for $\bar{u}_1$

In the presence of the action of control inputs  $\bar{u}_2$  and  $\bar{u}_d$ , as given by (3.1.5), the dynamics of the augmented system (3.2.4) are

$$\begin{aligned}\dot{\bar{x}} &= A_{\text{aug}} \bar{x} + B_1 \bar{u}_1 + D \bar{w} \\ \bar{y}_1 &= C_{\text{aug}} \bar{x} + \bar{v}_y\end{aligned}\quad (3.3.1)$$

where

$$\begin{aligned}A_{\text{aug}} &\triangleq (A + B_2 G_2 C_2 + B_d G_d C_d) \\ C_{\text{aug}} &\triangleq (C_1 + C_u G_d C_d)\end{aligned}\quad (3.3.2)$$

and the performance index  $J_1$  becomes

$$J_1 = E \left\{ \lim_{T \rightarrow \infty} \frac{1}{T} \int_0^T (\bar{x}^T (Q_1 + C_2^T G_2^T F_1 G_2 C_2) \bar{x} + \bar{u}_1^T R_1 \bar{u}_1) dt \right\} \quad (3.3.3)$$

Equations (3.3.1) and (3.3.3), in the case of uncorrelated process and measurement noises ( $\bar{w}$  and  $\bar{v}_y$ ) and for  $V_y > 0$  (i.e.  $V_y$  - positive definite), describe the standard non-singular linear quadratic Gaussian regulator problem for controller  $\bar{u}_1$ . The optimal controller is known [12] to have the form

$$\bar{u}_1 = K_1 \hat{\bar{x}} \quad (3.3.4)$$

where  $\hat{\bar{x}}$  is the minimum mean-square estimate of the system state vector  $\bar{x}$ . The gain matrix  $K_1$  is given by

$$K_1 = -R_1^{-1} B_1^T P \quad (3.3.5)$$

with  $P > 0$  and symmetric, the solution of the algebraic Ricatti equation

$$A_{aug}^T P + P A_{aug} + (Q_1 + C_2^T G_2^T F_1 G_2 C_2) - P B_1^T R_1^{-1} B_1 P = 0 \quad (3.3.6)$$

The dynamics of the Kalman state estimator are

$$\dot{\hat{\chi}} = A_{aug} \hat{\chi} + B_1 \bar{u}_1 + M_1 (\bar{y}_1 - C_{aug} \hat{\chi}) \quad (3.3.7)$$

where the Kalman filter gain matrix  $M_1$  is given by

$$M_1 = \Sigma C_{aug}^T V_y^{-1} \quad (3.3.8)$$

with  $\Sigma (> 0)$  the solution of the algebraic Ricatti equation

$$A_{aug} \Sigma + \Sigma A_{aug}^T + D W D^T - \Sigma C_{aug}^T V_y^{-1} C_{aug} \Sigma = 0 \quad (3.3.9)$$

### 3.4 Solution for $\bar{u}_2$ and $\bar{u}_d$

The optimal controller  $\bar{u}_1$  as derived above has the form

$$\bar{u}_1 = K_1 \hat{\chi}; \quad \dot{\hat{\chi}} = A_1 \hat{\chi} + M_1 \bar{y}_1 \quad (3.4.1)$$

where  $A_1 \triangleq (A_{aug} + B_1 K_1 - M_1 C_{aug})$ . Then in the presence of this control action  $\bar{u}_1$ , the system dynamics (3.2.4, 3.3.4, 3.3.7) can be written in terms of the augmented state vector  $\bar{q} \triangleq \text{COL} (\bar{\chi}, \hat{\chi})$  as

$$\dot{\bar{q}} = \begin{bmatrix} A & B_1 K_1 \\ M_1 C_1 & A_1 \end{bmatrix} \bar{q} + \begin{bmatrix} B_2 \\ 0 \end{bmatrix} \bar{u}_2 + \begin{bmatrix} B_d \\ M_1 C_u \end{bmatrix} \bar{u}_d + \begin{bmatrix} D & 0 \\ 0 & M_1 \end{bmatrix} \begin{bmatrix} \bar{w} \\ \bar{v}_y \end{bmatrix} \quad (3.4.2)$$

which can further be written in a compact form, with appropriate definitions of matrices, as

$$\dot{\bar{q}} = A'_1 \bar{q} + B'_2 \bar{u}_2 + B'_d \bar{u}_d + D' \bar{w}' \quad (3.4.3)$$

The intensity of the process  $\bar{w}'$  is  $W' = \begin{bmatrix} W & 0 \\ 0 & V_y \end{bmatrix}$ .

The index of performance to be minimized by  $\bar{u}_2$  and  $\bar{u}_d$  then becomes

$$J_2 = E \left\{ \lim_{T \rightarrow \infty} \frac{1}{T} \int_0^T (\bar{q}^T Q' \bar{q} + \bar{u}_2^T F_2 \bar{u}_2 + \bar{u}_d^T F_d \bar{u}_d) dt \right\} \quad (3.4.4)$$

with

$$Q' \triangleq \begin{bmatrix} Q_2 & 0 \\ 0 & K_1^T R_2 K_1 \end{bmatrix}.$$

The design objective can then be stated as that of finding the optimal controller  $\bar{u}_2$  and optimal display control  $\bar{u}_d$  which minimize the cost  $J_2$  as given by (3.4.4), subject to (3.4.3).

Proceeding in a way as detailed in Appendix A, it can be shown that the gains  $G_2$  and  $G_d$  which correspond to the simultaneous optimality of the two controllers  $\bar{u}_2$  and  $\bar{u}_d$  are given by

$$G_2 = -F_2^{-1} [B_2^T \ 0] H L \begin{bmatrix} C_2^T \\ 0 \end{bmatrix} ([C_2 \ 0] L \begin{bmatrix} C_2^T \\ 0 \end{bmatrix})^{-1} \quad (3.4.5)$$

and

$$G_d = -F_{2d}^{-1} \begin{bmatrix} B_d \\ M_1 C_u \end{bmatrix}^T H L \begin{bmatrix} C_d^T \\ 0 \end{bmatrix} ([C_d \ 0] L \begin{bmatrix} C_d^T \\ 0 \end{bmatrix})^{-1} \quad (3.4.6)$$

Here,  $L = E\{\bar{q} \bar{q}^T\}$  satisfies the relation

$$A_c L + L A_c^T + D' W' D'^T = 0 \quad (3.4.7)$$

and  $H$  satisfies

$$A_c^T H + H A_c + \bar{Q} = 0 \quad (3.4.8)$$

where the following definitions have been used

$$A_c \triangleq \begin{bmatrix} A_{aug} & B_1 K_1 \\ M_1 C_{aug} & A_1 \end{bmatrix}; \quad \bar{Q} \triangleq Q' + \begin{bmatrix} C_2^T G_2^T F_2 G_2 C_2 + C_d^T G_d^T F_{2d} G_d C_d & 0 \\ 0 & 0 \end{bmatrix}$$

The solutions (3.4.5) and (3.4.6) are derived from the gradient condi-



tions

$$\frac{\partial \bar{J}_2}{\partial G_2} = 2\{F_2 G_2 [C_2 \ 0] L \begin{bmatrix} C_2^T \\ 0 \end{bmatrix} + [B_2^T \ 0] H L \begin{bmatrix} C_2^T \\ 0 \end{bmatrix}\} = 0 \quad (3.4.9)$$

and

$$\frac{\partial \bar{J}_2}{\partial G_d} = 2\{F_{2d} G_d [C_d \ 0] L \begin{bmatrix} C_d^T \\ 0 \end{bmatrix} + \begin{bmatrix} B_d \\ M_1 C_u \end{bmatrix}^T H L \begin{bmatrix} C_d^T \\ 0 \end{bmatrix}\} = 0 \quad (3.4.10)$$

respectively, as shown in Appendix A.

Equations (3.4.7) to (3.4.10) then give the four necessary conditions for the simultaneous optimality of the display and control augmentation for the task, as defined by the performance index  $J_2$ , given that Controller 1 is of the form stated in (3.4.1).

### 3.5 Application to Pilot-in-the-Loop Synthesis

In the preceding sections, a dual performance optimization problem was discussed and the necessary conditions for the optimality of the various controllers, and the expressions for the resulting gain matrices, were derived. The association of Controller 2 ( $\bar{u}_2$ ) with plant augmentation, and of display control ( $\bar{u}_d$ ) with the display augmentation should be apparent in the above formulation. In this section it will be shown that Controller 1 ( $\bar{u}_1$ ) can be made to closely approximate the OCM model of human behaviour by an appropriate choice of the relevant parameters. In this manner the cooperative methodology, as developed above, can be used to do "pilot in the loop" synthesis of the display/control augmentation design.

Consider the Optimal Control Model as discussed in Appendix B.

With  $\bar{u}_p \triangleq \bar{u}_o(t)$  and  $\bar{x}_p^T \triangleq [\bar{x}^T, \bar{u}_p^T(t)]$ , the dynamics of the augmented system in Equation (B.4) are

$$\dot{\bar{x}}_p(t) = A_o \bar{x}_p(t) + B_{1o} \bar{u}_o(t) + D_o \bar{w}(t) \quad (3.5.1)$$

with  $A_o$ ,  $B_{1o}$ , and  $D_o$  as in (3.1.1).

The observations available to the pilot, as given by (B.2) can be rewritten as

$$\bar{y}_p(t) = C_o \bar{x}_p(t-\tau) + \bar{v}(t-\tau) \quad (3.5.2)$$

where  $C_o = [C \mid d]$ , and the pilot's cost function (B.3) becomes

$$J_p(\mu^*) = E\left\{\lim_{T \rightarrow \infty} \frac{1}{T} \int_0^T (\bar{x}_p^T C_o^T \bar{x}_p + \bar{u}_o^T G \bar{u}_o) dt\right\} \quad (3.5.3)$$

Comparing the above formulation for  $\bar{u}_o$  with that for Controller 1 ( $\bar{u}_1$ ) as in Section (3.3) we notice that Equations (3.5.1) to (3.5.3) have the same form as Eqns (3.3.1) to (3.3.3), but for the simplification that the time delay,  $\tau$ , has been eliminated in the observations for  $\bar{u}_1$ . The absence of the time delay simplifies the dynamic order of the pilot model by eliminating the linear predictor in the control structure (B.17, B.18). The motor noise ( $v_m$  in (B.12)) is however accounted for in this formulation in that it may appear as an additional disturbance in Eqn. (3.3.1). The structure of the pilot model as represented by Controller 1 ( $\bar{u}_1$ ) is as shown in Figure (3.2).

It is worth mentioning here that, though the simplified pilot model is used in the synthesis procedure presented in this report, the complete model (with predictor, etc.) is used to evaluate these designs. Moreover, at each iteration of the synthesis process, the parameters (e.g. noise intensities) in the simplified model are updated to yield

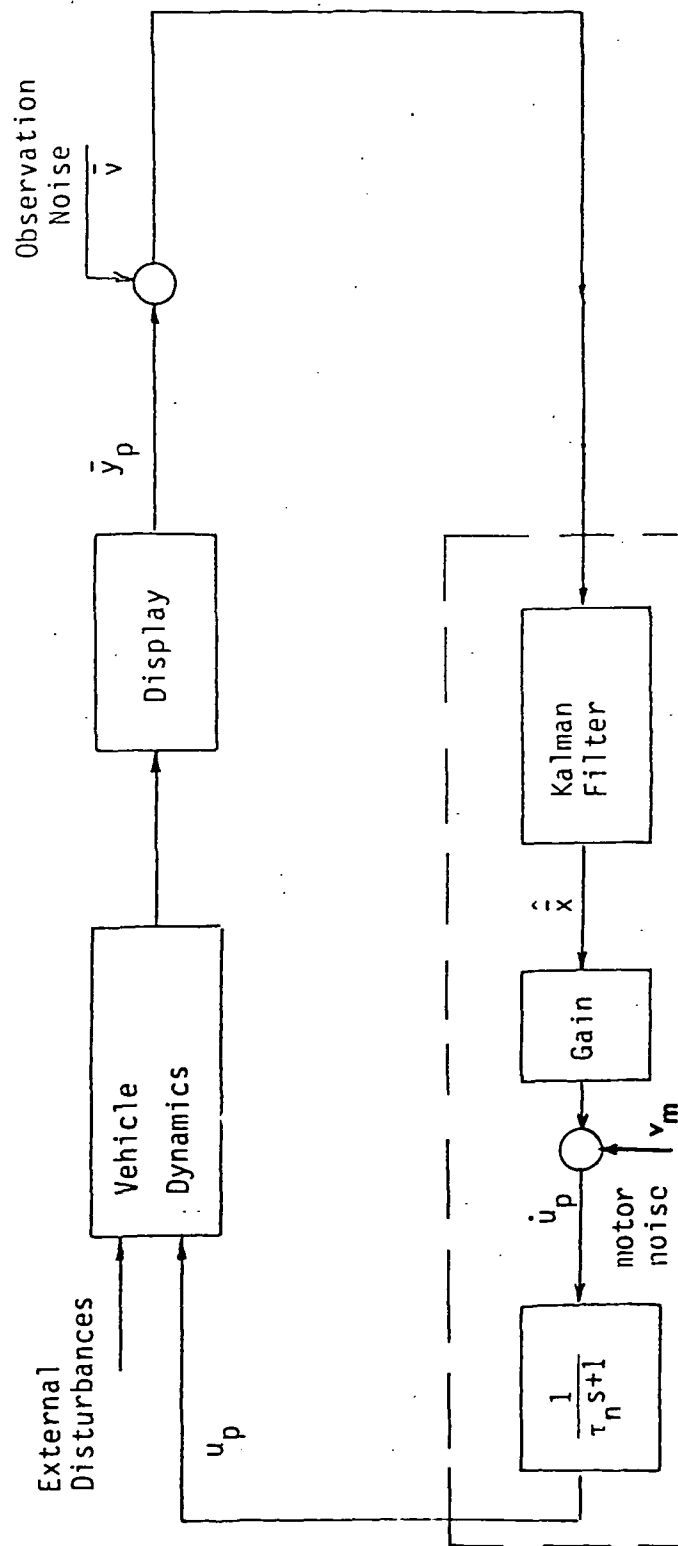


Figure 3.2 Simplified Pilot Model Block Diagram

results that are consistent with the complete OCM model. It has been shown in [9] and [16] that by selecting proper noise intensities for the control noise  $\bar{v}_m$  and the measurement noise  $\bar{v}_y$ , the simplified model may yield the same human operator dynamics as the complete OCM model.

### 3.6 Numerical Solution Algorithm

For the case of only control augmentation ( $\bar{u}_2$ ) being designed, the problem reduces to one discussed extensively by Innocenti in [8,9] as the Linear Optimal Cooperative Regulator (LOCR) problem. With the display-related terms removed from the problem formulation, the necessary conditions for optimality as derived above reduce to those in [8,9].

For the case of only display control law being designed, the necessary conditions simplify, with the terms related to Controller 2 ( $\bar{u}_2$ ) removed from the problem formulation. The block diagram for the controller interaction is the same as in Figure (3.1) but without Controller 2. A brief description of the solution algorithm, along with a flow chart for the computer program written to implement the display synthesis procedure, is provided here. Since the algorithm is very similar to that in [8,9], the reader is referred to the references for a more detailed description.

The problem formulation for the case of display augmentation only can be summarized as follows:

Given the linear time invariant system

$$\begin{aligned}\dot{\bar{x}} &= A\bar{x} + B_1\bar{u}_1 + B_d\bar{u}_d + D\bar{w} \\ \bar{y}_1 &= C_1\bar{x} + C_u\bar{u}_d + \bar{v}_y\end{aligned}\tag{3.6.1}$$

$$\bar{y}_d = C_d \bar{x}$$

we wish to determine the optimal controllers  $\bar{u}_1$  and  $\bar{u}_d$  that minimize respectively

$$J_1 = E\left\{\lim_{T \rightarrow \infty} \frac{1}{T} \int_0^T (\bar{x}^T Q_1 \bar{x} + \bar{u}_1^T R_1 \bar{u}_1) dt\right\} \quad (3.6.2)$$

and

$$J_2 = E\left\{\lim_{T \rightarrow \infty} \frac{1}{T} \int_0^T (\bar{x}^T Q_2 \bar{x} + \bar{u}_1^T R_2 \bar{u}_1 + \bar{u}_d^T F_{2d} \bar{u}_d) dt\right\} \quad (3.6.3)$$

subject to the constraint

$$\bar{u}_d = G_d \bar{y}_d \quad (3.6.4)$$

In Equations (3.6.1) to (3.6.4) all the vectors and matrices are as defined in Section (3.2).

The numerical procedure solves for the display control law ( $\bar{u}_d$ ) which satisfies the necessary conditions of optimality for the cost  $J_2$  (3.4.7 to 3.4.10), given that the corresponding Controller 1 ( $\bar{u}_1$ ) is optimal with respect to the cost  $J_1$  (or satisfies 3.3.5 to 3.3.9). The algorithm for the solution procedure is summarized in Fig. (3.3) and a step-by-step description of the algorithm is given in the following.

Step-1. This step consists of selecting a starting display control law  $\bar{u}_d$  to initialize the numerical optimization procedure. A reasonable choice (as is shown in later application) is to select  $G_d$  such that the display variables  $\bar{x}_d$ , as given by (3.1.2), closely approximate those observations of the pilot which are of primary importance for accomplishing the assigned task.

Another important choice to be made, before starting the iterative

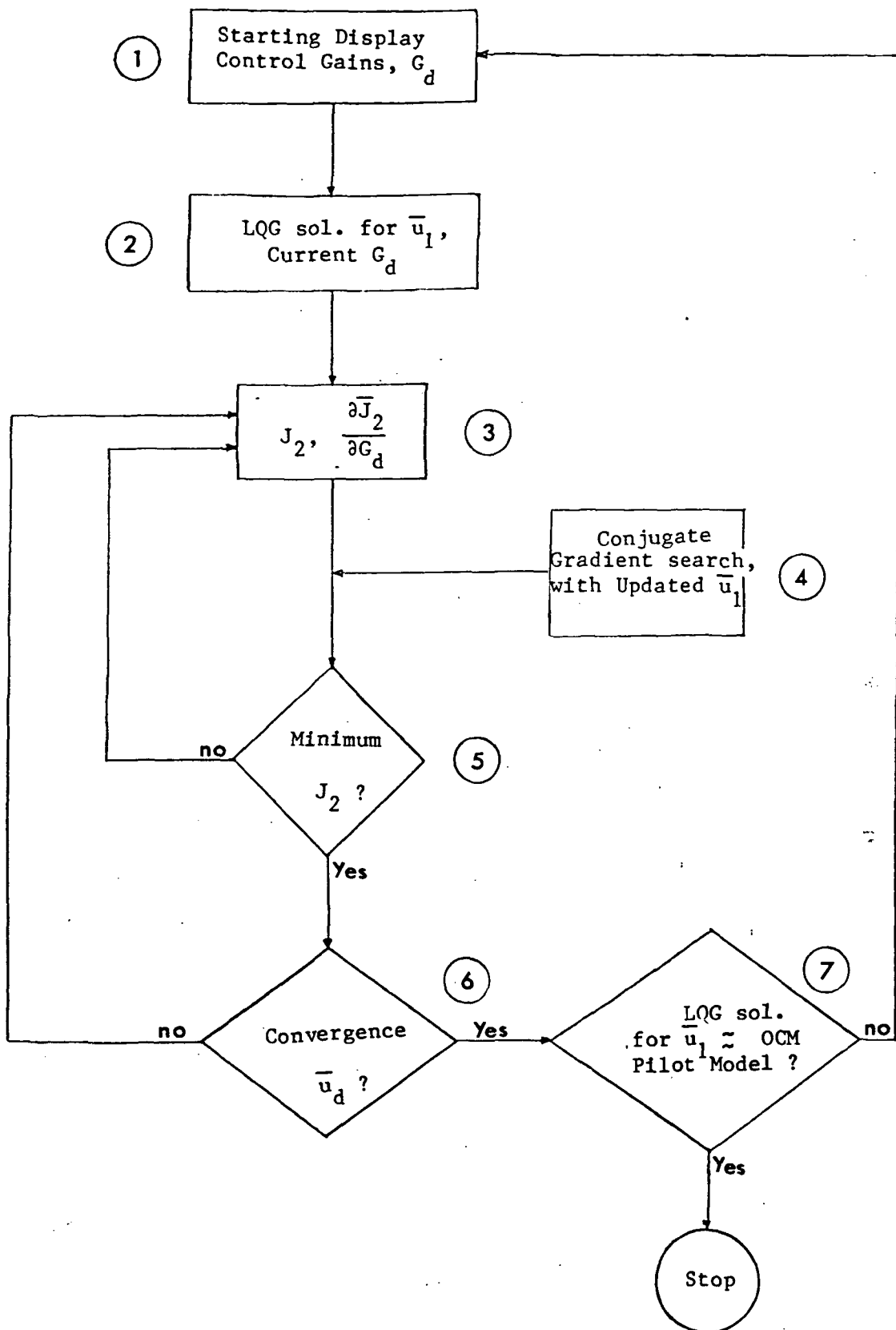


Figure 3.3 Flowchart for Numerical Procedure

procedure, is that for the intensities of the noise processes  $\bar{w}$  and  $\bar{v}_y$ . These should be chosen such that the optimal Controller 1, for the starting display augmentation, closely represents the OCM pilot model.

Step-2. Solve for the optimal Controller 1 ( $\bar{u}_1$ ), as detailed in Section (3.3), for the initial display augmentation, and compare with the corresponding OCM pilot model to confirm that the choice for the noise intensities is appropriate.

Step-3. Form the closed loop system, as in (3.4.3) and (A.4 of Appendix A), for the current display augmentation ( $\bar{u}_d$ ) and the corresponding optimal Controller 1. Solve the Lyapunov equations (3.4.7) and (3.4.8) for the matrices L and H, respectively. Obtain the cost  $J_2$  as in (A.6) and the gradient  $\frac{\partial \bar{J}_2}{\partial G_d}$  as in (3.4.10).

Step-4. Next a conjugate gradient search procedure is used to upgrade the display control law  $\bar{u}_d$ . This consists of making incremental changes in the gain matrix  $G_d$  in the negative gradient direction till a value of  $G_d$  is reached for which the cost  $J_2$  shows an increase as compared to its value over the previous step. Note that at each incremental step the controller  $\bar{u}_1$  is updated to be the LQG controller for the current display law  $\bar{u}_d$ .

Step-5. Calculate  $\frac{\partial \bar{J}_2}{\partial G_d}$  for the display control gains  $G_d$  obtained at the end of Step 4 and check whether the necessary condition (3.4.10) for  $J_2$  to be minimum is satisfied. If yes, then go to Step 6 other-

wise go back to Step 3.

Step-6. Check for the convergence of the entire iterative process. This is done by evaluating the difference between the display control gains  $G_d$  obtained at the end of Step 5 and those at the start of Step 3. If this difference is less than some bound  $\epsilon$ , then proceed to Step 7, otherwise go back to Step 3 and repeat the gradient search procedure.

Step-7. The Controller  $\bar{u}_1$  and the display control law  $\bar{u}_d$  at the end of Step 6 are the optimal solution for the problem formulated as above. But we further require that the Controller 1 be an approximate representation of the human behaviour as modeled by the optimal control-theoretic model. Therefore the control gains and closed loop statistics obtained at the end of Step 6 are compared with the results of the evaluation of the corresponding display augmented system using the OCM model. If a reasonable agreement is obtained between the two results, then the display control law obtained is pilot-optimal and the iteration process is stopped. Otherwise the noise intensities  $\bar{v}_y$  and  $\bar{w}$  are updated and the iteration process started anew from Step 1.



## CHAPTER 4

### APPLICATION OF DISPLAY DESIGN METHODOLOGY TO $K/s^2$ PLANT

Using the algorithm discussed in Chapter 3, various display augmentation control laws,  $\bar{u}_d$ , will be synthesized for the  $K/s^2$  plant. The control laws are evaluated, using the full-order OCM model, in terms of the mean square values of the variables of interest, and the power spectrum of the human operator's control input. Detailed frequency domain analysis is also carried out for the various displays.

#### 4.1 Problem Formulation and Synthesis Results

The dynamics of the  $K/s^2$  plant augmented with the display may be expressed in the form

$$\begin{bmatrix} \dot{\bar{x}} \\ \dot{x}_d \end{bmatrix} = \begin{bmatrix} A_o & 0 \\ 0 & a_d \end{bmatrix} \begin{bmatrix} \bar{x} \\ x_d \end{bmatrix} + \begin{bmatrix} B_o \\ 0 \end{bmatrix} \delta + \begin{bmatrix} 0 \\ B_d \end{bmatrix} u_d + \begin{bmatrix} D_o \\ 0 \end{bmatrix} w \quad (4.1.1)$$

with  $A_o$ ,  $B_o$ ,  $D_o$  and the intensity  $W$  of the white noise process  $w$  as defined in Section (2.1), and  $B_d = 1$ . Here the display dynamics are as in (2.2.1), and  $u_d$  is the display control law to be determined.

As discussed in Chapter 3, Controller  $\bar{u}_1$  in the cooperative problem formulation is analogous to the control rate  $\bar{u}_p$  of the OCM. So defining  $u_1 \triangleq \dot{\delta}$ , the dynamics of Eqn. (4.1.1) can be written as

$$\begin{bmatrix} \dot{\bar{x}} \\ \dot{x}_d \\ \dot{\delta} \end{bmatrix} = \begin{bmatrix} A_o & 0 & B_o \\ 0 & a_d & 0 \\ 0 & 0 & 0 \end{bmatrix} \begin{bmatrix} \bar{x} \\ x_d \\ \delta \end{bmatrix} + \begin{bmatrix} 0 \\ 0 \\ 1 \end{bmatrix} u_1 + \begin{bmatrix} 0 \\ 1 \\ 0 \end{bmatrix} u_d + \begin{bmatrix} D_o & 0 \\ 0 & 0 \\ 0 & \frac{1}{\tau_n} \end{bmatrix} \begin{bmatrix} w \\ v_m \end{bmatrix} \quad (4.1.2)$$

where the control noise term,  $v_m$ , is the human's "motor noise". The

outputs available for feedback to Controller 1 ( $u_1$ ) are the same as the human's observations. Therefore for the display augmented case

$$\bar{y}_1 = [x_d, \dot{x}_d]^T + \bar{v}_y \quad (4.1.3)$$

where  $\bar{v}_y$  is the human's observation noise. To be consistent with the analysis of Chapter 2, the responses driving the display are chosen to be

$$\bar{y}_d = [x_2, x_3]^T \quad (4.1.4)$$

where  $x_2(t)$  and  $x_3(t)$  are the position error and the plant velocity, respectively, and are as defined in Section (2.1). Then the display controller, to be designed, has the form

$$\begin{aligned} \dot{x}_d &= a_d x_d + u_d \\ u_d &= G_d \bar{y}_d \end{aligned} \quad (4.1.5)$$

with  $G_d = [g_{d2}, g_{d3}]$ . The human operator's objective for the display-augmented system is to regulate the displayed variable  $x_d$ . Thus the controller  $u_1$  minimizes the cost function  $J_1$ , where

$$J_1 = E\left\{\lim_{T \rightarrow \infty} \frac{1}{T} \int_0^T (x_d^2 + r_1 u_1^2) dt\right\} \quad (4.1.6)$$

Here the choice of  $r_1$  depends on the desired neuro-muscular-lag time constant  $\tau_n$  of the human as modeled. For the purposes of the display design for the  $K/s^2$  plant,  $r_1$  was continually adjusted to yield  $\tau_n \approx 0.1$  secs.

The objective in the display design is to help the human operator regulate the tracking error  $e$  ( $= x_2$ ), in the presence of the velocity disturbance, and with minimal workload. This objective can be formulated as that of finding the optimal display control law  $u_d$  of the form

(4.1.5) which minimizes the cost function  $J_2$ , where

$$J_2 = E\left\{\lim_{T \rightarrow \infty} \frac{1}{T} \int_0^T (q_e e^2 + r_2 u_1^2 + f_{2d} u_d^2) dt\right\} \quad (4.1.7)$$

Equations (4.1.2) to (4.1.7) then define the problem formulation for the display design for the  $K/s^2$  plant, within the framework of the cooperative methodology. Using the algorithm discussed earlier, the optimal display control gains,  $G_d$ , are determined for various values of relative weighting on the error in cost function  $J_2$ . Here relative error weighting is defined as the ratio  $\frac{q_e}{r_2}$  which is varied by changing  $q_e$  and/or  $r_2$ . The results are presented in Table 4.1. Note that in (4.1.7),  $f_{2d}$  needs to be positive definite in order to get a finite optimal solution to the problem. However, since the display control does not reflect any measure of energy, the weighting  $f_{2d}$  may be chosen to achieve some selected overall display gain, or sensitivity. For the results presented in this section, simply a constant value of  $f_{2d} = .001$  is used, and note that the display sensitivity  $\left| \frac{x_d}{e} \right|_{ss}$  is not constant.

Since the algorithm that synthesizes the optimal gains is iterative, a starting display gain matrix has to be specified. For the results presented in Table 4.1,  $G_d = [20, 0]$  is used for the starting display control law. (Note from Section (2.1), the starting gains are such that the displayed variable  $x_d$  is just lagged error). Also, for comparison with the results of Section (2.2),  $a_d = -20 \text{ sec}^{-1}$  was chosen (this corresponds to  $\tau_d = 0.05 \text{ secs}$ ). The weighting  $r_1$  in  $J_1$ , and the variances for the noise processes  $\bar{v}_y$  and  $v_m$  are constantly updated in the iteration process in order to make the controller  $u_1$  closely approximate the OCM model with the parameters selected as in Section (2.1).

TABLE 4.1: OPTIMAL DISPLAY DESIGNS FOR  $K/s^2$  PLANT

$$\tau_d = .05 \text{ secs} , \quad G_d = [g_{d2}, g_{d3}]$$

Case	$q_e$	$r_2$	Optimal $G_d$
1.	1	$2 \times 10^{-4}$	[36.6, 11.9]
2.	2	$2 \times 10^{-4}$	[49.2, 13.0]
3.	2	$1 \times 10^{-4}$	[64.4, 16.3]
4.	4	$1 \times 10^{-4}$	[88.1, 17.3]
5.	4	$5 \times 10^{-5}$	[118.2, 22.6]

From the results presented in Table 4.1 it is noted that as the relative weighting on the error is increased, the display sensitivity ( $\tau_d g_{d2}$ ) becomes larger. This is because a low value for  $f_{2d}$  was chosen as discussed earlier. But, as the analysis in the following section will show, it is the relative position and velocity gain magnitudes in the display which are of most interest, rather than the absolute values of the display gains.

#### 4.2 Evaluation of the Display Quickening Control Laws

The display gains obtained in Section (4.1) are now to be evaluated using the full-order human operator model, with the same parameters in the model as given in Section (2.1). For the purposes of comparison, the initial display case ( $G_d = [20, 0]$ ) and the limiting case of no display lag are also evaluated.

The display designs of Section (4.1) are referred to as Designs 1 to 5, as defined in Table 4.1. The limiting case of no display lag is referred to as "A", the initial display case as "B" and the case of best performance obtained through trial and error in Section (2.2) as "C".

##### 4.2.1 Mean-Square Analysis

The OCM analysis results, in terms of the mean-square values of the tracking error, the human's control rate, and control input for the various cases of display augmentation mentioned above, are listed in Table 4.2. These results are also plotted in Figures (4.1) and (4.2). Fig. (4.1) is a plot of mean-square error vs. mean-square control rate, and Fig. (4.2) is a plot of mean-square error vs. mean-square control input. The scales are chosen to be compatible with Figs. (2.2) and (2.3).

TABLE 4.2: OCM ANALYSIS RESULTS FOR VARIOUS CASES

Case	M.S. Error (e) (in. <sup>2</sup> )	M.S. Input ( $\delta$ ) (in. <sup>2</sup> )	M.S. Control Rate ( $\dot{\delta}$ ) (in. <sup>2</sup> /sec <sup>2</sup> )
1.	0.014	0.389	18.64
2.	0.0132	0.492	23.72
3.	0.0131	0.514	24.78
4.	0.01272	0.650	31.58
5.	0.01269	0.665	32.40
A.	0.0131	1.141	54.73
B.	0.0157	1.353	67.44
C.	0.0127	0.789	38.49

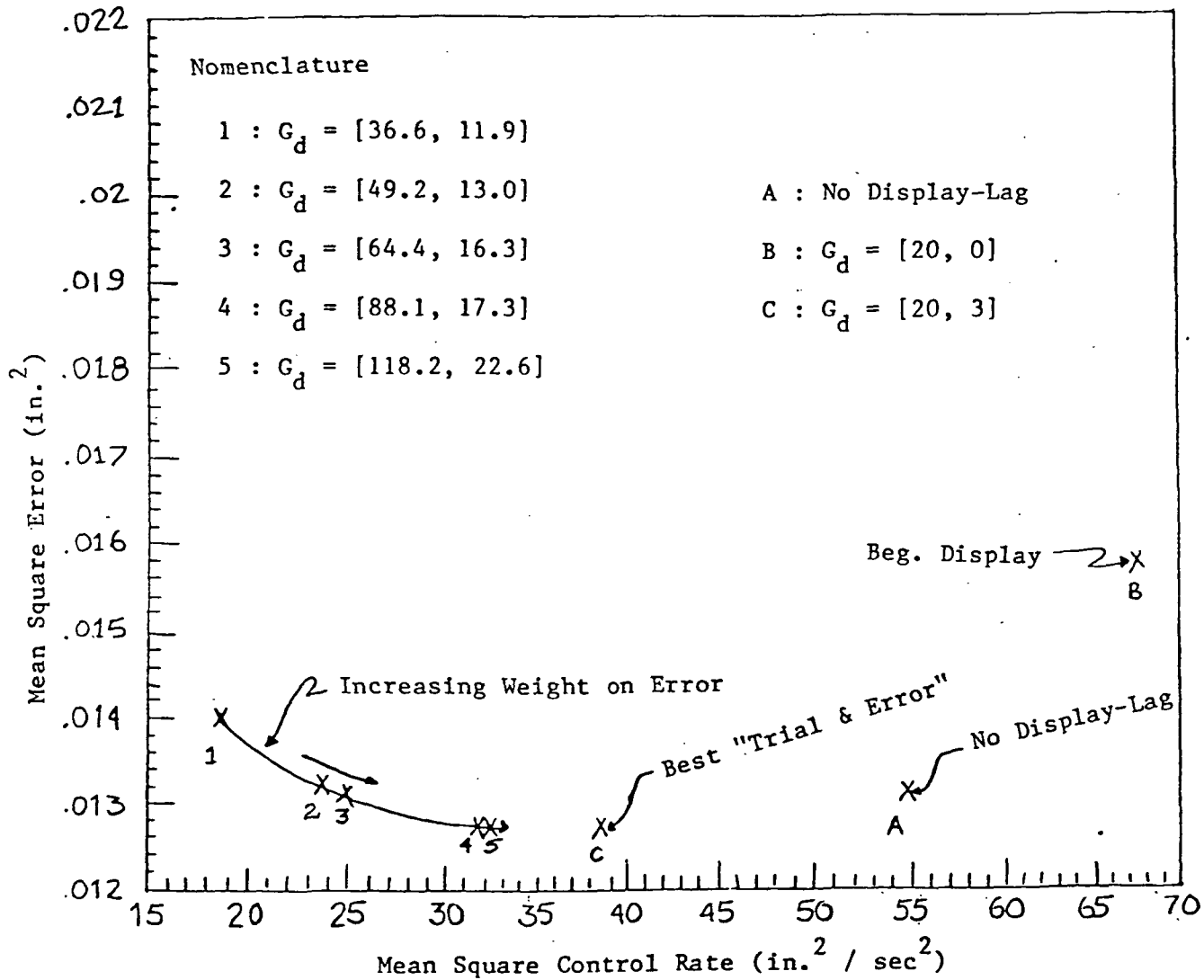


Figure 4.1 Error vs. Manual Control Rate for Various Displays

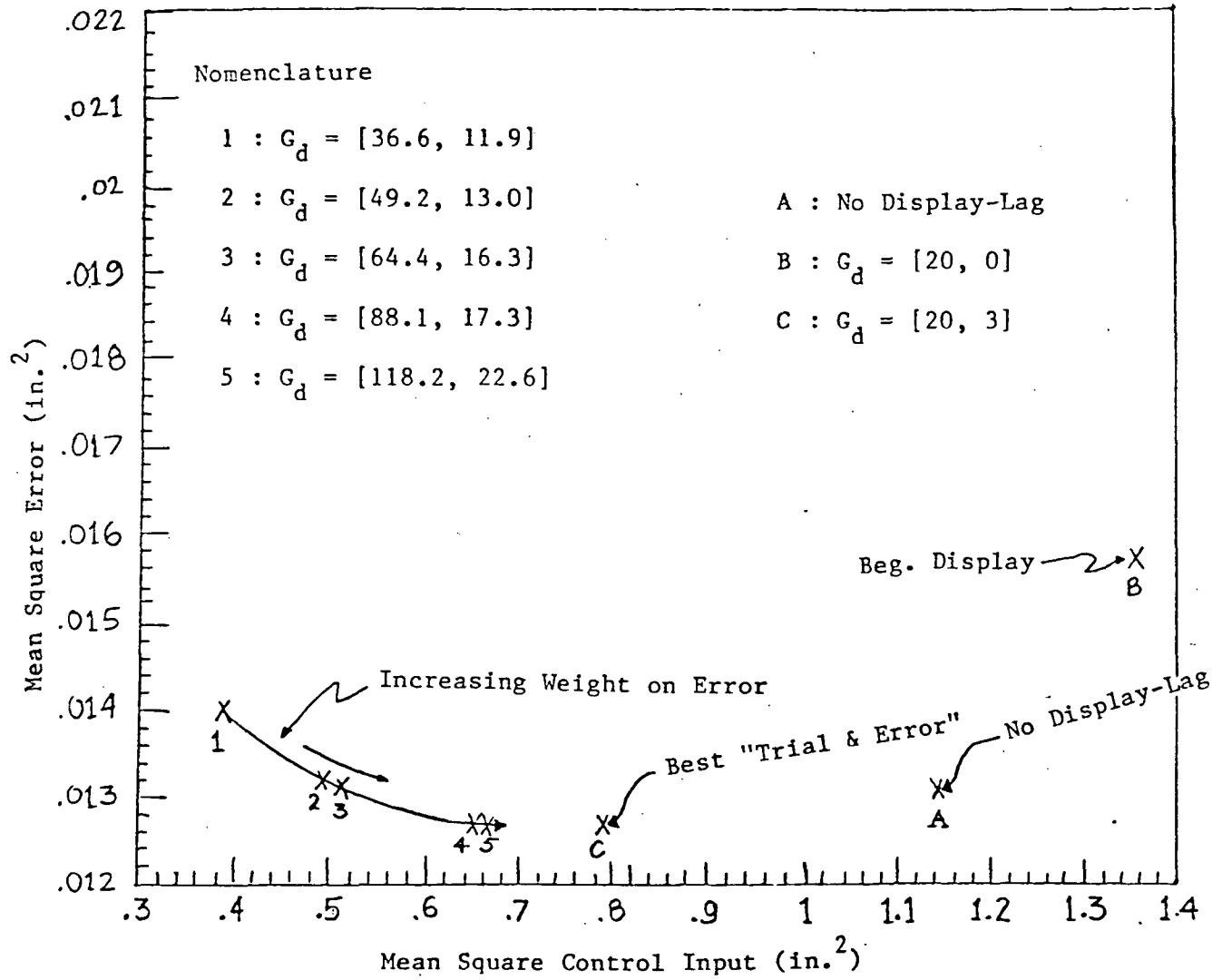


Figure 4.2 Error vs. Manual Control Activity for Various Displays



From these results it is clear that as the relative weighting on the error in the cost function  $J_2$  is increased, the optimal cooperative display design methodology leads to display gains which give improved performance at the expense of increased control activity. It is noted that for all the 5 cases obtained using the cooperative methodology, the final optimal display gains are such that the performance is significantly improved as compared to the starting display (B), and at the same time the "workload" ( $\delta$ ) and the control effort ( $\delta$ ) are considerably reduced. If the weighting on the error is high (Cases 4 and 5), performance comparable to the limiting case (A) and the best performance case (C) is obtained, along with reduced workload and control effort. Moreover it appears that for the selected display bandwidth ( $a_d = -20 \text{ sec}^{-1}$ ), tracking performance (rms error) better than that of Case 5 cannot be obtained. Increasing the weight on error in the cost function  $J_2$  any further would only have the effect of leading to a display design requiring higher control effort without any noticeable improvement in performance.

#### 4.2.2 Power Spectrum Analysis

Using the OCM modeling technique, the power spectra of the human's control inputs and the system responses can also be estimated. Note that the mean-square value  $\sigma_x^2$  of a zero mean process  $x$  is related to the area under its power spectral density  $\Sigma_x(\omega)$ , or

$$\sigma_x^2 = \frac{1}{\pi} \int_0^{\infty} \Sigma_x(\omega) d\omega \quad (4.2.1)$$

Figure (4.3) provides a comparison of the power spectra of the human operator's control input ( $\delta$ ) for the displays 1, 3, and 5, and the lim-

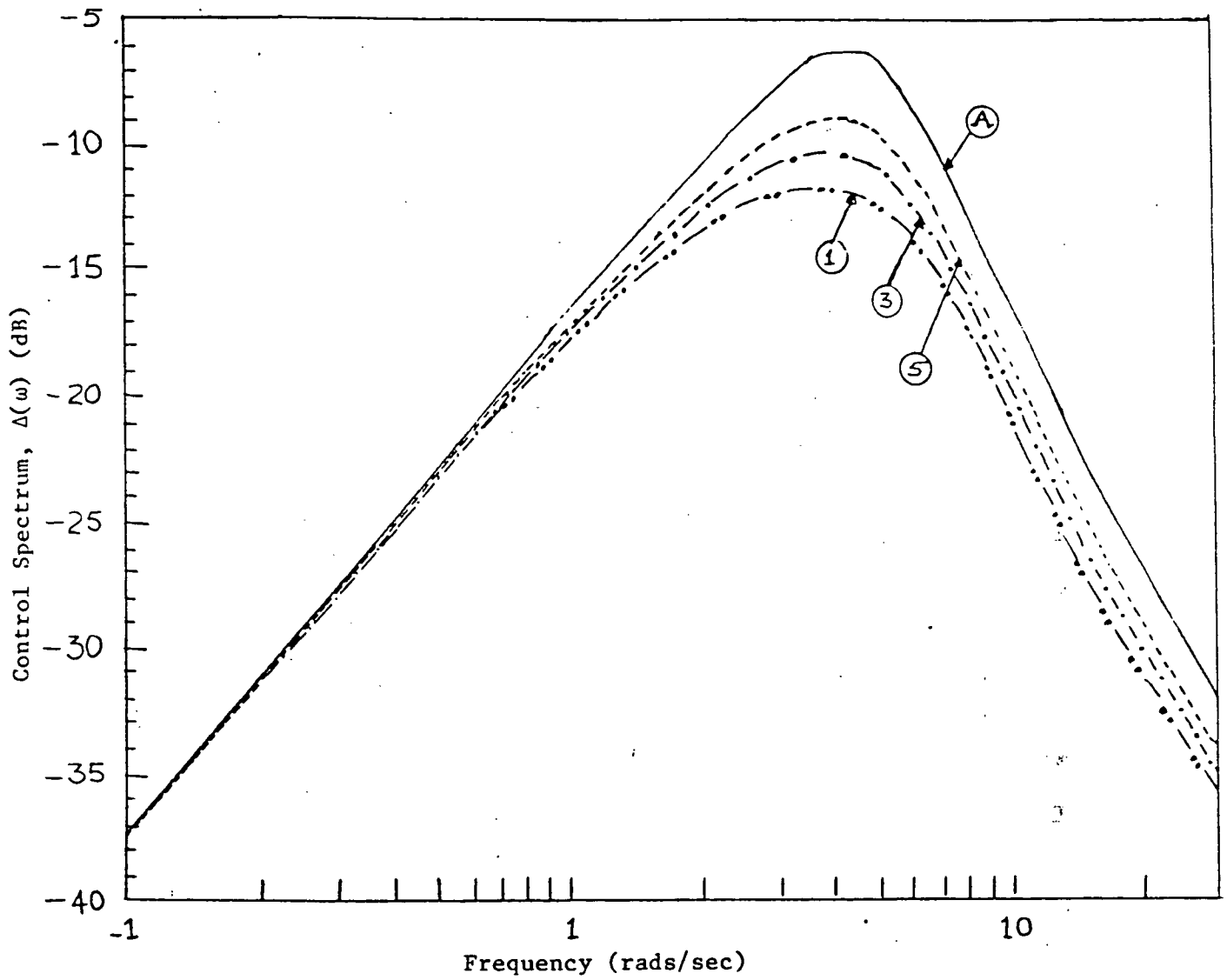


Figure 4.3 Comparison of Human Operator's Control Spectrum,  $\Delta(\omega)$

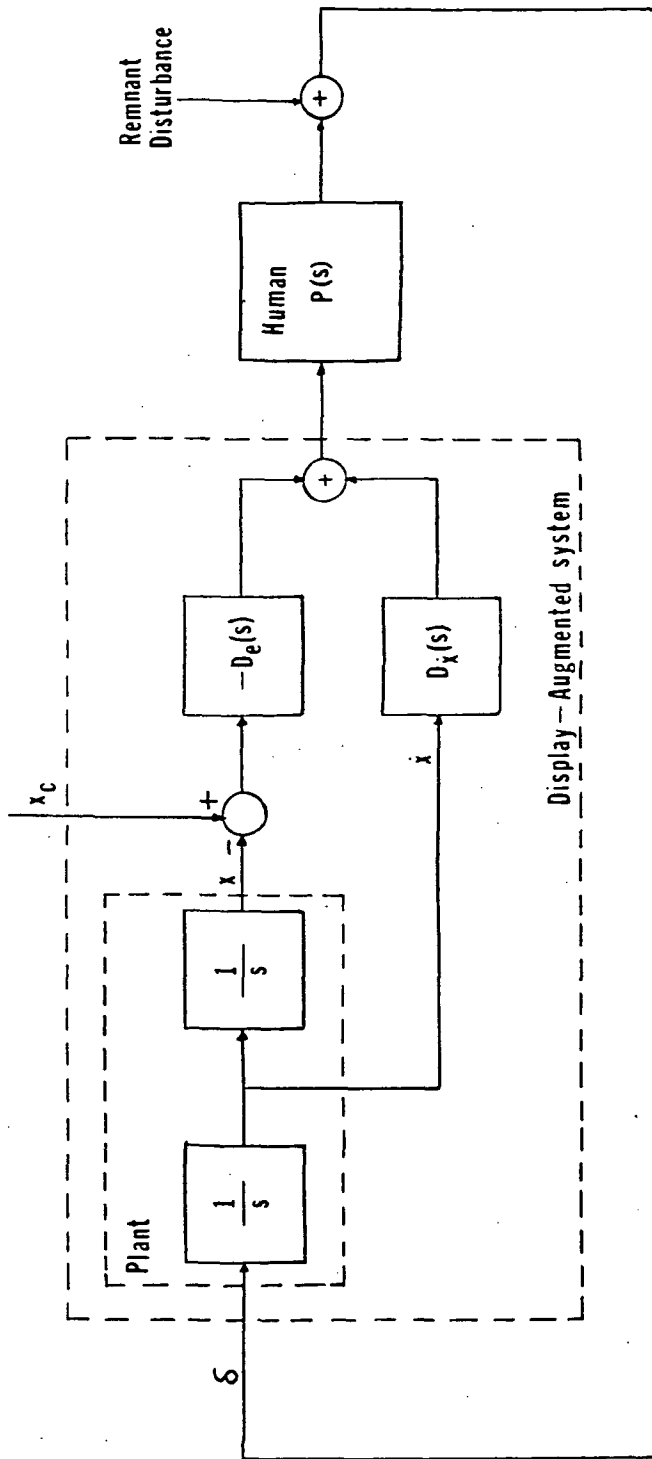
iting case A. The plots in Figure (4.3) show that the control power required is lower for all the optimally synthesized displays when compared to the idealized Case A with no display lag. Moreover, the peak value increases as the weighting on the error in the cost  $J_2$  is increased, corresponding to the human's task becomes increasingly more difficult from display design 1 to design 5. The power spectral densities of the human's control input  $\delta$  for all the displays are shown in the Figures (C.1) to (C.6) in Appendix C. These figures include: 1) the total control input power (in dB), 2) the portion of the control correlated with the command driving the system, and 3) the human operator's remnant, or the uncorrelated portion of the control input.

Since the mean-square value of the errors for the display cases 1 to 5 and the limiting Case A were not significantly different, (see Table 4.2), the power spectral densities of the errors for these cases would be expected to be similar. This was indeed found to be the case and so the error power spectral density plots are not included in the report.

#### 4.2.3 Frequency Domain Analysis

The human operator model can also be represented in the frequency domain in terms of the transfer matrix between the human's observations and his control inputs [6,13]. Since the Bode characteristics of the plant and the display are known, frequency-domain analysis of the manually-controlled display-augmented systems can be carried out, once the human describing functions are estimated from the model.

With the human operator so represented, the block diagram for the task is shown in Fig. (4.4). The display-augmented system is defined as



$$D_e(s) \triangleq \frac{g_{d2}}{s - a_d} \quad ; \quad D_x(s) \triangleq \frac{g_{d3}}{s - a_d}$$

Figure 4.4 Block Diagram for Display Augmented Plant

$$G(s) \triangleq \frac{x_d(s)}{\delta(s)}$$

and the human describing function is

$$P(s) \triangleq \frac{\delta(s)}{x_d(s)}$$

For the displays 1, 3, 5, and A,  $G(s)$  and  $P(s)$  are compared in Figures (4.5) and (4.6), respectively. (The Bode-plots of  $G(s)$  and  $P(s)$  for the cases 1 to 5 and the Case A are shown in Appendix C.) From these frequency responses in Fig.(4.5) and Fig.(4.6), the open-loop Bode-plots may also be determined (not shown). It appears that open-loop magnitude crossover ( $\omega$  such that  $|P(j\omega) G(j\omega)| = 0$  dB) is approximately constant at between 2-2.5 rads/sec for all these cases, consistent with the command signal bandwidth (break at 2 rads/sec). Also, as the weighting on error increases (Case 1  $\rightarrow$  Case 5), the sensitivity (gain) of the total plant plus display increases. From Fig. (4.5) it is clear that all the synthesized displays provide additional lead between 1 and 10 rads/sec. As the weighting on the error in the cost  $J_2$  is increased (Case 1  $\rightarrow$  Case 5), this phase lead provided by the synthesized display gains decreases.

The human operator's phase compensation in Fig. (4.6) is more easily interpreted by looking at this phase compensation with the time delay ( $\tau$ ) of 0.2 seconds removed. This adjusted phase is then given by:

$$pc(\omega) = \angle P(j\omega) + 57.3 \tau \omega \quad (4.2.2)$$

A comparison of this adjusted phase for the various display cases is provided in Figure (4.7). From these plots it appears that the human would need to generate much higher phase lead for Case A as compared to all the optimal display augmentation cases. For Cases 1-5, the required

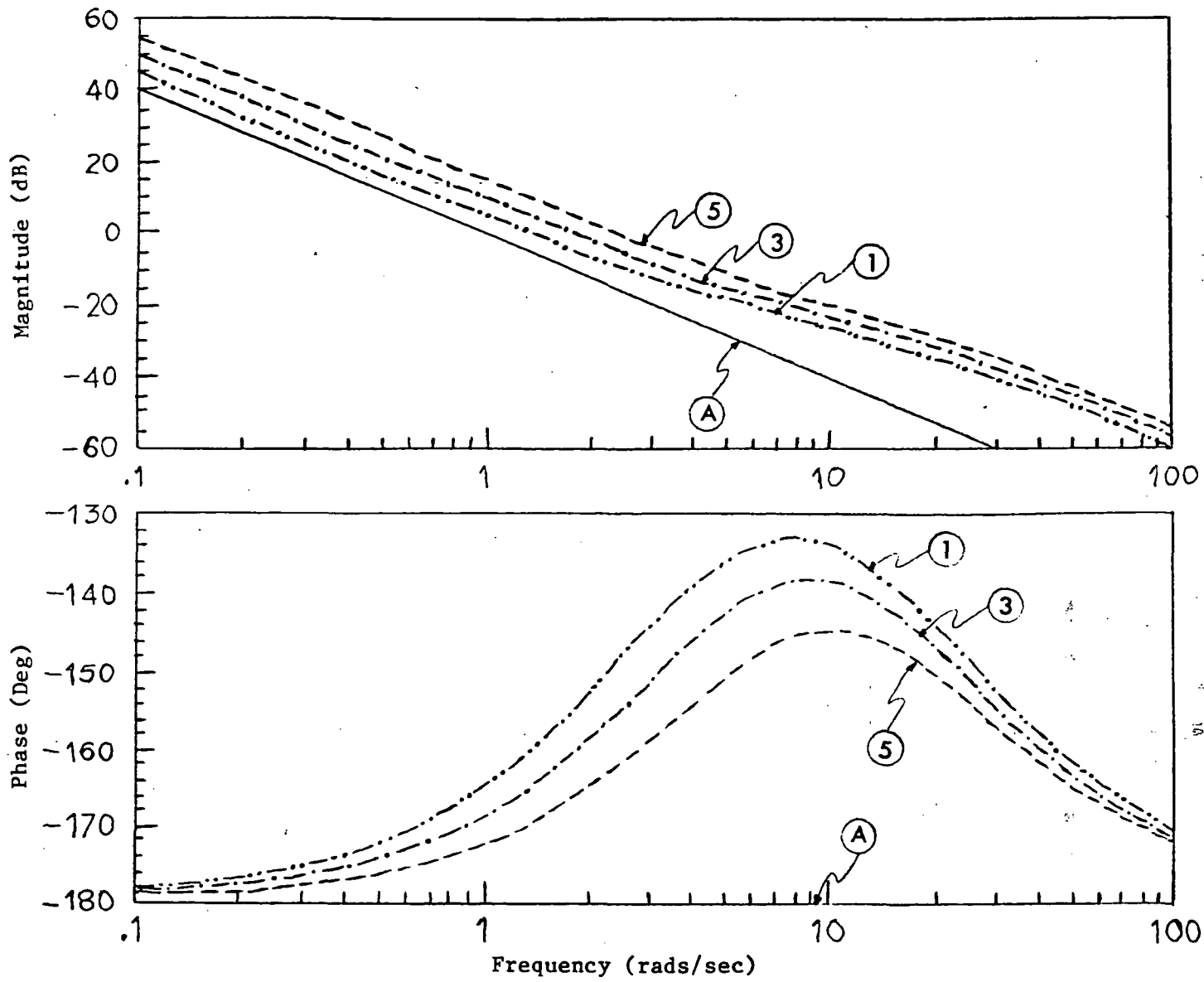


Figure 4.5 Comparison of Display Augmented Plants,  $G(s)$

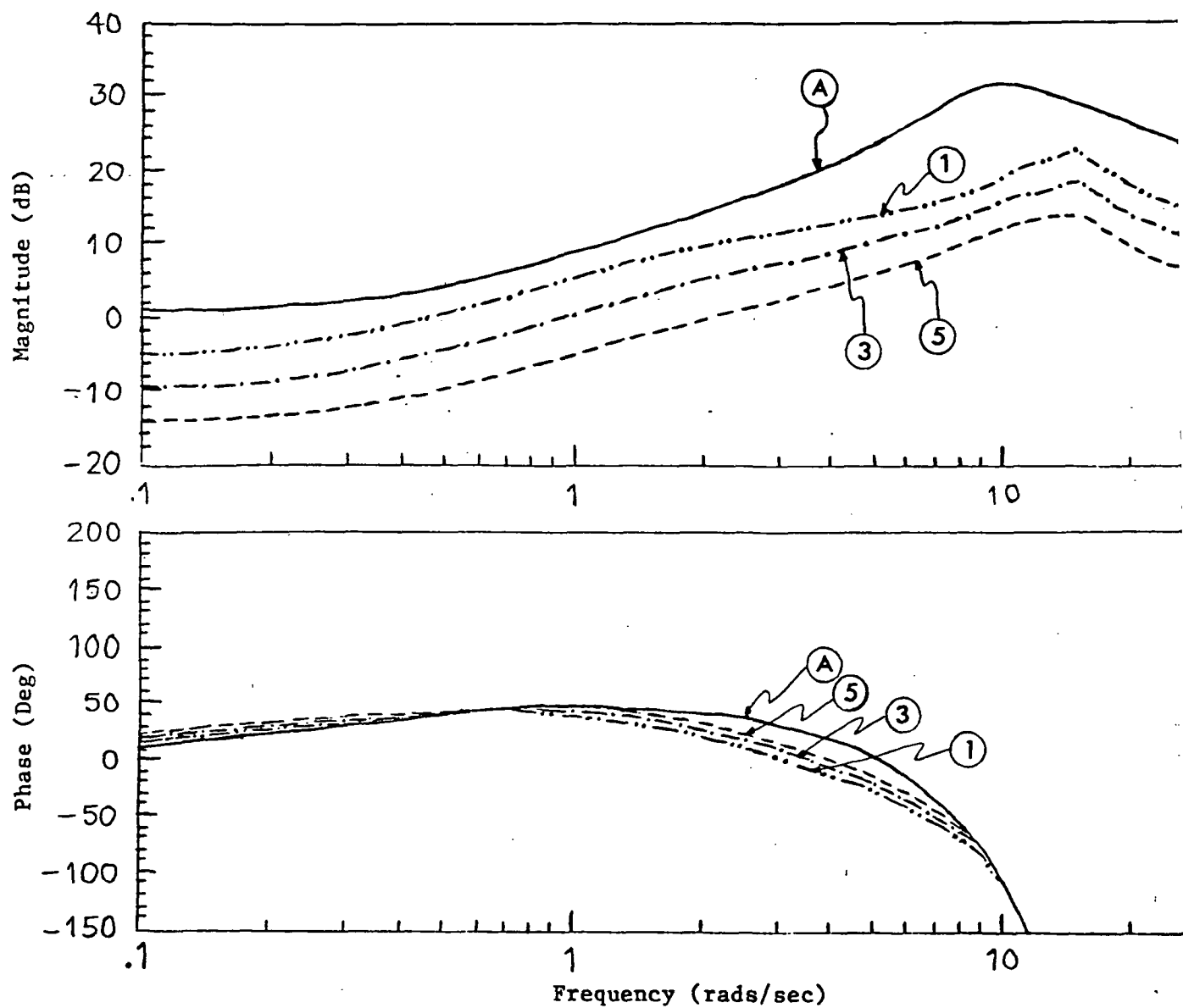


Figure 4.6 Comparison of Human Describing Functions,  $P(s)$

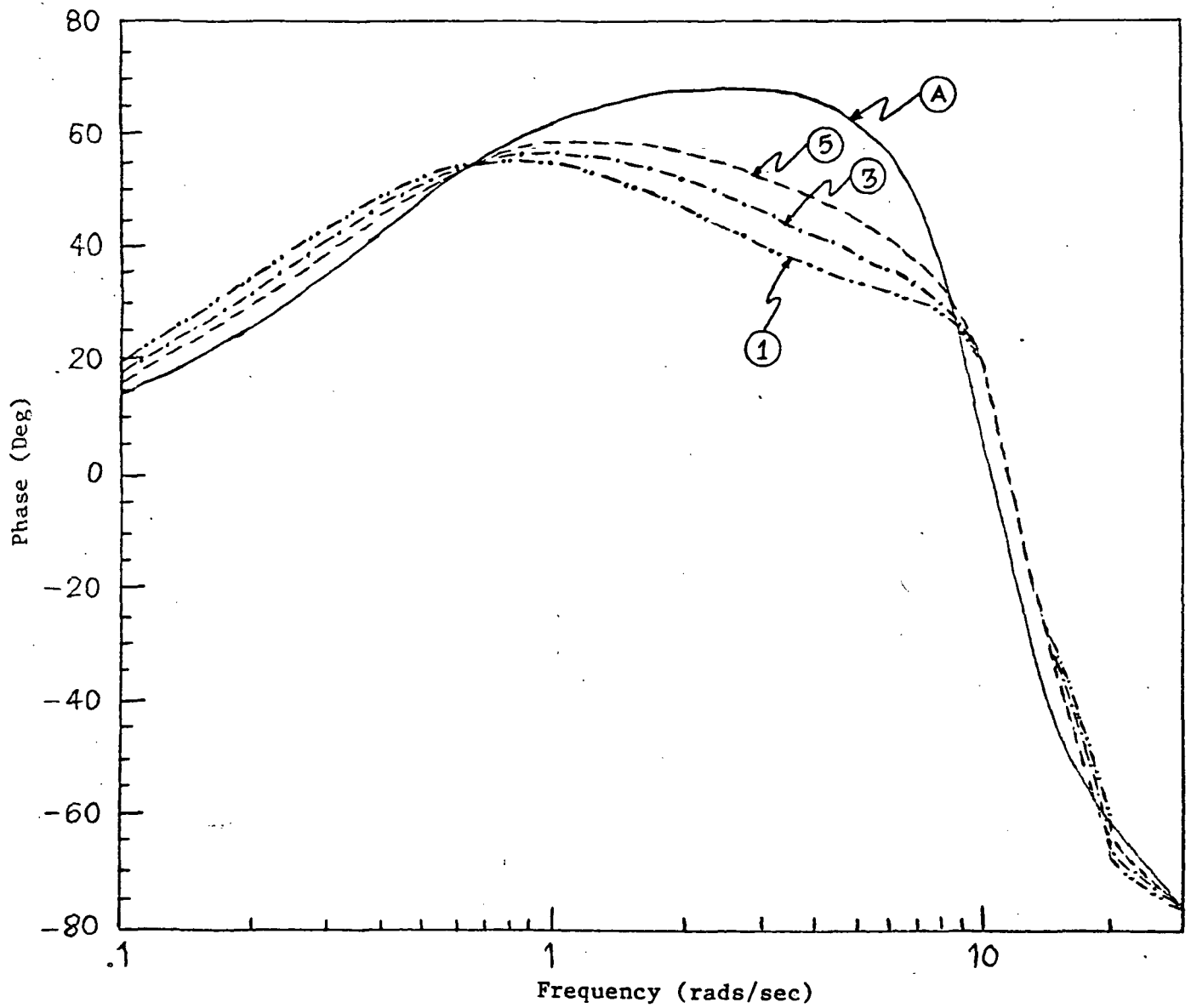


Figure 4.7 Comparison of Human's Phase Compensation  
(adjusted phase)



phase lead increases with the increase of error weighting in the cost function  $J_2$ . Thus, using the phase lead as a measure of workload, the trends in Figure (4.7) indicate that the display augmentation reduces the human's workload. Moreover, the plots predict increasing workload as the error weighting ( $q_e$ ) is increased in the synthesis of the display.

With  $G(s)$  and  $P(s)$  known, the closed loop transfer function,  $T(s) = \frac{x(s)}{x_c(s)}$ , is easily obtained, through algebraic manipulations using the block diagram of Fig. (4.4), to be

$$\frac{x(s)}{x_c(s)} = \frac{-\frac{1}{s^2} P(s) D_e(s)}{1 - \frac{1}{s^2} P(s) [D_e(s) + s D_x(s)]} \quad (4.2.3)$$

Here  $D_e(s) \triangleq \frac{g_{d2}}{s - a_d}$  and  $D_x(s) \triangleq \frac{g_{d3}}{s - a_d}$ ,  $x_c(s)$  is the commanded position and  $x(s)$  is the plant position state. Closed-loop frequency response for Cases 1,3 and 5 of display augmentation is compared in Fig. (4.8). The magnitude and phase plots in Fig. (4.8) indicate that as the error weighting ( $q_e$ ) is increased, the synthesized display is such that tracking performance is improved.

Hence, both by comparing these results from the display augmentation synthesis technique with the results of Chapter 2, and through additional closed-loop analysis, one can conclude that this synthesis technique appears to lead to desirable results.

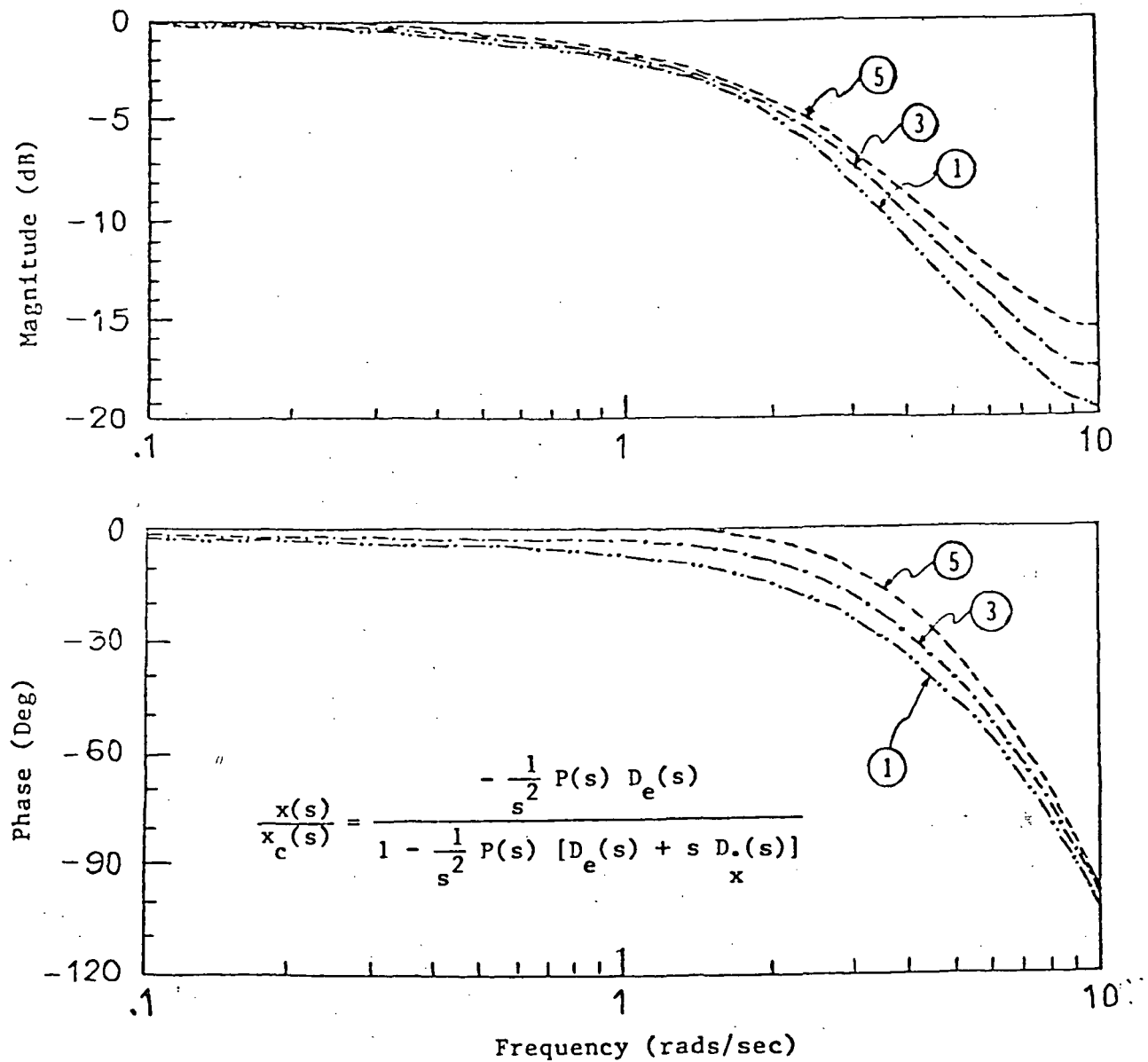


Figure 4.8 Comparison of Closed-Loop Frequency Response for Displays 1,3 and 5

## CHAPTER 5

### APPLICATION OF COOPERATIVE METHODOLOGY TO A MORE COMPLEX DISPLAY DESIGN

In this chapter, an example application of the optimal cooperative methodology to a higher-order system in a multi-input task is presented. The intent is to demonstrate the application of the cooperative methodology to complex systems and the design presented here should not be considered a finalized design. The chosen plant to be controlled represents the unaugmented longitudinal dynamics of an aircraft, and the task is that of tracking a normal-acceleration command while regulating Mach number. The control inputs available to the pilot are the elevator stick and throttle, and the pilot may be assumed to be controlling the aircraft remotely from the ground, for example. The chosen model and the task formulation are discussed in detail.

The task is first described and modeled, using an initial unaugmented status display. Then an optimal display augmentation control law is synthesized using the proposed algorithm. The pilot's performance for the unaugmented and the augmented display systems is then evaluated and compared. Based on these evaluations, improvement in performance and reduction in the pilot workload is predicted for the optimally augmented display.

#### 5.1 System Dynamics

The dynamics are those for an F-15 type aircraft without any flight control augmentation, but including a Mach sensor (with lag), a thrust lag modeling the engine, and a fast first order actuator for the eleva-

tor control. (This model is from Ref.[21], but without the command augmentation system.) The vehicle state vector is

$\bar{x}_v^T = [V, \alpha, q, \theta, \delta_e, M, \delta T]$  - the perturbed forward velocity (ft/sec), angle of attack (.01 rads), pitch rate (.01 rads/sec), pitch attitude (.01 rads), the elevator deflection (.01 rads), sensed Mach number (.001 Mach), and the thrust acceleration (ft/sec<sup>2</sup>).

The pilot control vector is  $\bar{\delta}^T = [\delta_{ec}, \delta T_c]$  - the commanded elevator deflection and the commanded thrust acceleration. The state-space representation of the model is

$$\dot{\bar{x}}_v = A_v \bar{x}_v + B_v \bar{\delta} \quad (5.1.1)$$

where the matrices  $A_v$  and  $B_v$  are as given in Appendix D. The states are the perturbed values about the trim conditions also listed in Appendix D.

The pilot's assumed objective here is to track a normal acceleration command ( $a_{zc}$ ) while regulating Mach number to the best of his ability. Rather than the deterministic normal acceleration command ( $a_{zc}$ ) used for the pushup-pullover maneuver in previous studies [4,5], the command signal to be tracked is generated, for the purpose of display control law synthesis, by using a second order Markov process with a break frequency of 1 rad/sec and a damping ratio of 0.7. With

$\bar{x}_c^T \triangleq [a_{zc}, \dot{a}_{zc}]$ , the command system is represented in the state variable form as

$$\dot{\bar{x}}_c = \begin{bmatrix} 0 & 1 \\ -1 & -1.4 \end{bmatrix} \bar{x}_c + \begin{bmatrix} 0 \\ 1 \end{bmatrix} w_c \quad (5.1.2)$$

The intensity of the white noise process  $w_c$  is chosen to be  $W_c = 181$  so

as to yield the rms command of  $\sigma_{a_{zc}} = 8 \text{ ft/sec}^2$  (or  $0.25 \text{ g's}$ ).

Defining  $\bar{x}_O^T \triangleq [\bar{x}_C^T, \bar{x}_V^T]$ , the vehicle dynamics augmented with the command system are written in the state-space form as

$$\dot{\bar{x}}_O = A_O \bar{x}_O + B_O \bar{\delta} + D_O w_C \quad (5.1.3)$$

with appropriate definitions of  $A_O$ ,  $B_O$  and  $D_O$ . The time response of the variables  $a_z$ ,  $M$  and  $\theta$  is obtained for unit step control inputs. The time histories for step elevator input are shown in Figures (5.1 (a)-(c)) and those for step throttle input in Figures (5.2 (a)-(c)).

## 5.2 Task Modeling

For the initial unaugmented status display, the pilot's observations are assumed to be the normal acceleration command signal, the  $a_z$  tracking error ( $e_{az} = a_{zc} - a_z$ ), the sensed (lagged) Mach number and pitch attitude. It will again be assumed that the pilot can reconstruct the rates of the displayed signals. Then the pilot's observation vector,  $\bar{y}_p^T = [a_{zc}, \dot{a}_{zc}, e_{az}, \dot{e}_{az}, M, \dot{M}, \theta, \dot{\theta}]$ , is of the form

$$\bar{y}_p = C_O \bar{x} + E_O \bar{\delta} \quad (5.2.1)$$

with  $C_O$  and  $E_O$  as given in Appendix D. A conceptual display format for this status display is shown in Fig. (5.3).

For the augmented display system, the pilot's observations are to be  $x_{d1}$ ,  $x_{d2}$ ,  $a_{zc}$  and  $\theta$ , along with the associated rates. (Note that compared to the status display case,  $e_{az}$  and  $M$  are replaced by the "intelligent" display variables  $x_{d1}$  and  $x_{d2}$ , while  $a_{zc}$  and  $\theta$  are maintained in the pilot's observation vector). Therefore the outputs available for feedback by the pilot are

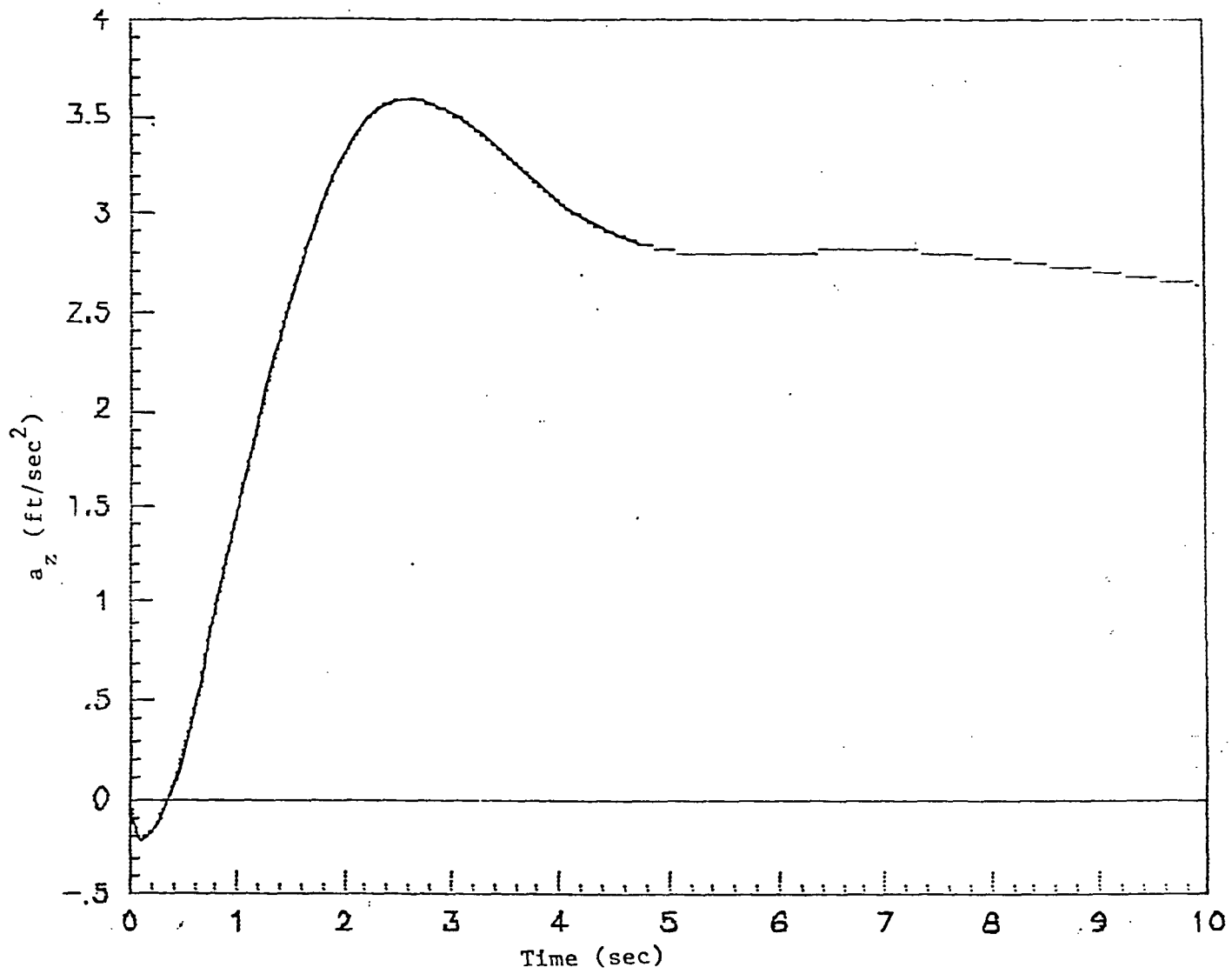


Figure 5.1(a)  $a_z$  Response to Step Elevator Input  
( $\delta e_c = 0.01$  rads, +ve down)

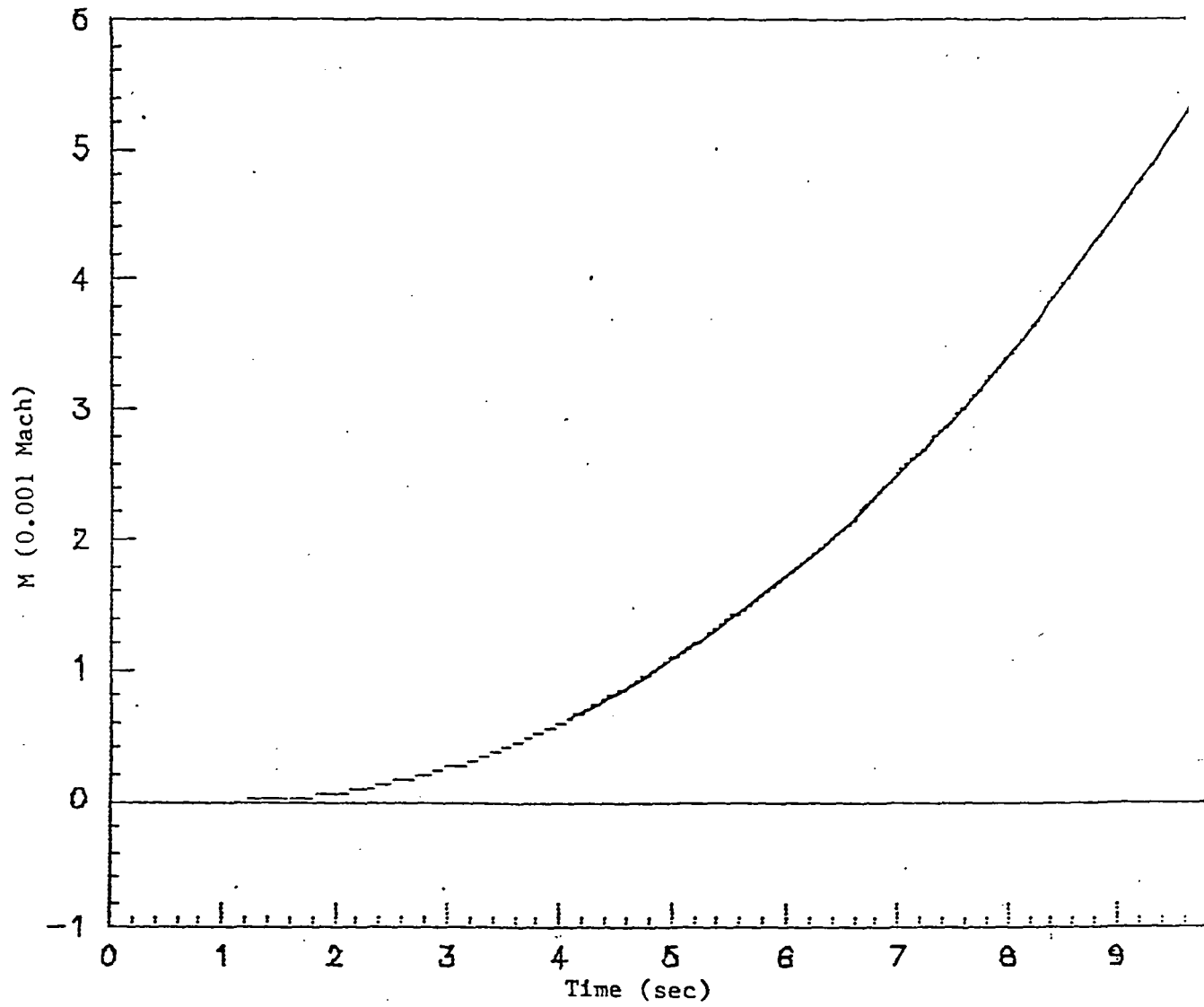


Figure 5.1(b) Mach Response to Step Elevator Input

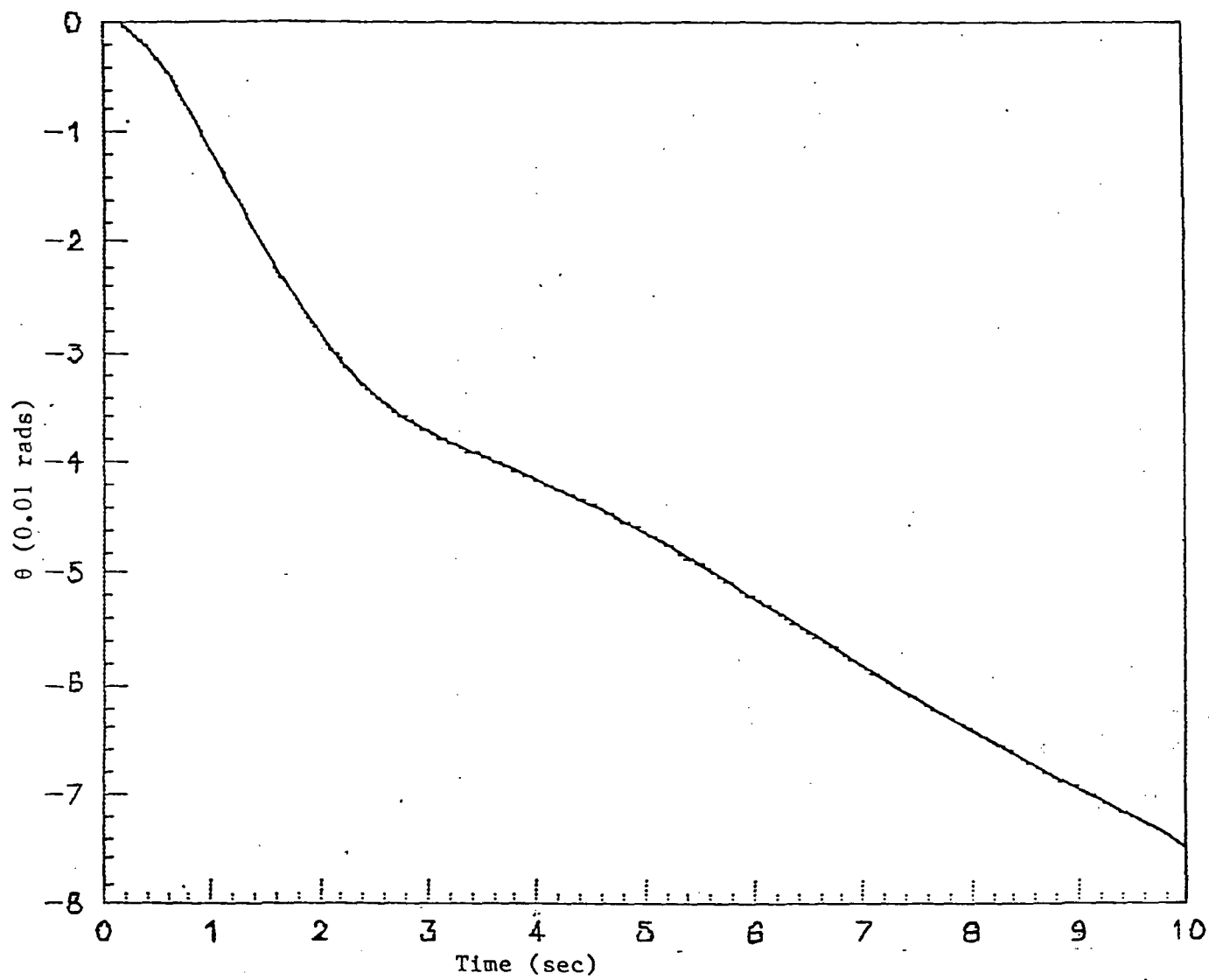


Figure 5.1(c)  $\theta$  Response to Step Elevator Input



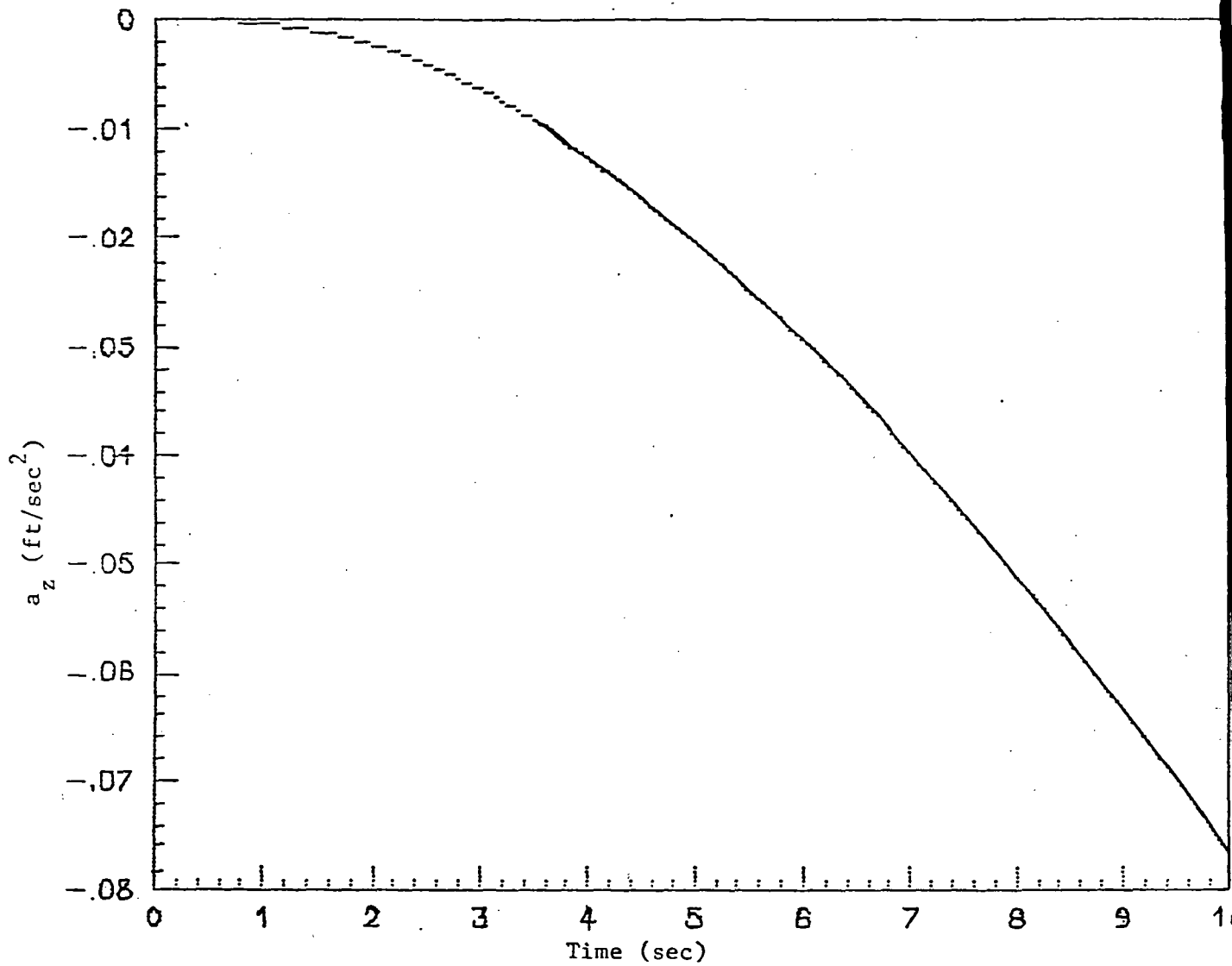


Figure 5.2(a)  $a_z$  Response to Step Throttle Input  
( $\delta T_c = 1 \text{ ft}/(\text{sec}^2)$ , +ve thrust)

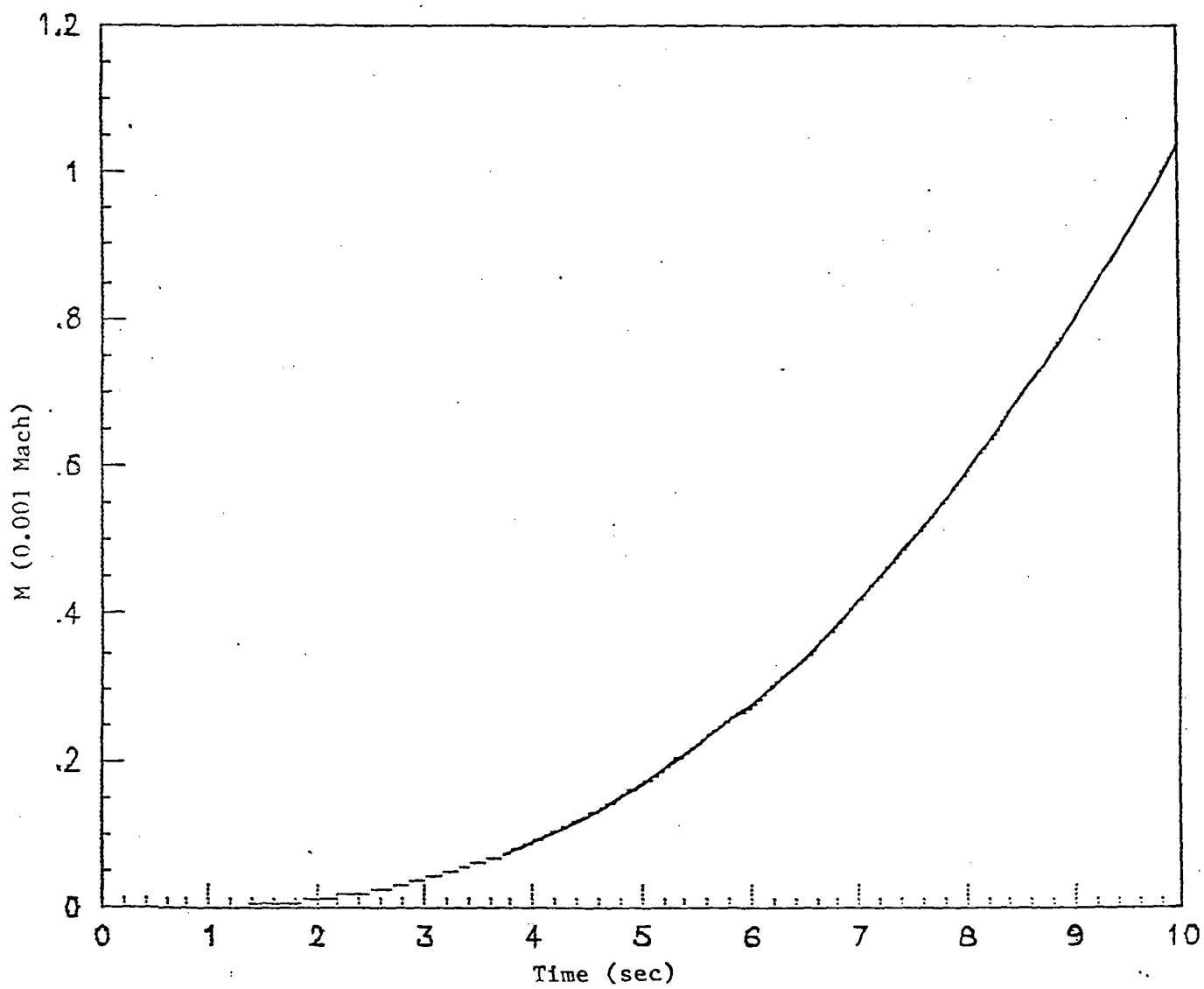


Figure 5.2(b) Mach Response to Step Throttle Input

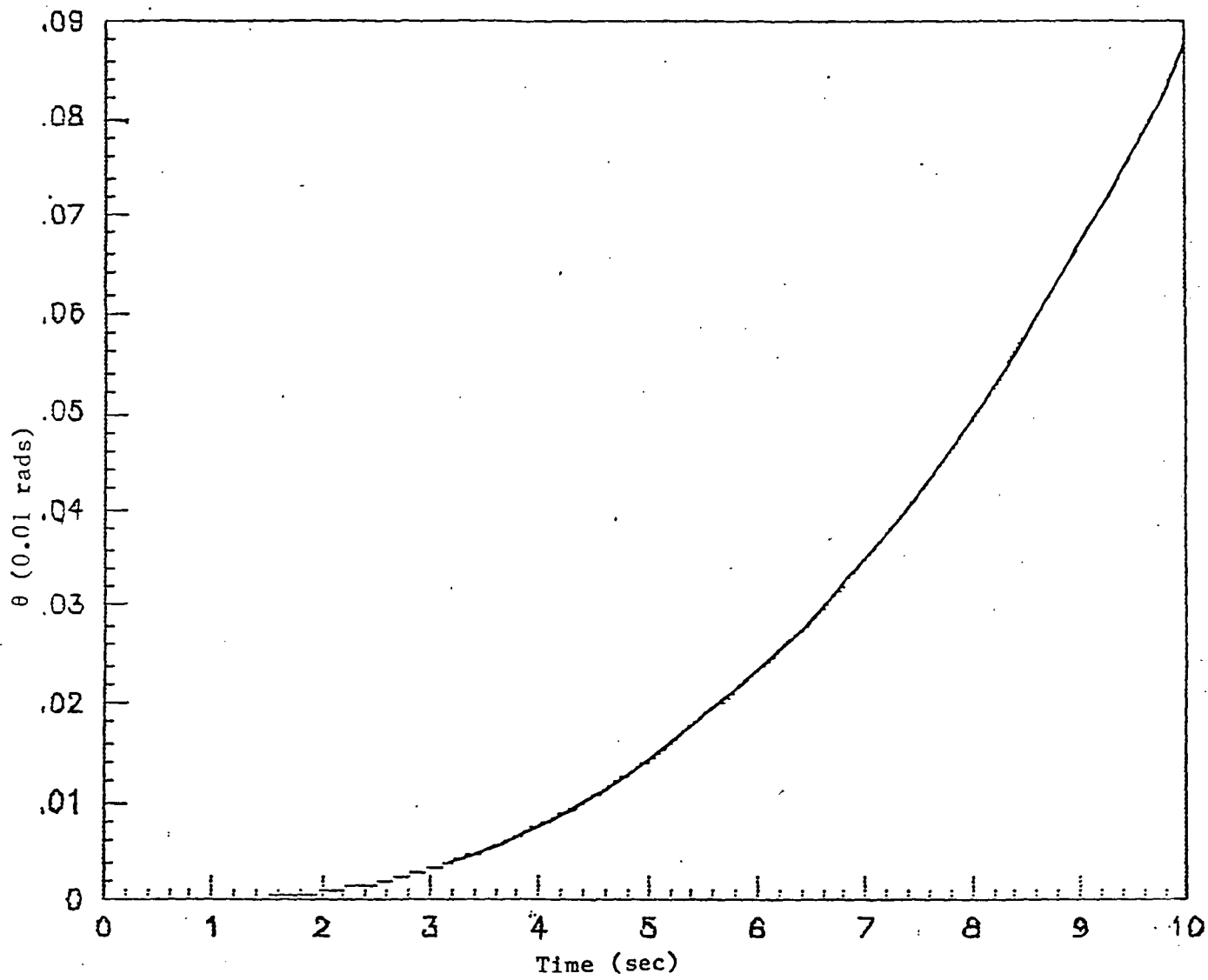
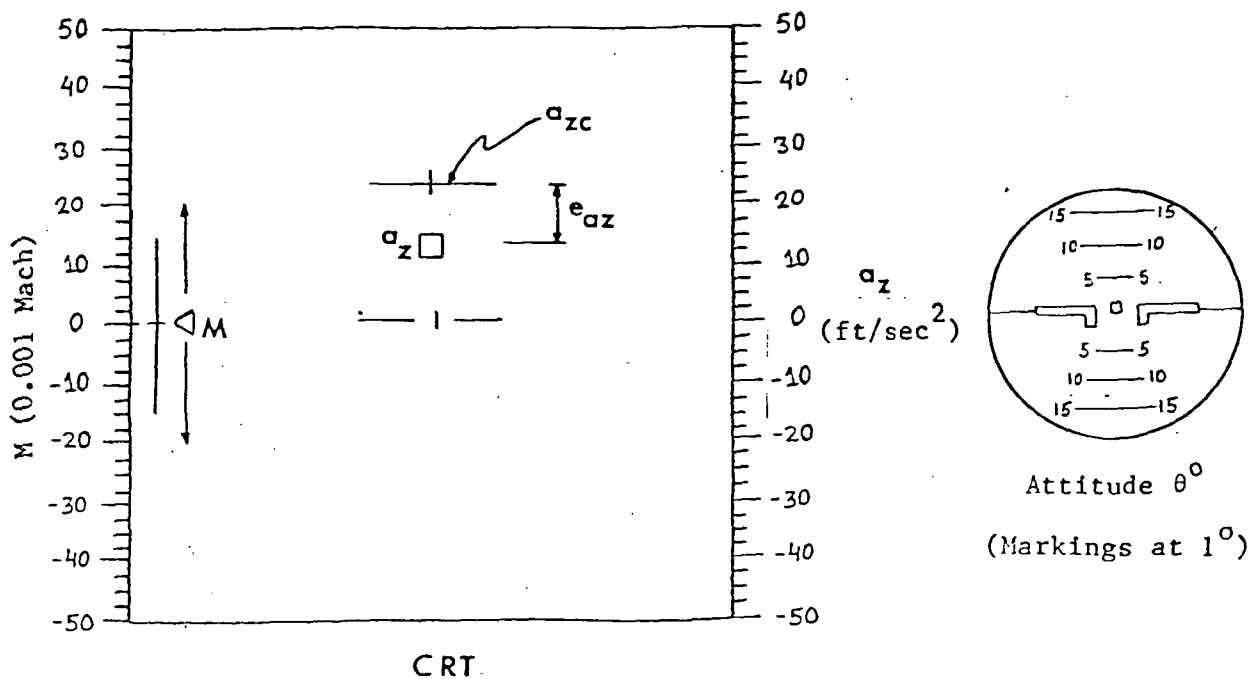


Figure 5.2(c)  $\theta$  Response to Step Throttle Input



(Assumed Markings at  $0.5 \text{ ft/sec}^2$  and  $0.5 \text{ M}$ )

- Pilot's objective:
- (a) Keep  $\square$  over the  $a_{zc}$  bar
  - (b) Keep  $\triangle$  within  $\pm (15) \text{ M}$

Figure 5.3 Conceptual Display Format for Status Display

$$\bar{y}_p = [x_{d1}, \dot{x}_{d1}, x_{d2}, \dot{x}_{d2}, a_{zc}, \dot{a}_{zc}, \theta, \dot{\theta}]^T$$

A conceptual display format for the augmented system is shown in Fig.

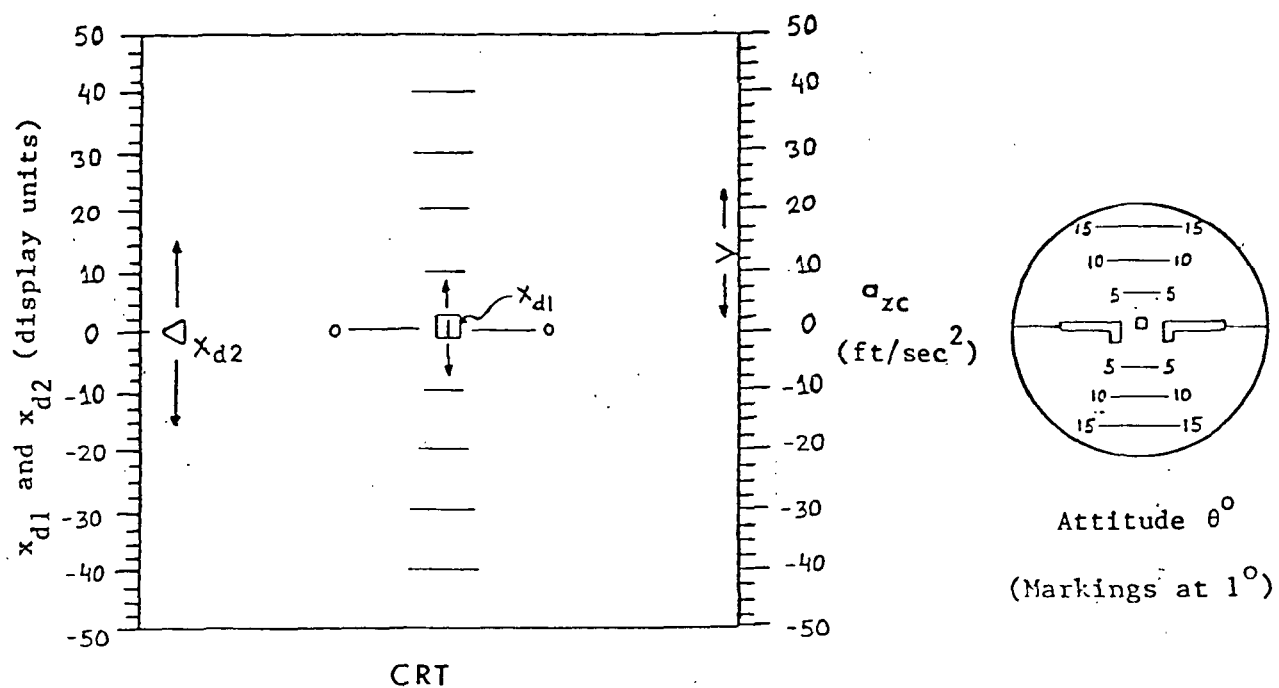
(5.4).

Reasonable pilot modeling parameters for this analysis are as follows:

- (i) Pilot's observation time delay,  $\tau$ , set to 0.2 seconds.
- (ii) Observation noise ratio set at -12 dB for all observations.
- (iii) Motor noise ratio set at -12 dB for both control channels.
- (iv) The weighting on the control rates in the pilot's cost function adjusted to yield a neuromotor lag time constant of 0.2 secs in the elevator channel and 5 secs in the throttle channel.
- (v) The pilot's fractional attention allocation ( $f_i$ ) was set at 0.3 for each of the observations  $a_{zc}$ ,  $e_{az}$  and  $M$ , and 0.1 for  $\theta$ .
- (vi) The pilot's indifference thresholds for the various observations are set to values listed in Table 5.1.

Though parametric performance analysis is not too sensitive to many of these variables, the values of observation and motor noise ratios are chosen to be higher than in Chapter 2 in order to be consistent with the pilot behaviour observed in real-time simulations of complex tasks.

Also the pilot's neuromotor lag time constant for the throttle channel is set at 5.0 secs to reflect the fact that the pilot changes the throttle setting very slowly, since the engine response is slow. Finally, from Fig. (5.3), it is seen that though the pilot observes  $a_{zc}$ ,  $e_{az}$  and



(Assumed Markings at 0.5 display units for  $x_{d1}$  and  $x_{d2}$ )

Pilot's objective: (a) Keep  $\square$  at 0 marking for  $x_{d1}$

(b) Keep  $\triangle$  at 0 marking for  $x_{d2}$

Figure 5.4 Conceptual Display Format for Augmented Display

TABLE 5.1 PILOT PERCEPTION THRESHOLDS

Observation	Threshold	Rate Threshold
$a_{zc}$ (ft/sec <sup>2</sup> )	0.5	1.0
$e_{az}$ (ft/sec <sup>2</sup> )	0.5	1.0
M(.001 Mach)	0.5	1.0
$\theta$ (.01 rads)	0.2	0.4
$x_{d1}$ (display units)	0.5	1.0
$x_{d2}$ (display units)	0.5	1.0

$M$  ( $a_{zc}$ ,  $x_{d1}$  and  $x_{d2}$  for the case of augmented display - Fig. (5.4)) from the same physical display, he still needs to scan their values separately. So we will consider his attention to be divided equally between the three primary observations, with attitude information only secondary to the task. The choice of the values for pilot's thresholds is based on the assumed display size and minimum resolution in the conceptual display format of Figs. (5.3) and (5.4). The thresholds for the rates are twice the thresholds for the corresponding displayed variable, for all the pilot's observations.

For the unaugmented status display, the pilot's objective function is taken to be

$$J_p(\bar{\delta}) = E\left\{\lim_{T \rightarrow \infty} \frac{1}{T} \int_0^T (e_{az}^2 + .0001M^2 + .05(\delta T_c)^2 + g_1(\dot{\delta}_{ec})^2 + g_2(\dot{\delta T_c})^2) dt\right\} \quad (5.2.2)$$

which reflects the pilot's emphasis on tracking the  $a_z$  command, and also is consistent with the units of  $a_z$  and  $M$  in the dynamic model. This objective corresponds to the pilot attempting to keep the square, in the display format of Fig. (5.3), over the  $a_{zc}$  bar, while at the same time maintaining the Mach needle within  $\pm (15)$ . Note in this case the pilot's commanded thrust ( $\delta T_c$ ) is explicitly included in the cost objective. This was found to be necessary to keep the commanded thrust within limits deliverable by the engine. The weightings in (5.2.2) were determined after a few trials of the modeling procedure. Finally, in (5.2.2),  $g_1$  and  $g_2$  are chosen to be consistent with the assumed pilot's neuromotor lag time constants for the two control channels.

### 5.3 Optimal Display Synthesis for F-15 Model



For designing display augmentation for the aircraft discussed above, the basic display dynamics may be taken to be of the form

$$\begin{bmatrix} \dot{x}_{d1} \\ \dot{x}_{d2} \end{bmatrix} = \begin{bmatrix} -20 & 0 \\ 0 & -20 \end{bmatrix} \begin{bmatrix} x_{d1} \\ x_{d2} \end{bmatrix} + \begin{bmatrix} 1 & 0 \\ 0 & 1 \end{bmatrix} \begin{bmatrix} u_{d1} \\ u_{d2} \end{bmatrix}$$

or

$$\dot{\bar{x}}_d = A_d \bar{x}_d + B_d \bar{u}_d \quad (5.3.1)$$

with

$$\begin{aligned} \bar{u}_d &= G_d \bar{y}_d \\ \bar{y}_d &= C_d \bar{x}_o \end{aligned} \quad (5.3.2)$$

where  $\bar{x}_o$  is as defined in (5.1.3). In (5.3.2),  $\bar{y}_d$  is chosen by the designer, and the display gains  $G_d$  are to be synthesized so as to be optimal for the task to be performed. For the display design presented in this section,  $\bar{y}_d$  is chosen to be

$$\bar{y}_d^T = [a_{zc}, \dot{a}_{zc}, v, \alpha, q, \theta, \delta_e, M] \quad (5.3.3)$$

which means that all the vehicle states as well as the command states are available for driving the display. Note that in (5.3.1), the display bandwidth is chosen to be faster than the pilot's dynamics. Also two display states (along with two display control laws) are chosen.

Defining Controller 1 to be the pilot's inputs, or  $\bar{u}_1 \triangleq \bar{\delta}$ , the dynamics of (5.1.3), augmented with the display system and pilot's control inputs can be written as

$$\begin{bmatrix} \dot{\bar{x}}_o \\ \dot{\bar{x}}_d \\ \dot{\bar{\delta}} \end{bmatrix} = \begin{bmatrix} A_o & 0 & B_o \\ 0 & A_d & 0 \\ 0 & 0 & 0 \end{bmatrix} \begin{bmatrix} \bar{x}_o \\ \bar{x}_d \\ \bar{\delta} \end{bmatrix} + \begin{bmatrix} 0 \\ 0 \\ I \end{bmatrix} \bar{u}_1 + \begin{bmatrix} 0 \\ B_d \\ 0 \end{bmatrix} \bar{u}_d + \begin{bmatrix} D_o & 0 \\ 0 & 0 \\ 0 & I \end{bmatrix} \begin{bmatrix} w_c \\ v_m \end{bmatrix} \quad (5.3.4)$$

where the two-dimensional white-noise process  $\bar{v}_m$  is the pilot's motor noise in the two control channels.

With the augmented display (see Fig. (5.4)), the pilot's task is that of regulating the display states  $x_{d1}$  and  $x_{d2}$ . This can be modeled as finding the optimal Controller 1 ( $\bar{u}_1$ ) which minimizes the cost function  $J_1$  given by

$$J_1(\bar{u}_1) = E\left\{\lim_{T \rightarrow \infty} \frac{1}{T} \int_0^T (x_{d1}^2 + x_{d2}^2 + 0.05(\delta T_c)^2 + g_1(\delta_{ec})^2 + g_2(\delta T_c)^2) dt\right\} \quad (5.3.5)$$

The objective function  $J_2$  to be minimized by the display control law  $\bar{u}_d$  is, however, taken to be

$$J_2 = J_p(\bar{\delta}) + E\left\{\lim_{T \rightarrow \infty} \frac{1}{T} \int_0^T .00001(u_{d1}^2 + u_{d2}^2) dt\right\} \quad (5.3.6)$$

Note here that  $J_p(\bar{\delta})$  is as in (5.2.2), or the pilot's objective with the status display. The weights on the display controls ( $u_{d1}$  and  $u_{d2}$ ) are chosen to be very small initially, at least, so that their contribution to  $J_2$  is negligible as compared to  $J_p(\bar{\delta})$ . The choice of  $J_2$  as above is consistent with our objective of finding a display control law which helps the pilot perform his overall task of tracking the  $a_z$  command while regulating the Mach number.

In order to initialize the numerical solution technique, an initial guess for the display control gains is made such that  $x_{d1}$  corresponds to  $-e_{az}$  (i.e.  $a_z - a_{zc}$ ) and  $x_{d2}$  to  $0.01 M$  in the steady state. Recalling Eqns.(5.3.2) and (5.3.3), then, the starting display control gains are

$$G_{d\_start} = \begin{bmatrix} -20 & 0 & -0.082 & -32.21 & 0 & 0 & -5.096 & 0 \\ 0 & 0 & 0 & 0 & 0 & 0 & 0 & 0.2 \end{bmatrix} \quad (5.3.7)$$

For this choice of  $G_d$ ,  $J_1(\bar{u}_1)$  for the initial display law closely

represents  $J_p(\bar{\delta})$  of the original status-display case.

The optimal display control gains determined from the algorithm converged to

$$G_d^* = \begin{bmatrix} -26.08 & -6.329 & -1.475 & -38.05 & -12.06 & -4.019 & 4.923 & 3.219 \\ -18.72 & -16.74 & 0.8258 & -13.44 & -36.74 & -15.40 & 33.06 & -0.202 \end{bmatrix} \quad (5.3.8)$$

In the synthesis process for the optimal display, the weightings  $g_1$  and  $g_2$  in the cost function  $J_1(\bar{u}_1)$  and the variances for the noise processes  $\bar{v}_m$  and  $\bar{v}_y$  are constantly updated so as to make the controller  $\bar{u}_1$  closely approximate the full-order pilot model.

#### 5.4 Comparison of the Displays

The pilot's performance, as predicted by model-based evaluation, is compared for the two cases - the status display and the "optimal" display augmentation synthesized as above. As in the case of  $K/s^2$  plant, the criteria used for comparison are - rms values of the variables of interest, control and error spectra, and frequency domain analysis. Time histories for step control inputs are also provided to gain a better understanding of the significance of the "intelligent" display variables  $x_{d1}$  and  $x_{d2}$ . For brevity, the status display is referred to as Display A and the optimal display as Display B in the following discussion.

##### 5.4.1 Time Histories

For Display B, the time histories for the two display variables  $x_{d1}$  and  $x_{d2}$  for a unit step elevator input are shown in Figs. (5.5 (a)-(b)) and those for a unit throttle input are shown in Figs. (5.6 (a)-(b)). Significant coupling is evident in this case, especially for elevator

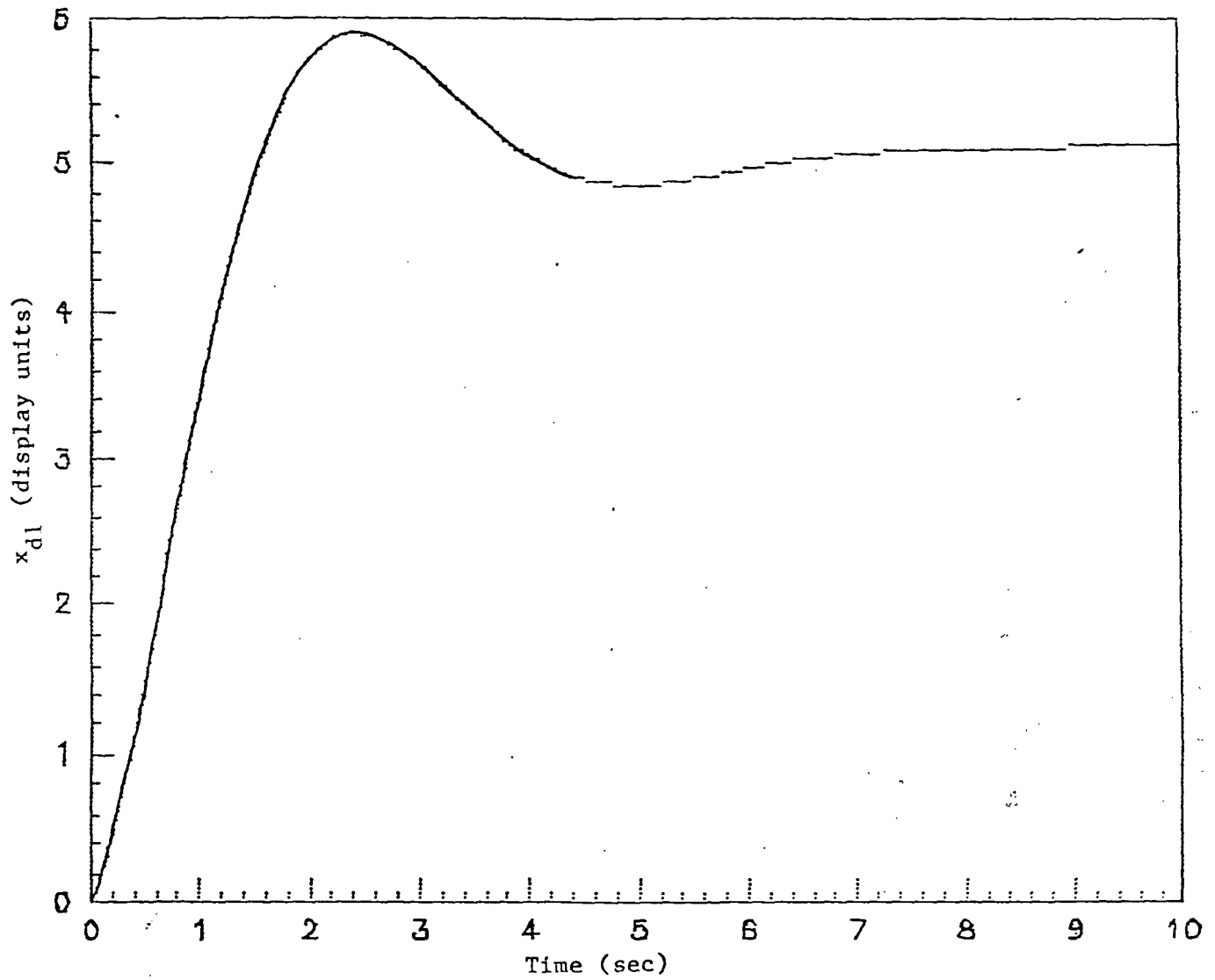


Figure 5.5(a)  $x_{d1}$  Response to Step Elevator Input  
( $\delta e_c = 0.01$  rads, +ve down)

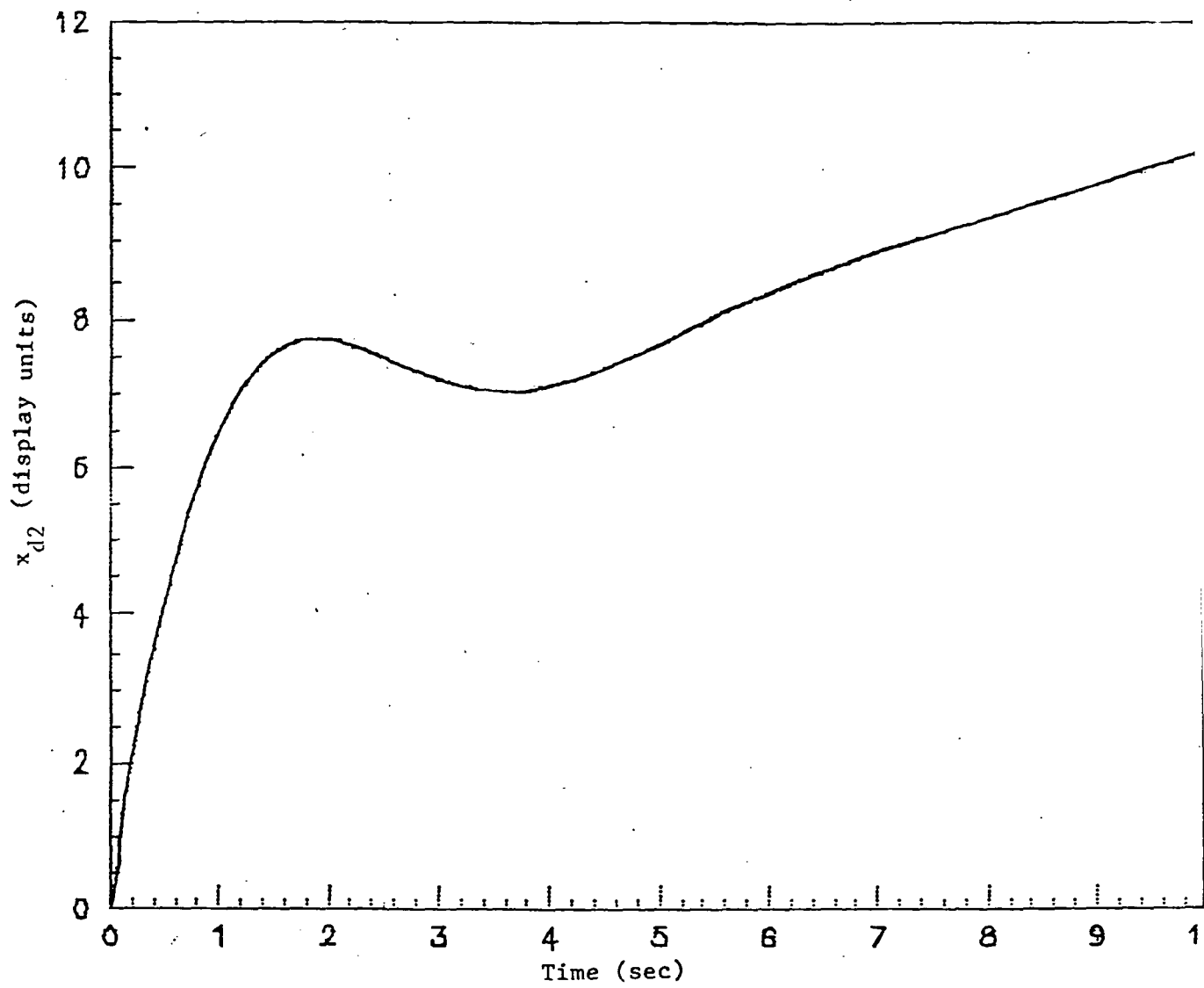


Figure 5.5(b)  $x_{d2}$  Response to Step Elevator Input

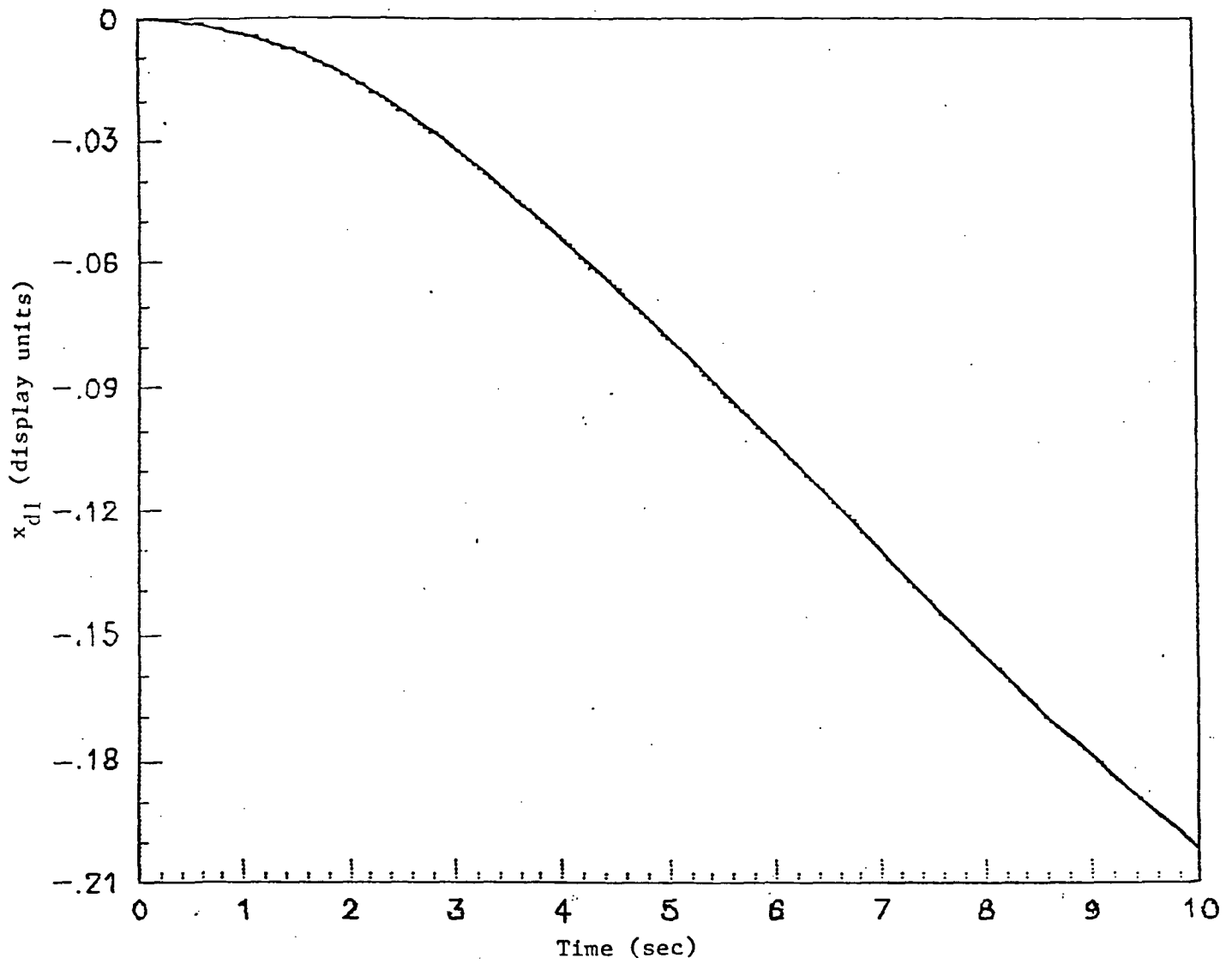


Figure 5.6(a)  $x_{d1}$  Response to Step Throttle Input  
( $\delta T_c = 1 \text{ ft}/(\text{sec}^2)$ , +ve thrust)

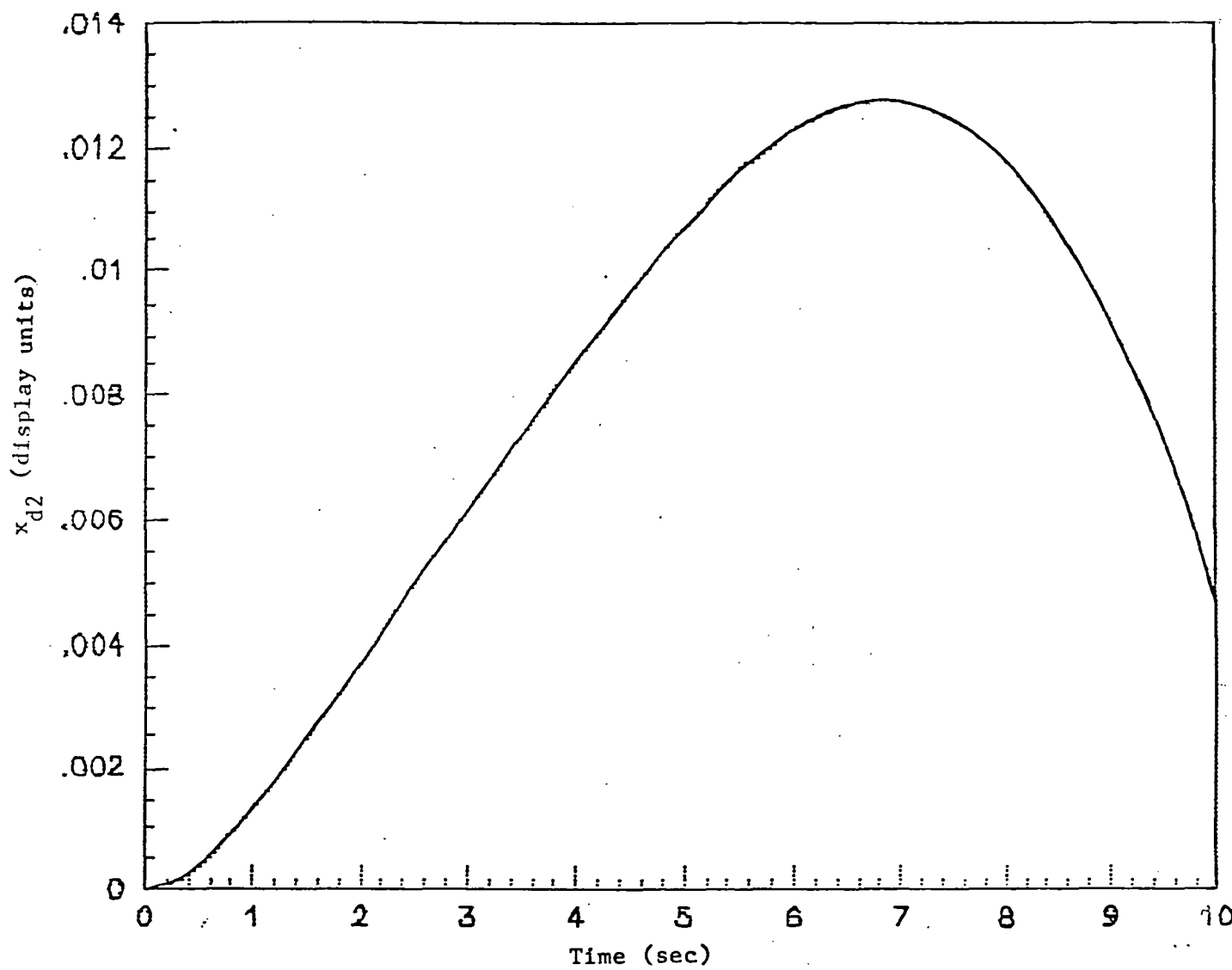


Figure 5.6(b)  $x_{d2}$  Response to Step Throttle Input

commands. From these time responses, it would appear that the strategy for the pilot might be to attempt to "control"  $x_{d1}$  with the throttle and  $x_{d2}$  with the elevator. This is due to the fact that  $x_{d2}$  is essentially uncontrollable from throttle inputs. For a step normal acceleration command, there will be an instantaneous change in both  $x_{d1}$  and  $x_{d2}$  (as is apparent from the optimal display gains  $G_d^*$  in (5.3.9)). In order to follow the command, then, the pilot's strategy would appear to be to apply the elevator to regulate  $x_{d2}$  and simultaneously use the throttle to null out the effects of the elevator command and the normal acceleration command on  $x_{d1}$ . The ultimate success of this strategy as well as comparison with that for the case of status display (Display A), of course, requires additional analysis and simulation.

#### 5.4.2 Frequency Domain Analysis

The block diagram representations for the pilot's task formulated as above are shown in Figures (5.7) and (5.8) for Displays A and B, respectively. Note that in each case the pilot has four observations and two controls available to him. (The rate observations, as stated earlier, are reconstructed by the pilot from the displayed signals.) So the frequency-domain representation of the pilot consists of a  $2 \times 4$  transfer matrix. For Display A the pilot representation is

$$P(s) = \begin{bmatrix} \frac{P}{a} \frac{\delta e}{z_c} & \frac{P}{e} \frac{\delta e}{a_z} & \frac{P}{M} \frac{\delta e}{\theta} & \frac{P}{\theta} \frac{\delta e}{\theta} \\ \frac{P}{a} \frac{\delta T}{z_c} & \frac{P}{e} \frac{\delta T}{a_z} & \frac{P}{M} \frac{\delta T}{\theta} & \frac{P}{\theta} \frac{\delta T}{\theta} \end{bmatrix} \quad (5.4.1)$$

and for Display B

$$P(s) = \begin{bmatrix} \frac{P}{a} \frac{\delta e}{z_c} & \frac{P}{x_{d1}} \frac{\delta e}{x_{d1}} & \frac{P}{x_{d2}} \frac{\delta e}{x_{d2}} & \frac{P}{\theta} \frac{\delta e}{\theta} \\ \frac{P}{a} \frac{\delta T}{z_c} & \frac{P}{x_{d1}} \frac{\delta T}{x_{d1}} & \frac{P}{x_{d2}} \frac{\delta T}{x_{d2}} & \frac{P}{\theta} \frac{\delta T}{\theta} \end{bmatrix} \quad (5.4.2)$$



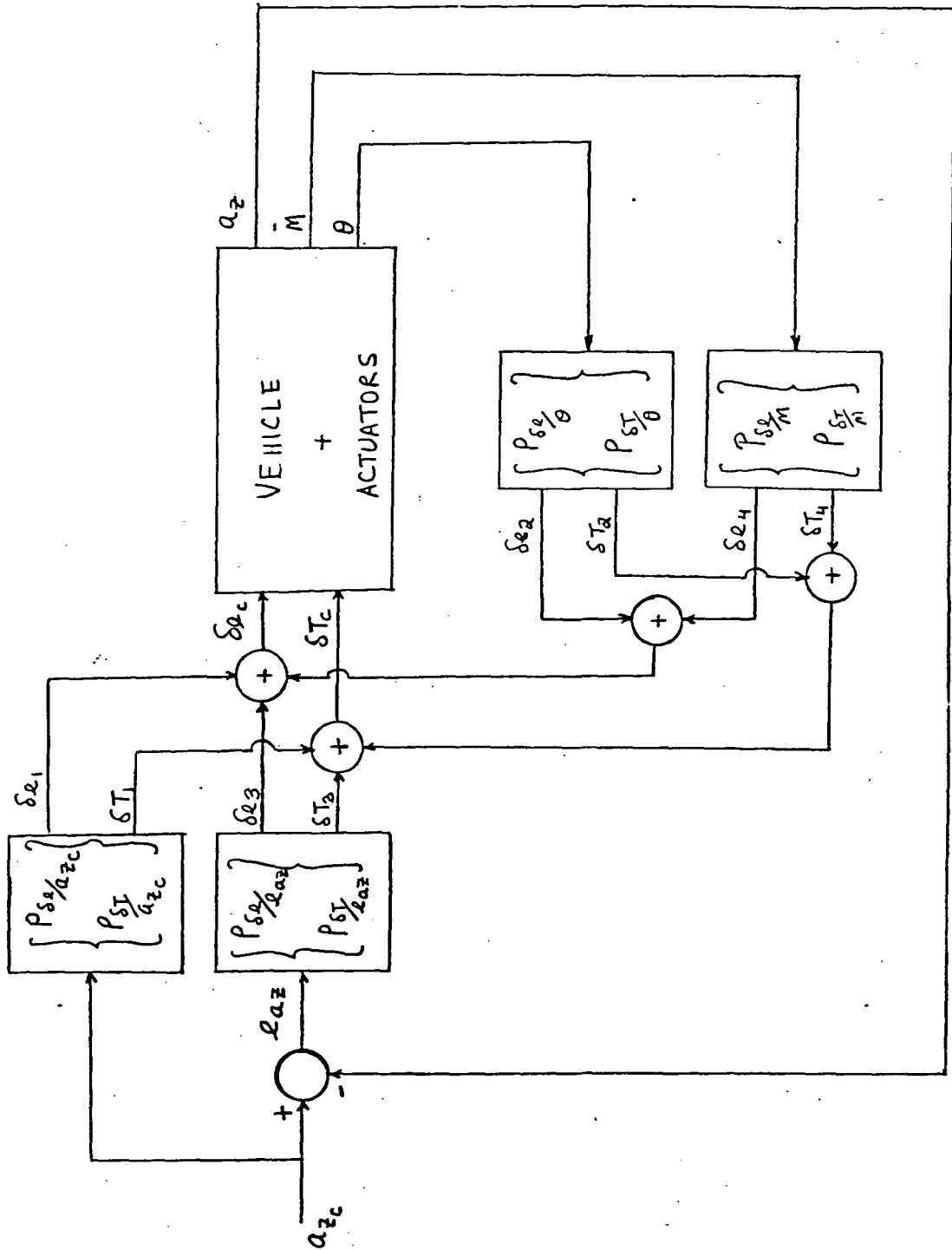


Figure 5.7 Block Diagram for Status Display

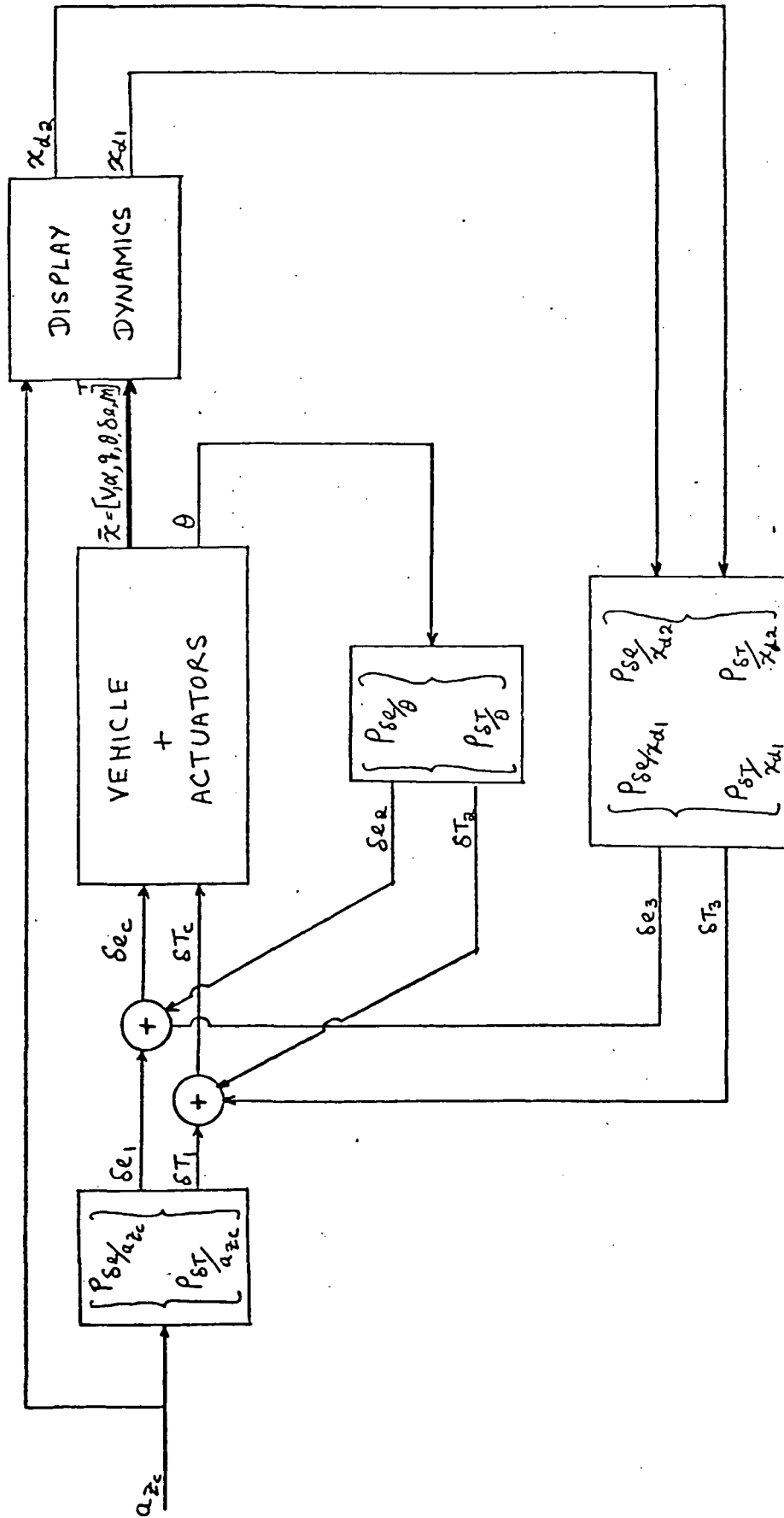


Figure 5.8 Block Diagram for Augmented Display

Here  $P_{\frac{\delta_e}{a_{zc}}}$  is the pilot describing function from the normal acceleration command observation  $a_{zc}$  to the commanded elevator input  $\delta_{ec}$ . The other elements of (5.4.1) and (5.4.2) are similarly defined. The Bode-plots for the eight pilot describing functions for Display A are presented in Figures (D.1) to (D.8) and those for Display B in Figures (D.9) to (D.16) in Appendix D, for reference.

With the pilot represented by eight transfer functions, it is not straightforward to define a meaningful measure of pilot workload in the frequency-domain. Since the vehicle dynamics and the display dynamics are known and the various pilot describing functions are available as above, additional frequency-domain analysis, as in the case of the  $K/s^2$  plant, may in principal be performed using the block diagrams of Figures (5.6) and (5.7). However, the results presented in Chapter 4 showed that the performance and workload information obtained from statistical and spectral analysis of the model-based predictions is consistent with that derived from the other frequency-domain analysis. Therefore, results from statistical and spectral analysis will be used to evaluate and compare the two Displays A and B.

#### 5.4.3 RMS Analysis

Using the complete human operator model, closed-loop analysis was performed for both the status display (A) and the optimal augmented display (B). The rms values for the variables of interest for the two displays are shown in Table 5.2. From these results it is clear that there is a slight improvement in  $a_z$  tracking performance for the case with display augmentation, and Mach number regulation is much improved. Both the pilot control inputs and control rates are lower for the

TABLE 5.2 OCM ANALYSIS RESULTS

## (a) Performance Measures

Classification	$e_{az}$ ft/sec <sup>2</sup>	$\dot{e}_{az}$	M .001 Mach	$\theta$ .01 rads
A: Status Display	7.009	11.920	39.11	8.45
B: Optimal Display	6.659	9.349	11.32	3.36

## (b) Workload Measures

Classification	$\delta_{ec}$ .01 rads	$\dot{\delta}_{ec}$	$\delta T_c$ ft/sec <sup>2</sup>	$\dot{\delta T}_c$
A: Status Display	2.95	13.21	2.566	0.1742
B: Optimal Display	1.78	8.06	0.819	0.1228

optimal display case, indicating that the designed display augmentation should lead to reduction in pilot workload.

#### 5.4.4 Spectral Analysis

The power spectra of the  $a_z$  tracking error and both the control inputs for the Displays A and B are shown in Figures (D.1) to (D.6) in the Appendix D. These plots show the total power (in dB), the portion correlated with the command driving the system, and the uncorrelated part, or the contribution due to the pilot's remnant.

The  $a_z$  tracking error power spectrum for the Displays A and B is compared in Figure (5.9). This power for Display B (augmented case) is slightly higher than Display A at low frequencies, but is less than Display A for frequencies above 0.7 rads/sec. Even though the rms tracking error with the optimal display (B) is not too much lower than that with the status display (A), the augmentation appears to reduce the errors at the more-demanding higher frequencies.

The pilot's commanded elevator power spectrum and commanded thrust power spectrum for Displays A and B are compared in Figures (5.10) and (5.11), respectively. From these figures it is clear that the power for both pilot control inputs is much lower at all frequencies for the optimal display case. As was the case of  $K/s^2$  plant, this is an indication that the pilot's workload in accomplishing the task should be reduced.

Thus, from this initial example application, it appears that the suggested display augmentation synthesis technique can lead to desirable results when applied to manual control of complex dynamics. As further experience is gained in applying the technique, even better performance

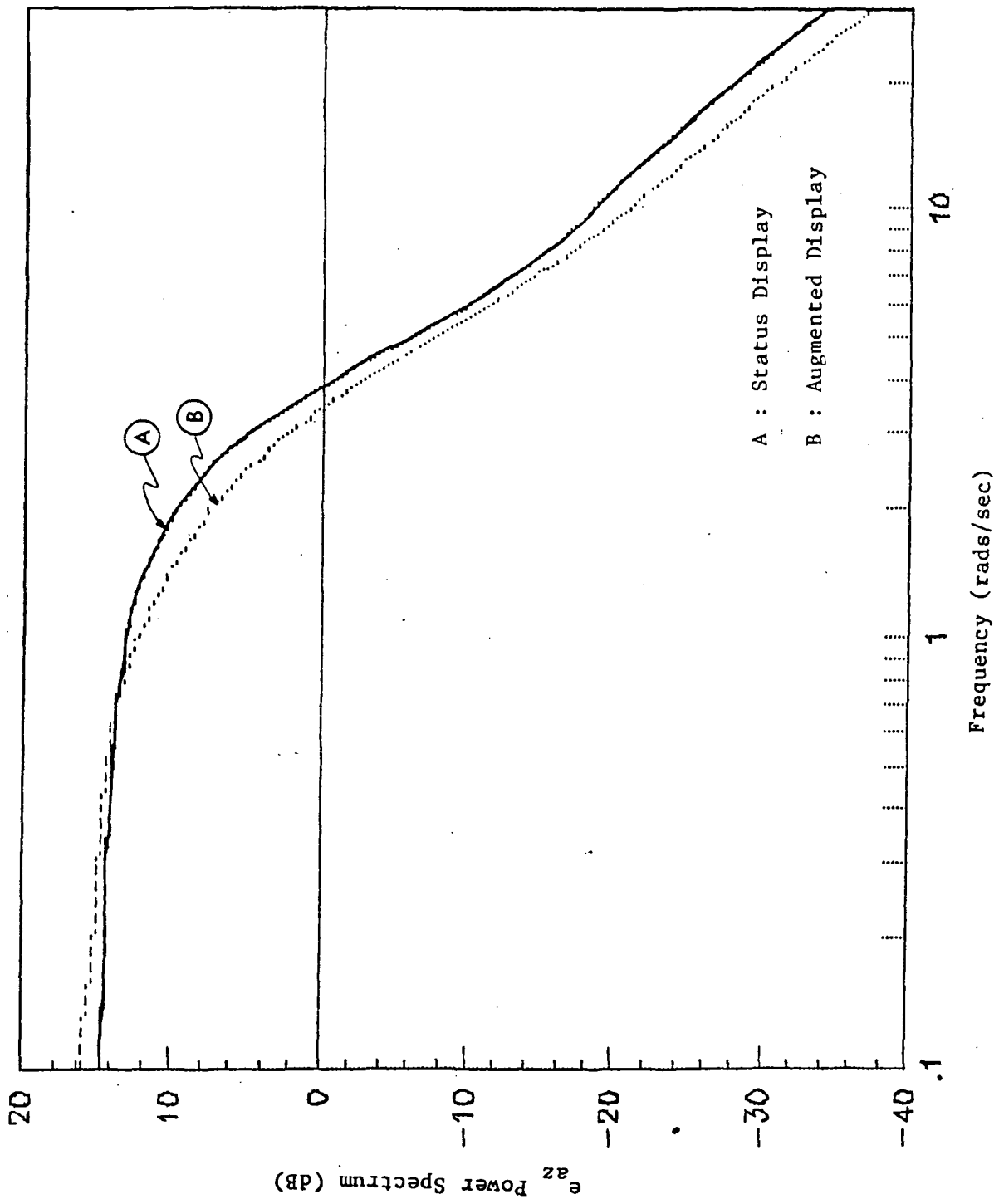


Figure 5.9 Comparison of  $e_{az}$  Power Spectrum

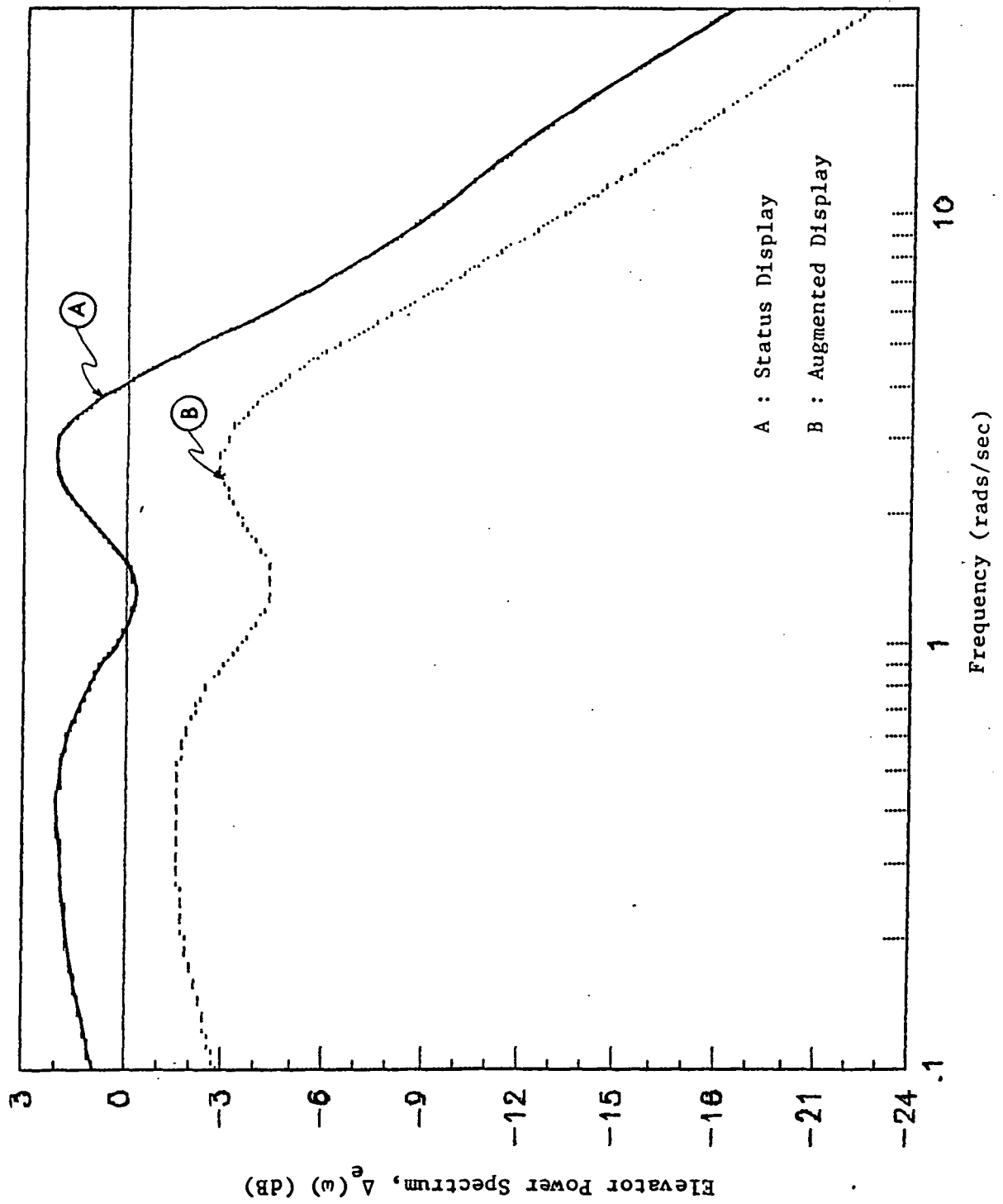


Figure 5.10 Comparison of Pilot Commanded Elevator Spectrum

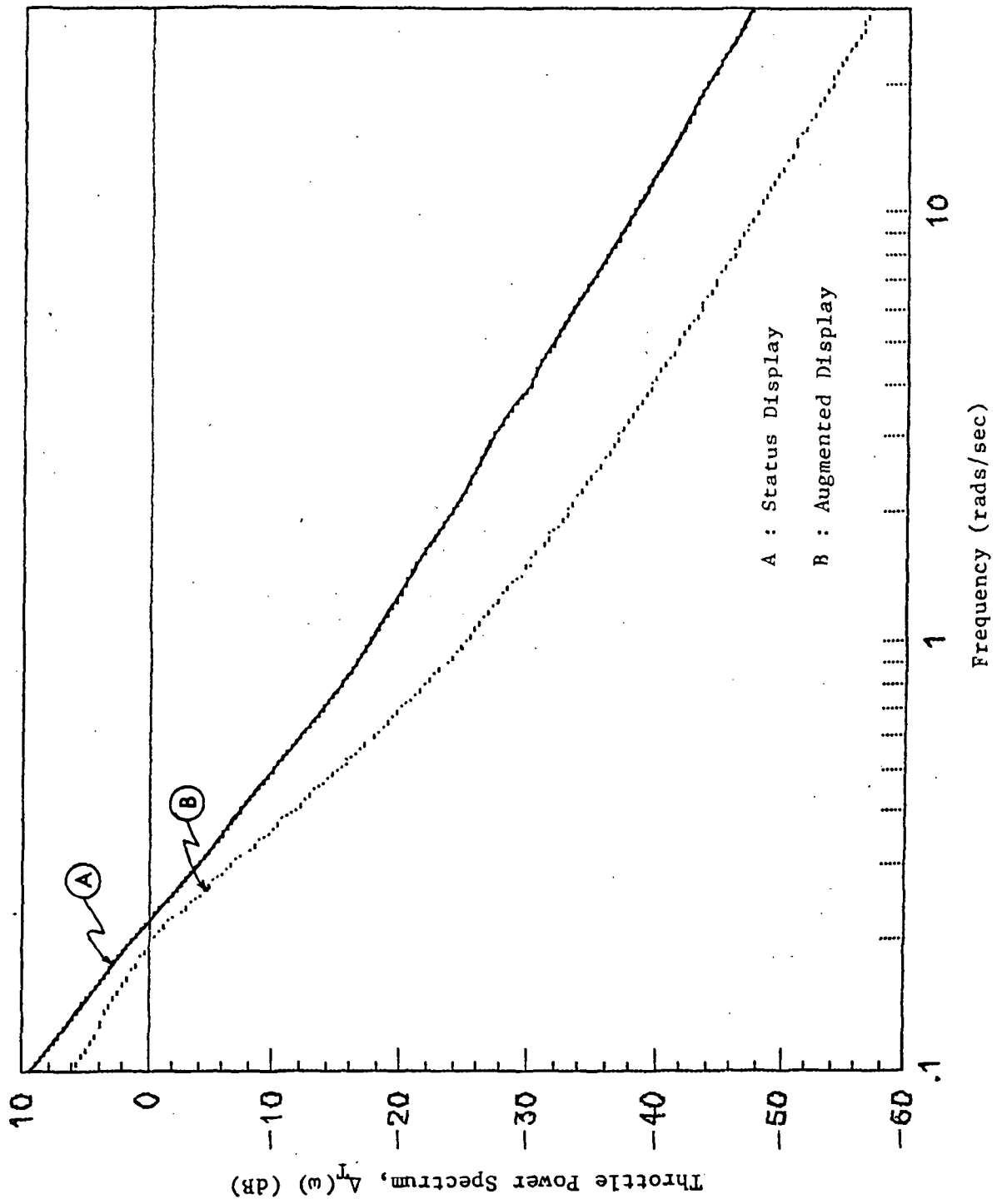


Figure 5.11 Comparison of Pilot Commanded Throttle Spectrum



**Page Intentionally Left Blank**

CHAPTER 6SUMMARY

The objective of this effort was to develop an analytical technique to aid in the design of display augmentation. The main differences between display augmentation and control augmentation were pointed out using simplified block diagrams. Although different from augmenting plant dynamics, it is usually possible to improve human operator performance in manual-control tasks by providing the human with an augmented display.

Model-based evaluations were performed for various empirically-derived display "quickenings" control laws for a simple  $K/s^2$  plant in a compensatory tracking task. The results of this analysis, in terms of mean square values of tracking error and manual control activity and rate, showed that significant reduction in human operator workload and improvement in performance is possible through a proper design of the signal being displayed to the human.

The cooperative control synthesis technique previously developed to design pilot-optimal control augmentation was then extended to incorporate the simultaneous design of pilot-optimal display augmentation. The problem formulation for the cooperative synthesis technique was discussed in detail and the necessary conditions for optimality were derived. A numerical algorithm for applying the methodology to perform pilot-in-the-loop synthesis of optimal display augmentation control laws was then presented.

The application of the methodology to a simple system was demonstrated by synthesizing various display augmentation control laws for

the  $K/s^2$  plant. By varying the weighting parameters in the cost function, it was shown that this methodology has the potential of providing a systematic approach to design of task tailored display augmentation. The synthesized display designs were evaluated, using the full-order human operator model, in terms of the mean square values of the variables of interest and the power spectrum of the human operator's control input. The evaluation results predicted a reduction in human operator workload and improvement in tracking error performance with the augmented displays. Moreover, when compared to the empirically-derived display "quickenings" control laws, the results tended to validate the cooperative approach to display design.

Detailed frequency domain analysis was also performed for the synthesized displays, using the frequency-domain representation of the human operator model. All the augmented displays were shown to provide the human operator with some lead information, reducing the required human operator phase compensation from the case with no display augmentation. A comparison of the closed-loop frequency responses for the various synthesized displays indicated that the cooperative methodology does lead to desired results.

An initial application of the methodology to high-order system dynamics with a multi-control task was then demonstrated, using a normal-acceleration tracking task and an F-15 type aircraft model. The problem formulation was discussed in detail and a preliminary display design was synthesized using the cooperative technique. Analytical methods for evaluating the synthesized display for the complex task were again employed, and the results of the analysis were compared with those for an unaugmented status display. Based on the statistical analysis

results, improvement in performance and pilot workload is predicted for the synthesized optimally augmented display.

Since the model-based evaluation of the display designs predicts promising gains in pilot workload, it is suggested that these results be validated through real-time, man-in-the-loop simulation. For the display design synthesized for the aircraft model, further insight needs to be gained into the significance of the two display variables. Finally, the application of the cooperative methodology to display design for complex systems should be further explored, and systems considered for which other methods have been used to synthesize the display, to provide further comparison and validation.

REFERENCES

- [1] Poulton, "Tracking Skill and Manual Control," Academic Press, 1974.
- [2] Hoffman, W.C., Kleinman, D.L., and Young, L.R., "Display/Control Requirements for Automated VTOL Aircraft," NASA-CR 158905, ASI-TR-76-39.
- [3] Korn, J., Gully, Sol W., and Kleinman, D.L., "Validation of an Advanced Cockpit Display Design Methodology via Workload/Monitoring Tradeoff Analysis," 18th Annual Conference on Manual Control, Dayton, Ohio, June 1982.
- [4] Duke, E.L., Jones, F.P., and Roncoli, R.B., "Development of a Flight Test Maneuver Autopilot for a Highly Maneuverable Aircraft," AIAA Paper 83-0061, Jan. 1983.
- [5] Walker, R.A., Gupta, N.K., Duke, E.L., and Patterson, B., "Developments in Flight Test Trajectory Control," AIAA Paper 84-0240, Jan. 1984.
- [6] Kleinman, D.L., Baron, S., and Levison, W.H., "An Optimal Control Model of Human Response," Parts I and II, Automatica, vol. 6, pp. 357-383, 1970.
- [7] Schmidt, D.K., "Optimal Flight Control Synthesis via Pilot Modeling," AIAA Journal of Guidance and Control, July-August 1979.

- [8] Schmidt, D.K., and Innocenti, M., "Pilot Optimal Multivariable Control Synthesis by Output Feedback," NASA CR-16312, July 1981.
- [9] Innocenti, M., "Cooperative Pilot-Optimal Augmentation System Synthesis for Complex Flight Vehicles," Ph.D. Thesis, Purdue University, West Lafayette, Indiana, May 1983.
- [10] Schmidt, D.K., "On the Use of the OCM's Quadratic Objective Function as a Pilot Rating Metric," 17th Annual Conference on Manual Control, Los Angeles, CA, June 1981.
- [11] Wierwille, Walter W., and Connor, Sydney, A., "Evaluation of 20 Workload Measures Using a Psychomotor Task in a Moving-Base Aircraft Simulator," Human Factors, Vol. 25, pp. 1-16, 1983.
- [12] Kwakernaak, H., and Sivan, R., "Linear Optimal Control Systems," Wiley-Interscience, 1972.
- [13] Bacon, B.J., and Schmidt, D.K., "An Optimal Control Approach to Pilot/Vehicle Analysis and the Neal-Smith Criteria," NASA Contractor Report 170416, April 1984.
- [14] McRuer, D., Graham, D., Krendel, E., and Reisener, W. Jr., "Human Pilot Dynamics in Compensatory Systems," AFFDL-TR-65-15, July 1965.
- [15] Curry, R.E., Hoffman, W.C., and Young, L.R., "Pilot Modelling for Manned Simulation, Vols. I and II, AFFDL-TR-76-124, Dec. 1976.
- [16] Phatak, Anil V., "Investigation of Alternate Human Operator Optimal Control Model Structures," Air Force RMRL, contract

#F33615-78-C-0501.

- [17] Noble, B., Daniel, J.W., "Applied Linear Algebra," Prentice-Hall Inc., 1977.
- [18] Joshi, S.M., "Design of Optimal Partial State Feedback Controllers for Linear Systems in Stochastic Environments," Paper 6D-4, IEEE, Souteastcon, Charlotte, N.C., 1975.
- [19] Neal, T.P., and Smith, R.E., "An In-flight Investigation to Develop Control System Design Criteria for Fighter Airplanes," AFFDL-TR-70-74, Vol. I, Dec. 1970.
- [20] Anderson, M.R., and Schmidt, D.K., "Closed-loop, Pilot/Vehicle Analysis of the Approach and Landing Task," AIAA Paper No. 85-1851-CP, 1985 Guidance and Control Conference, Snowmass, Colorado.
- [21] Walker, R.A., and Gupta, N.K., "Flight Test Trajectory Control Analysis," NASA Contractor Report 170395, Feb. 1983
- [22] Pavassilopoulos, G.P., Medanic, J.V., Cruz, J.B. Jr., "On the existence of Nash Strategies and Solutions to Coupled Riccati Equations in Linear-Quadratic Games", JOTA, Vol. 28, No. 1, May 1979.
- [23] McRuer, D.T., and Krendel, E.S., "Dynamic Response of Human Operators", Wright Air Dev. Center WADC TR 56-524, Wright-Patterson Air Force Base, Ohio, Oct. 1957.
- [24] Levison, W.H., Kleinman, D.L., and Baron, S., "A Model for Human Controller Remnant", IEEE, Trans. Man-Machine Syst., Vol. 10, Dec. 1969

APPENDIX ADERIVATION OF NECESSARY CONDITIONS FOR CONTROLLER 2 ( $\bar{u}_2$ )

As stated in section (3.4), the system dynamics in the presence of the control action  $\bar{u}_1$  can be written in terms of the augmented state vector  $\bar{q}$  as

$$\dot{\bar{q}} = A_1' \bar{q} + B_2' \bar{u}_2 + B_d' \bar{u}_d + D' \bar{w} \quad (A.1)$$

where  $\bar{q}$ ,  $A_1'$ ,  $B_2'$ ,  $B_d'$ , and  $D'$  are as defined in section (3.4). The outputs  $\bar{y}_2$  and  $\bar{y}_d$  are given in terms of  $\bar{q}$  by

$$\begin{aligned} \bar{y}_2 &= [C_2 \ 0] \bar{q} = C_2' \bar{q} \\ \bar{y}_d &= [C_d \ 0] \bar{q} = C_d' \bar{q} \end{aligned} \quad (A.2)$$

and the index of performance  $J_2$  becomes

$$J_2 = E \left\{ \lim_{T \rightarrow \infty} \frac{1}{T} \int_0^T (\bar{q}^T Q' \bar{q} + \bar{u}_2^T F_2 \bar{u}_2 + \bar{u}_d^T F_{2d} \bar{u}_d) dt \right\} \quad (A.3)$$

with  $Q'$  again as defined in section (3.4).

The closed loop system under the action of Controller 2 ( $\bar{u}_2$ ) and the display control law  $\bar{u}_d$ , with the control laws as given by (3.1.5), can then be written in a compact form as

$$\dot{\bar{q}} = A_c \bar{q} + D' \bar{w} \quad (A.4)$$

where

$$A_c = \begin{bmatrix} A_{aug} & B_1 K_1 \\ M_1 C_{aug} & A_1 \end{bmatrix}$$

with  $A_{aug}$ ,  $C_{aug}$  and  $A_1$  as defined in Chapter 3.

The system given by (A.4) is identified as a linear stochastic time



invariant system driven by a white noise process  $\bar{w}'$ . From linear stochastic system theory [12], in the steady state case the system state covariance matrix  $L$  is obtained as the solution to the following Lyapunov equation

$$A_c L + L A_c^T + D' W' D'^T = 0 \quad (A.5)$$

where  $W'$  is the intensity of the process  $\bar{w}'$  and  $L = E[\bar{q} \bar{q}^T]$ .

Using the trace operator [17],  $J_2$  can be expressed as

$$J_2 = \text{tr}[\bar{Q}L] \quad (A.6)$$

where

$$\bar{Q} = Q' + \begin{bmatrix} C_2^T G_2^T F_2 G_2 C_2 + C_d^T G_d^T F_d G_d C_d & 0 \\ 0 & 0 \end{bmatrix}$$

(A.5) and (A.6) can now be treated as a constrained parameter optimization problem [18]. Defining  $H$  as a symmetric matrix of Lagrange multipliers, the cost  $J_2$  can be augmented with the constraint (A.5) to get

$$\bar{J}_2 = \text{tr}[\bar{Q}L] + \text{tr}[H(A_c L + L A_c^T + D' W' D'^T)] \quad (A.7)$$

The necessary conditions for optimality applied to (A.7) yield the following relations

$$\frac{\partial \bar{J}_2}{\partial L} = A_c^T H + H A_c + \bar{Q} = 0 \quad (A.8)$$

$$\frac{\partial \bar{J}_2}{\partial H} = A_c L + L A_c^T + D' W' D'^T = 0 \quad (A.9)$$

$$\frac{\partial \bar{J}_2}{\partial G_2} = 0 \quad (A.10)$$

$$\frac{\partial \bar{J}_2}{\partial G_d} = 0 \quad (A.11)$$

Equations (A.10) and (A.11) need further elaboration because the augmentation gains  $G_2$  and the display control gains  $G_d$  are embedded in the dynamics of the closed loop system.

(a)  $\frac{\partial \bar{J}_2}{\partial G_2}$ :

In  $\bar{J}_2$ , the terms containing  $G_2$  are  $\bar{Q}$  and  $A_c$ . Therefore

$$\frac{\partial \bar{J}_2}{\partial G_2} = \frac{\partial}{\partial G_2} \{ \text{tr}[\bar{Q}L] + 2\text{tr}[HLA_c^T] \} \quad (\text{A.12})$$

where the trace identity  $\text{tr}[HA_c L] = \text{tr}[HLA_c^T]$  has been made use of.

Further note that in  $A_c$ ,  $G_2$  appears both in  $A_{\text{aug}}$  as well as in  $A_1$ . But  $A_1$  is part of the optimal Controller 1 ( $\bar{u}_1$ ), as is apparent from (3.4.1), and since we are looking for a Nash solution, Controller 1 is to be considered fixed in the minimization process for  $J_2$ . Thus the only gains that may be adjusted in Controller 2 are those in  $A_{\text{aug}}$  where  $A_{\text{aug}} = A + B_2 G_2 C_2 + B_d G_d C_d$ . Then

$$\frac{\partial}{\partial G_2} \text{tr}[HLA_c^T] = \frac{\partial}{\partial G_2} \text{tr} \left\{ HL \begin{bmatrix} B_2 G_2 C_2 & 0 \\ 0 & 0 \end{bmatrix}^T \right\} \quad (\text{A.13})$$

Noting that

$$\begin{bmatrix} C_2^T G_2^T B_2^T & 0 \\ 0 & 0 \end{bmatrix} = \begin{bmatrix} C_2^T \\ 0 \end{bmatrix} G_2^T [B_2^T \ 0] \quad (\text{A.14})$$

(A.13) can be simplified to get

$$\frac{\partial}{\partial G_2} \text{tr} \left\{ HL \begin{bmatrix} C_2^T \\ 0 \end{bmatrix} G_2^T [B_2^T \ 0] \right\} = [B_2^T \ 0] HL \begin{bmatrix} C_2^T \\ 0 \end{bmatrix} \quad (\text{A.15})$$

Also from the definition of  $\bar{Q}$  we have

$$\begin{aligned}
\frac{\partial}{\partial G_2} \text{tr}[\bar{Q}L] &= \frac{\partial}{\partial G_2} \text{tr} \left\{ \begin{bmatrix} C_2^T G_2^T F_2 G_2 C_2 & 0 \\ 0 & 0 \end{bmatrix} L \right\} \\
&= \frac{\partial}{\partial G_2} \text{tr} \left\{ \begin{bmatrix} C_2^T \\ 0 \end{bmatrix} G_2^T F_2 G_2 [C_2 \ 0] L \right\} \\
&= 2F_2 G_2 [C_2 \ 0] L \begin{bmatrix} C_2^T \\ 0 \end{bmatrix}
\end{aligned} \tag{A.16}$$

Combining (A.15) and (A.16), the condition (A.10) can be written in the expanded form as

$$\frac{\partial \bar{J}_2}{\partial G_2} = 2\{F_2 G_2 [C_2 \ 0] L \begin{bmatrix} C_2^T \\ 0 \end{bmatrix} + [B_2^T \ 0] HL \begin{bmatrix} C_2^T \\ 0 \end{bmatrix}\} = 0 \tag{A.17}$$

(b)  $\frac{\partial \bar{J}_2}{\partial G_d}$ :

In  $\bar{J}_2$ , the terms containing  $G_d$  are  $\bar{Q}$  and  $A_c$ . Therefore as before

$$\frac{\partial \bar{J}_2}{\partial G_d} = \frac{\partial}{\partial G_d} \{\text{tr}[\bar{Q}L] + 2\text{tr}[HLA_c^T]\} \tag{A.18}$$

Again noting that in  $A_c$ ,  $A_1$  and  $M_1$  are part of the optimal controller 1 ( $\bar{u}_1$ ), the only free gains  $G_d$  to be adjusted are those appearing in  $A_{aug}$  and  $C_{aug}$ . Then

$$\frac{\partial}{\partial G_d} \text{tr}[HLA_c^T] = \frac{\partial}{\partial G_d} \text{tr} \left\{ HL \begin{bmatrix} B_d G_d C_d & 0 \\ M_1 C_u G_d C_d & 0 \end{bmatrix} \right\} \tag{A.19}$$

The matrix on the right hand side of (A.19) can be written as

$$\begin{bmatrix} B_d G_d C_d & 0 \\ M_1 C_u G_d C_d & 0 \end{bmatrix} = \begin{bmatrix} B_d \\ M_1 C_u \end{bmatrix} G_d [C_d \ 0] \tag{A.20}$$

which gives

$$\frac{\partial}{\partial G_d} \text{tr} \left\{ \text{HL} \begin{bmatrix} B_d G_d C_d & 0 \\ M_1 C_u G_d C_d & 0 \end{bmatrix} \right\} = \begin{bmatrix} B_d \\ M_1 C_u \end{bmatrix}^T \text{HL} \begin{bmatrix} C_d^T \\ 0 \end{bmatrix} \quad (\text{A.21})$$

Further, similar to the procedure used to get (A.16), we have

$$\frac{\partial}{\partial G_d} \text{tr}[\bar{Q}L] = 2F_{2d} G_d \begin{bmatrix} C_d & 0 \end{bmatrix} L \begin{bmatrix} C_d^T \\ 0 \end{bmatrix} \quad (\text{A.22})$$

Combining (A.21) and (A.22), (A.11) can be written in the expanded form as

$$\frac{\partial \bar{J}_2}{\partial G_d} = 2 \{ F_{2d} G_d \begin{bmatrix} C_d & 0 \end{bmatrix} L \begin{bmatrix} C_d^T \\ 0 \end{bmatrix} + \begin{bmatrix} B_d \\ M_1 C_u \end{bmatrix}^T \text{HL} \begin{bmatrix} C_d^T \\ 0 \end{bmatrix} \} \quad (\text{A.23})$$

(A.8), (A.9), (A.17) and (A.23) together give the necessary conditions for the simultaneously optimality of the augmentation controller  $\bar{u}_2$  and the display control law  $\bar{u}_d$ .

APPENDIX BTHE OPTIMAL CONTROL PILOT MODEL

The optimal control approach to human operator modeling was developed by Kleinman, Baron and Levison in the early 1970's. Since that time it has been used successfully to model manual pilot behaviour in a variety of complex tasks. A brief discussion of the actual model is given here as it forms the basis for the synthesis and analysis of display augmentation designs presented in this report. More detailed discussion of the structure of the model can be found in [6] and [13].

The model is based on the assumption that a "well-motivated" human pilot adjusts his gains and compensation for the vehicle and task such that an objective function,  $J_p$ , is minimized, subject to human limitations. Typically a piloting task, aircraft and display dynamics are represented in the block diagram shown in Figure (B.1) and by the time invariant differential equation

$$\dot{\bar{x}}(t) = A\bar{x}(t) + bu_p(t) + D\bar{w}(t) \quad (B.1)$$

where the A matrix can be an aggregation of task, plant and control system dynamics. The vehicle states are represented by the vector  $\bar{x}(t)$  while  $u_p(t)$  is the pilot input (assumed to be scalar here for the purposes of explanation - multi-input tasks are easily accommodated within the framework of the model) and  $w(t)$  is a "white" noise disturbance with intensity W.

An output vector  $\bar{y}_p(t)$  represents those variables which the pilot can observe, either through the cockpit display, out the windows or by the "seat of his pants". His observations are given by the relation

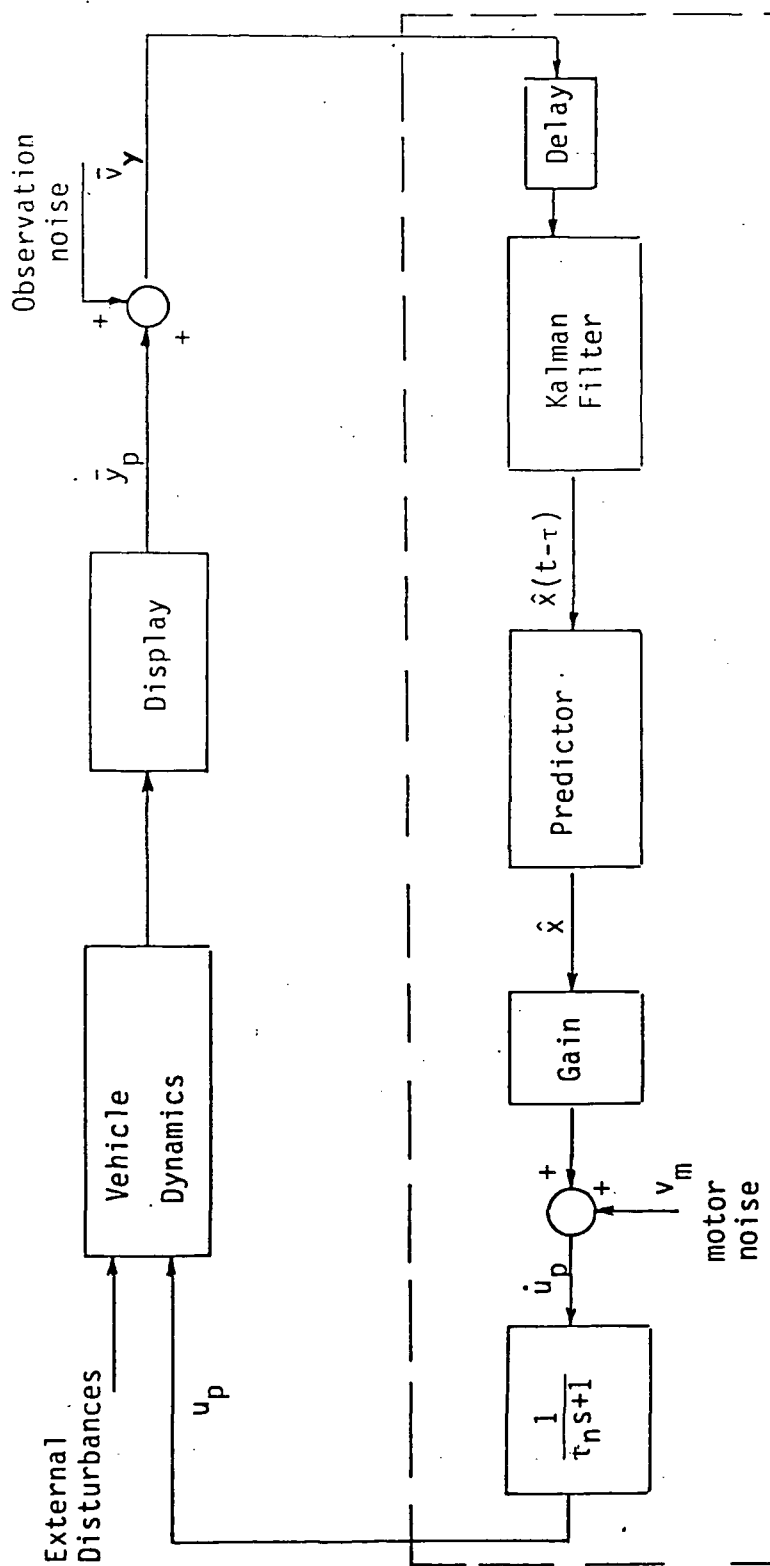


Figure B.1 OCM Block Diagram

$$\bar{y}_p(t) = C\bar{x}(t-\tau) + du_p(t-\tau) + \bar{v}_y(t-\tau) \quad (B.2)$$

where  $\tau$  is a pure delay associated with the inherent delay in the pilot's perception, and  $\bar{v}_y$  is a vector white noise process with intensity  $V_y$  which models the imperfection in the pilot's observations.

The pilot's task is reflected in the minimization of a quadratic performance index of the form

$$J_p(\mu^*) = E\left\{\lim_{T \rightarrow \infty} \frac{1}{T} \int_0^T \left( \sum_{i=1}^n q_i x_i^2 + r u_p^2 + g \dot{u}_p^2 \right) dt\right\} \quad (B.3)$$

subject to pilot observations  $y_p(\sigma)$  for time  $\sigma \leq t$  and with cost functional weightings  $q_i > 0$ ,  $r > 0$ , and  $g > 0$ .

Inclusion of the control rate,  $\dot{u}_p$ , in the cost function naturally leads to a first order lag in the pilot's control law analogous to the neuromotor lag of the McRuer crossover pilot model [14]. The time constant of the lag, furthermore, may be adjusted through variation of the control-rate weighting constant,  $g$ .

By defining a new state vector as

$$\bar{x}^T(t) = [\bar{x}^T(t), u_p(t)],$$

the augmented system can be represented as ( $\dot{u}_p(t) = \mu_o(t)$ )

$$\dot{\bar{x}}(t) = A_o \bar{x}(t) + b_o \mu_o(t) + D_o \bar{w}(t) \quad (B.4)$$

with

$$A_o = \begin{bmatrix} A & b \\ 0 & 0 \end{bmatrix}, \quad b_o = \begin{bmatrix} 0 \\ 1 \end{bmatrix}, \quad D_o = \begin{bmatrix} D \\ 0 \end{bmatrix}$$

The minimizing control law is

$$\mu_o^*(t) = -\hat{1}\bar{x}(t) \quad (B.5)$$

with

$$1 = \frac{1}{g} b_o^T K_o \quad (B.6)$$

where  $\hat{\bar{x}}(t)$  is the current estimate of the state  $\bar{x}(t)$ , and  $K_o$  is the unique positive definite solution of the Ricatti Equation

$$A_o^T K_o + K_o A_o + Q_o - \frac{1}{g} K_o b_o b_o^T K_o = 0 \quad (B.7)$$

with  $Q_o = \text{diag}(q_1, r)$ . Expanding the optimal control law as

$$\mu_o^*(t) = - \sum_{i=1}^n l_i \rho_i(t) - l_{n+1} u_p(t) \quad (B.8)$$

where  $\rho_i(t)$  is the current estimate of the system state  $x_i(t)$ , and letting

$$\tau_n = \frac{1}{l_{n+1}} \quad (B.9)$$

by iterating the control-rate weighting,  $g$ , the equivalent lag time constant,  $\tau_n = \frac{1}{l_{n+1}}$ , can be adjusted to a desired value. The control law can then be written as

$$\tau_n \dot{u}_p(t) + u_p(t) = \mu^*(t) \quad (B.10)$$

where

$$\mu^*(t) = -l_e \bar{\rho}(t) \quad (B.11)$$

with

$$l_e = \tau_n [l_1, l_2, \dots, l_n]$$

From the human operator viewpoint, an exact control input is not possible. This uncertainty is modeled by the addition of motor noise  $v_m$  in the control equation, or

$$\tau_n \dot{u}_p(t) + u_p(t) = \mu^*(t) + v_m(t) \quad (B.12)$$

where  $v_m(t)$  is a Gaussian "white" noise source with intensity,  $V_m$ . The



controller gains previously calculated are assumed to remain the same in the presence of motor noise. This assumption reduces the human operator model to sub-optimal control behaviour.

The current state estimate is derived from the combination of a Kalman state estimator and a least mean square predictor. The system is rewritten as

$$\begin{aligned}\bar{\mathbf{x}}^T(t) &= [\bar{\mathbf{x}}^T(t), u_p(t)] \\ \dot{\bar{\mathbf{x}}}(t) &= A_1 \bar{\mathbf{x}}(t) + b_1 u(t) + D_1 \bar{\mathbf{w}}_1(t) \\ \bar{\mathbf{y}}_p(t) &= C_1 \bar{\mathbf{x}}(t-\tau) + \bar{\mathbf{v}}_y(t-\tau), \quad \bar{\mathbf{v}}_y \sim N(0, V_y)\end{aligned}\tag{B.13}$$

where

$$\begin{aligned}A_1 &= \begin{bmatrix} A & b \\ 0 & -\frac{1}{\tau_n} \end{bmatrix}, \quad b_1 = \begin{bmatrix} 0 \\ \frac{1}{\tau_n} \end{bmatrix} \\ C_1 &= [C \mid d], \quad D_1 = \begin{bmatrix} D & 0 \\ 0 & \frac{1}{\tau_n} \end{bmatrix}\end{aligned}$$

The disturbance noise has the form  $\bar{\mathbf{w}}_1^T(t) = [\bar{\mathbf{w}}^T(t), v_m(t)]$  with covariance matrix

$$\begin{aligned}E\{\bar{\mathbf{w}}_1(t) \bar{\mathbf{w}}_1^T(\sigma)\} &= W_1 \delta(t-\sigma) \\ W_1 &= \begin{bmatrix} W & 0 \\ 0 & V_m \end{bmatrix}\end{aligned}\tag{B.14}$$

The Kalman filter generates an estimate,  $\hat{\bar{\mathbf{x}}}(t)$  of the model states  $\bar{\mathbf{x}}(t)$  from

$$\begin{aligned}\hat{\bar{\mathbf{x}}}(t-\tau) &= A_1 \hat{\bar{\mathbf{x}}}(t-\tau) + b_1 u(t-\tau) \\ &+ \Sigma_1 C_1^T V^{-1} [y_p(t) - C_1 \hat{\bar{\mathbf{x}}}(t-\tau)]\end{aligned}\tag{B.15}$$

where the error covariance matrix,  $\Sigma_1$ , is the solution of

$$A_1 \Sigma_1 + \Sigma_1 A_1^T + D_1^T W_1 D_1 - \Sigma_1 C_1^T V^{-1} C_1 \Sigma_1 = 0 \quad (B.16)$$

The least mean squared predictor is governed by the equation

$$\dot{\bar{\xi}}(t) = A_1 \bar{\xi}(t) + b_1 \mu(t) \quad (B.17)$$

Finally, the current state estimate is found by combining the Kalman state estimate and the predicted state through the relation

$$\bar{p}(t) = \bar{\xi}(t) + e^{A_1 \tau} [\hat{\chi}(t-\tau) - \bar{\xi}(t-\tau)] \quad (B.18)$$

In order to apply the optimal control model, it is necessary to know the various human response parameters  $\tau, \tau_n, V_y, V_m$  introduced above. Published data in manual control [14] indicates that typical values for the effective time delay are  $\tau=0.15-0.25$  secs. The neuromotor lag time constant  $\tau_n$  is of the order of  $\tau_n=0.1-0.6$  secs with  $\tau_n \approx 0.1$  being typical [23]. It should be noted that results reported in [14] indicate that  $\tau_n$  varies inversely with forcing function bandwidth.

Investigation of the properties of human controller remnant [24] have shown that the sources of remnant can be modeled on the basis of constant noise to signal ratios. Thus the observation noise associated with the  $i^{\text{th}}$  observed variable  $y_i$  has an intensity

$$(v_y^0)_{ii} = \rho_{yi} E\{y_i^2\} \quad (B.19)$$

where the constant  $\rho_{yi}$  is based on the human controller's attention being limited to the  $i^{\text{th}}$  observation only. Similarly, the motor-noise  $v_m(t)$  is modeled to have an intensity given by

$$v_m = \rho_u E\{u_p^2\} \quad (B.20)$$

The constants  $\rho_{yi}$  and  $\rho_u$  are referred to as observation noise ratio and

motor-noise ratio respectively, and are generally specified in terms of their decibel values. Model matching analyses have shown values of  $\rho_{y1}=0.01\pi$  (-20 dB) and  $\rho_u=0.003\pi$  (-25 dB) to provide a good fit with experimental data for manual control tasks involving single-axis tracking. These ratios have much higher values for complex multi-control tasks. Since the noise intensities are specified as ratios of the closed loop intensities of the corresponding signals, an iterative process is necessary to determine the optimal control model for which the relations (B.19) and (B.20) are satisfied.

Studies of human perception abilities have shown that if a quantity  $y_1$  is displayed explicitly to the human operator, he can extract the rate of change of that quantity,  $\dot{y}_1$ . Thus the rates of the displayed quantities should be included in the pilot's observation vector  $\bar{y}_p$ . Furthermore, if the human controller has more than one explicitly displayed observation available to him, his attention is divided between the various displays. The error induced due to this division of attention is modeled by modifying the observation noise corresponding to the  $i^{\text{th}}$  displayed variable as

$$(\dot{v}_y')_{11} = \frac{(v_y^0)_{11}}{f_1} \quad (\text{B.21})$$

where  $(v_y^0)_{11}$  is as given by Eqn. (B.19). Here  $f_1$  is the fraction of total attention allocated to the  $i^{\text{th}}$  observed variable and has limiting values at no attention ( $f_1=0$ ) and full attention ( $f_1=1$ ) [15]. The values of  $f_1$  are generally determined on the basis of the importance of that particular observation in successfully accomplishing the task as modeled by (B.3).

If a particular signal  $y_i$  is very small in magnitude, the human controller may not be able to detect its non-zero value (visual threshold) or may choose not to react to the small perturbations (indifference thresholds). This aspect of the human controller is modeled by modifying the observation noise intensity corresponding to the  $i^{\text{th}}$  displayed variable as

$$(v_y)_{ii} = \frac{(\dot{v}_y)_{ii}}{(N(\sigma_{yi}, \alpha_i))^2} \quad (\text{B.22})$$

where  $\sigma_{yi} = E\{y_i^2\}$  and  $N$  is the describing function of a dead-zone element [6].  $(\dot{v}_y)_{ii}$  is as obtained from (B.21) and  $\alpha_i$  is the value of the threshold for the  $i^{\text{th}}$  observation. Pyscophysical studies have shown that these thresholds typically correspond to values of 0.05 deg and 0.15 deg/sec at the pilot's eye. Also, a reasonable value for these thresholds is the minimum resolution marking on the display.

Finally, combining (B.19), (B.21), and (B.22), the intensity of the observation noise  $v_{yi}$  to be used in (B.2) to model the imperfections in the pilot's observations, is obtained to be

$$(v_y)_{ii} = \frac{\rho_{yi}}{f_i} \frac{\sigma_{yi}^2}{(N(\sigma_{yi}, \alpha_i))^2} \quad (\text{B.23})$$

with all the relevant quantities defined as above.

APPENDIX CANALYSIS RESULTS FOR  $K/s^2$  PLANT

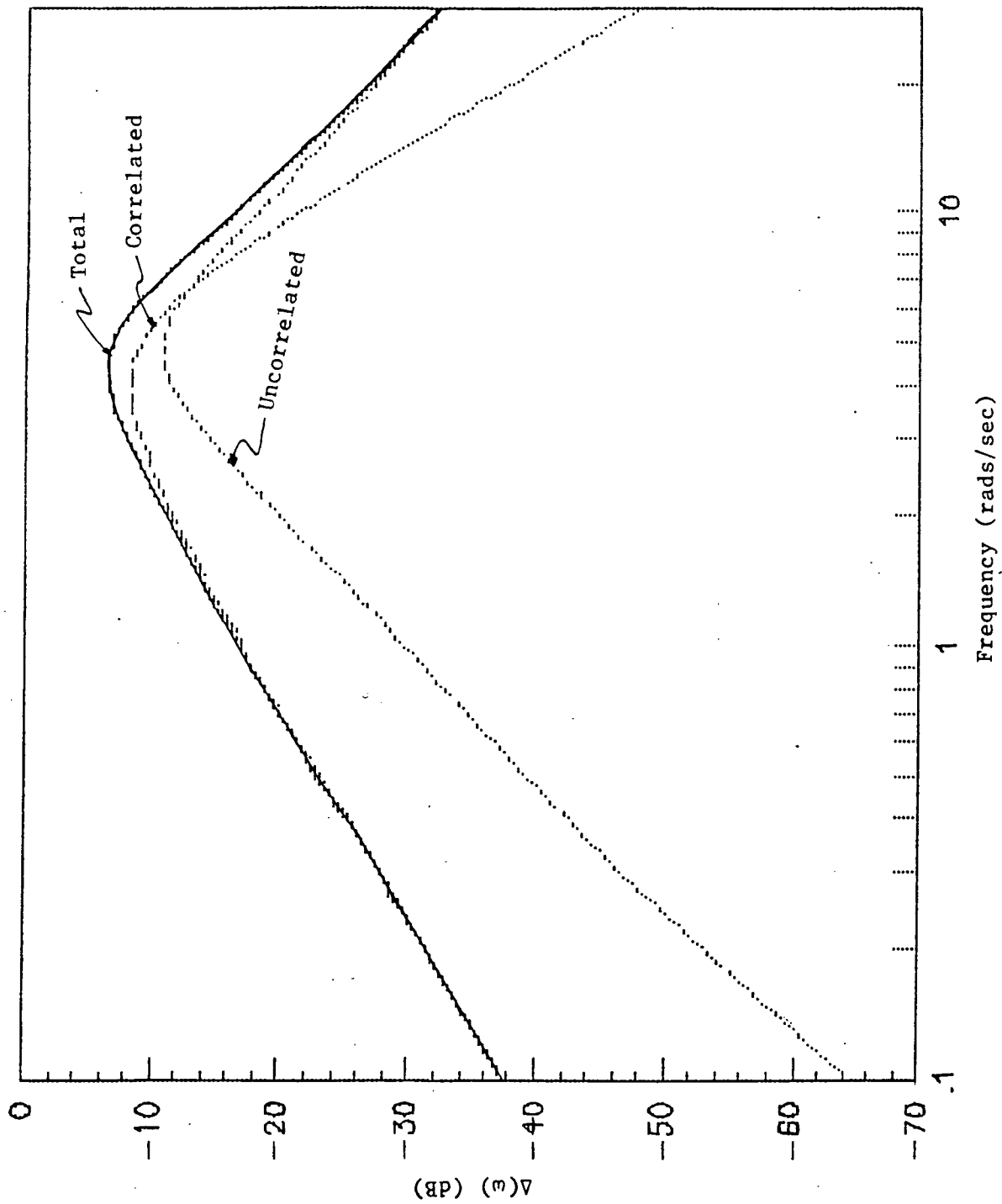


Figure C.1 Control Spectrum for Limiting Case - A

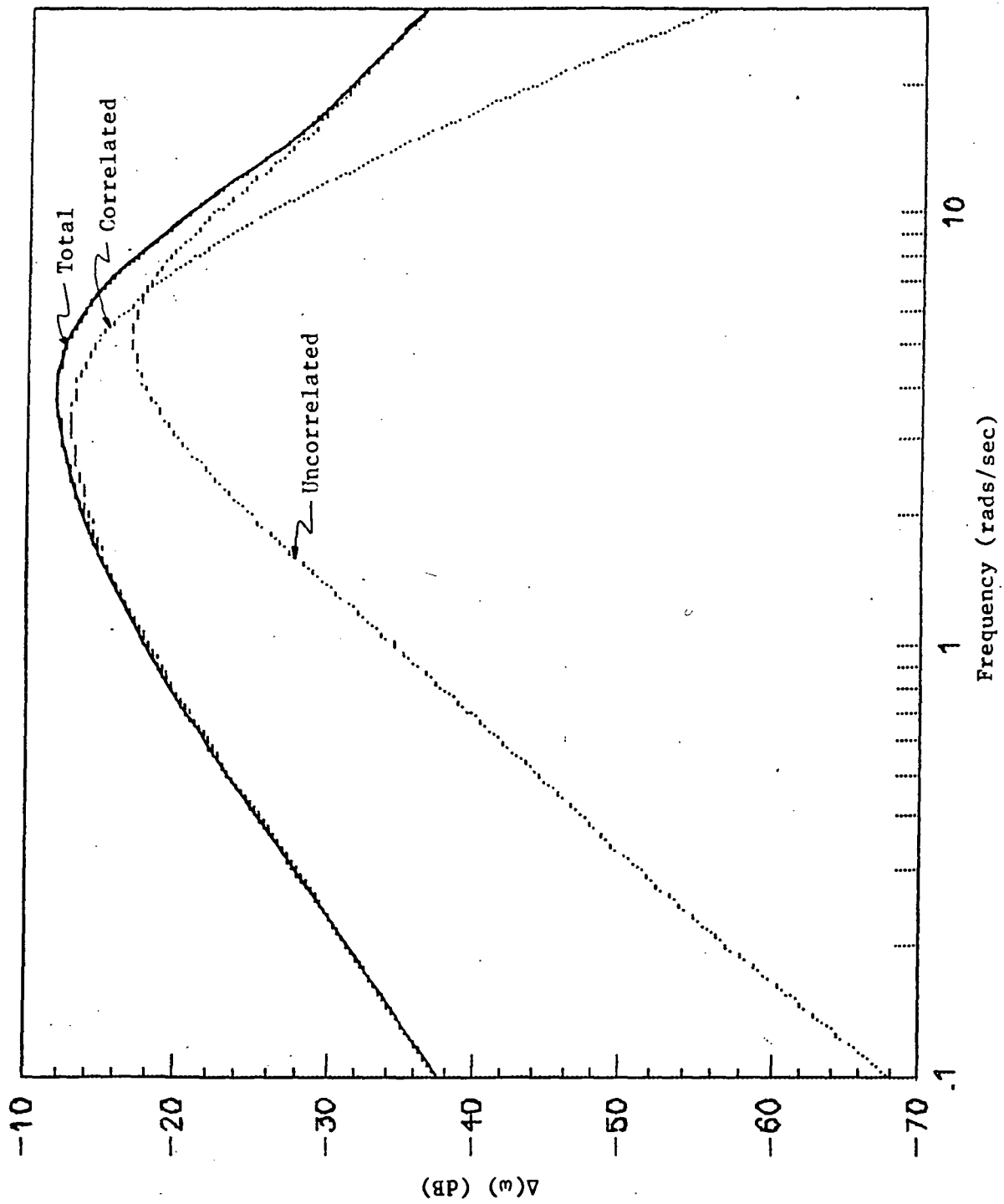


Figure C.2 Control Spectrum for Display 1

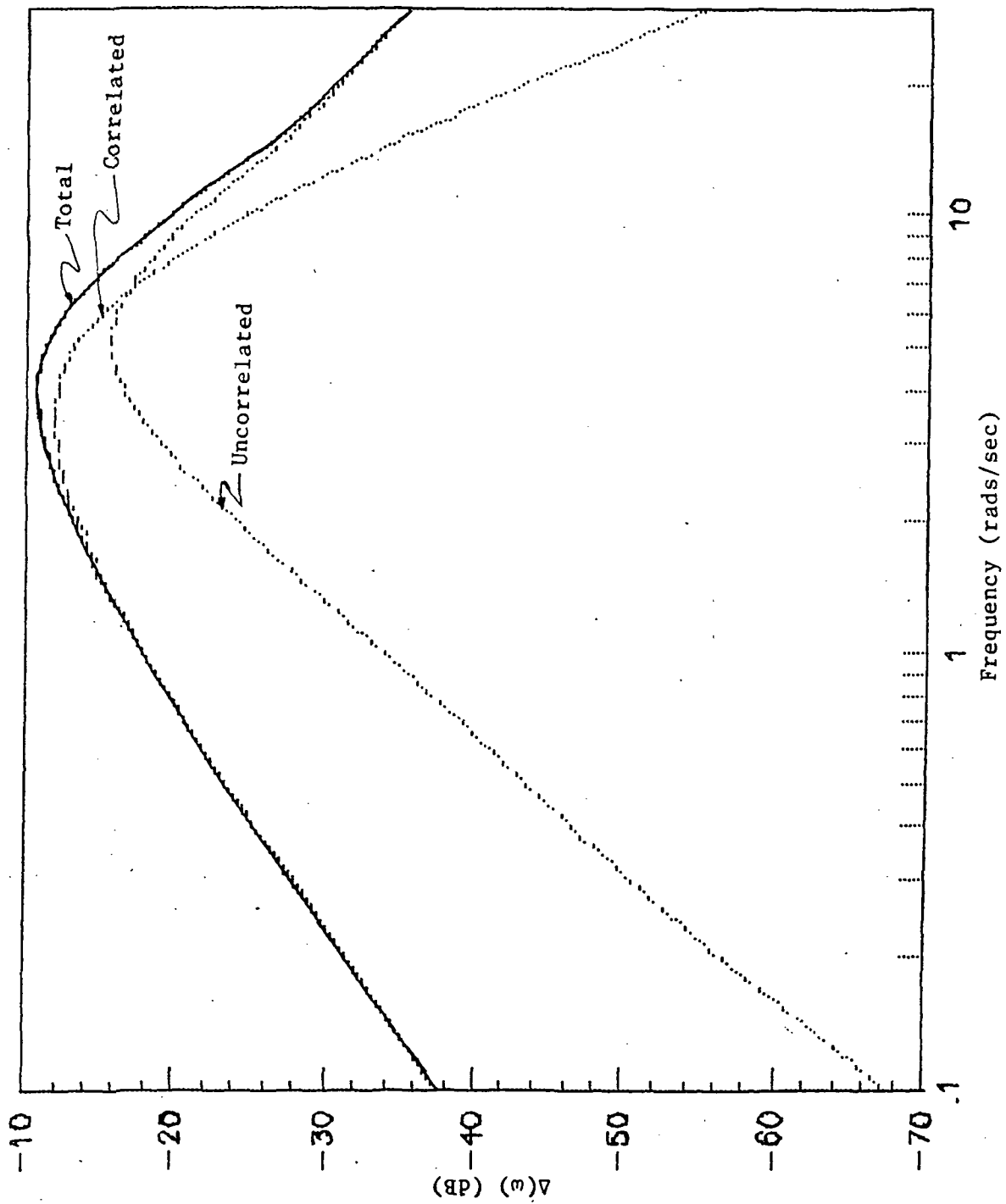


Figure C.3 Control Spectrum for Display 2



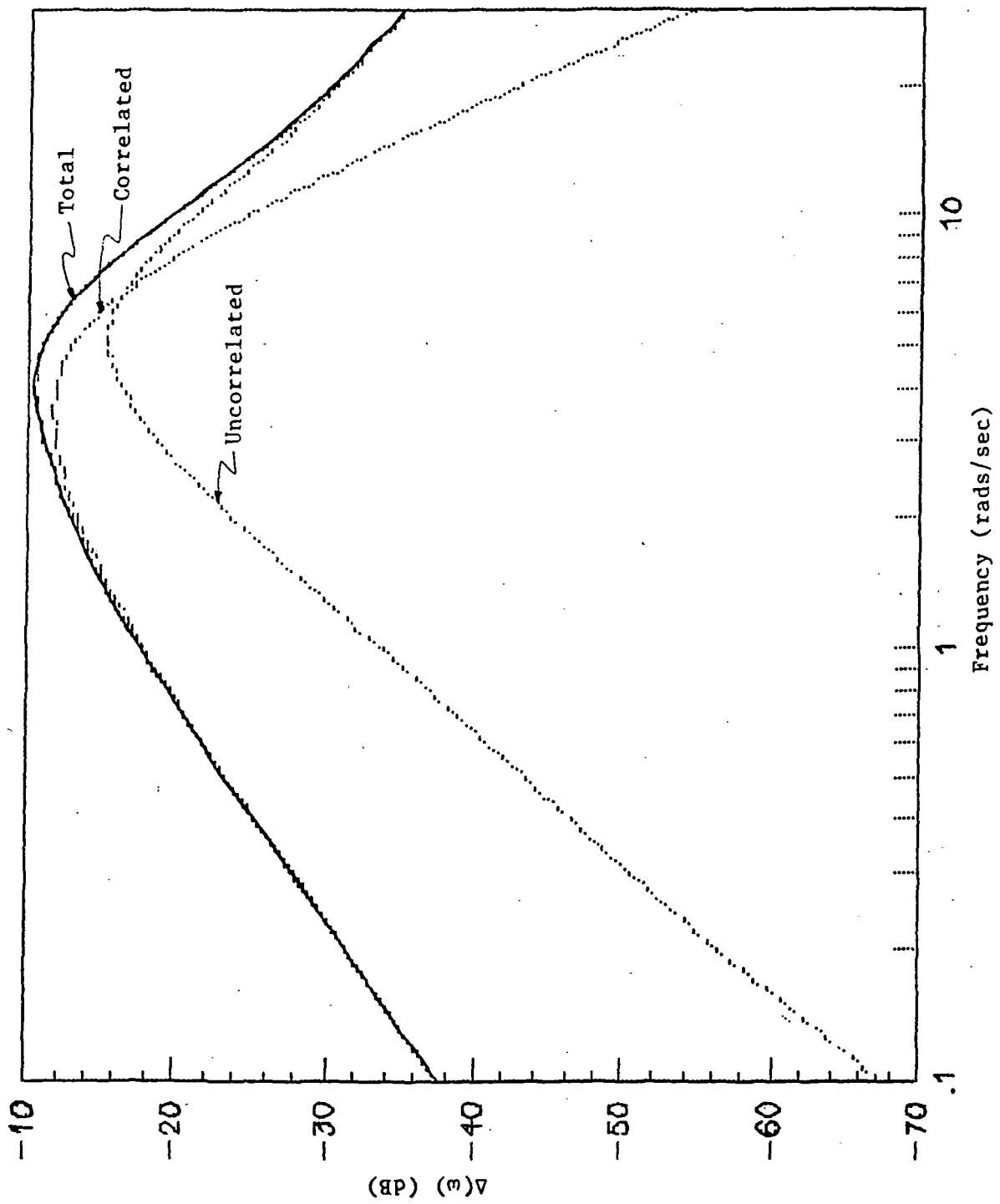


Figure C.4 Control Spectrum for Display 3

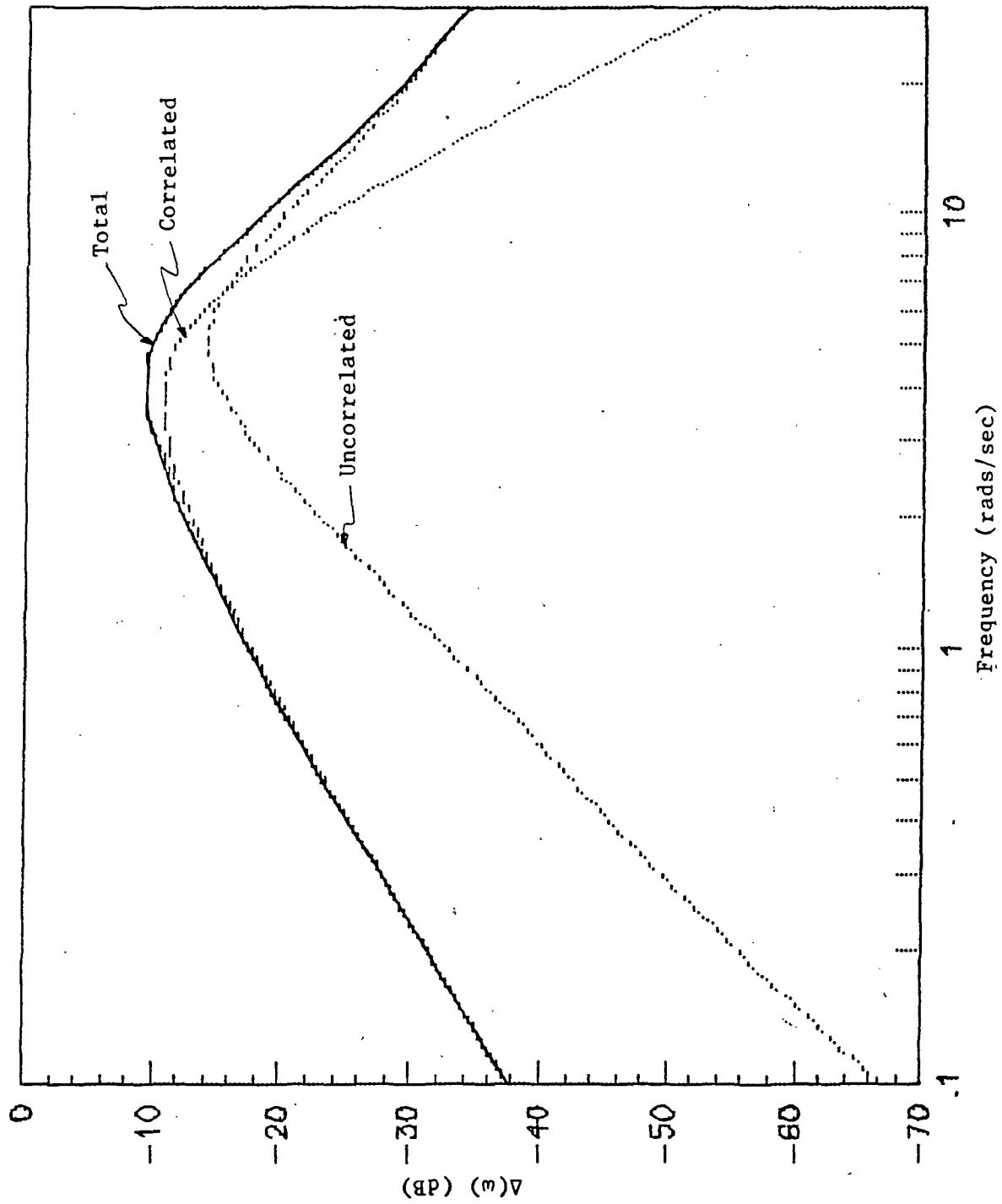


Figure C.5 Control Spectrum for Display 4

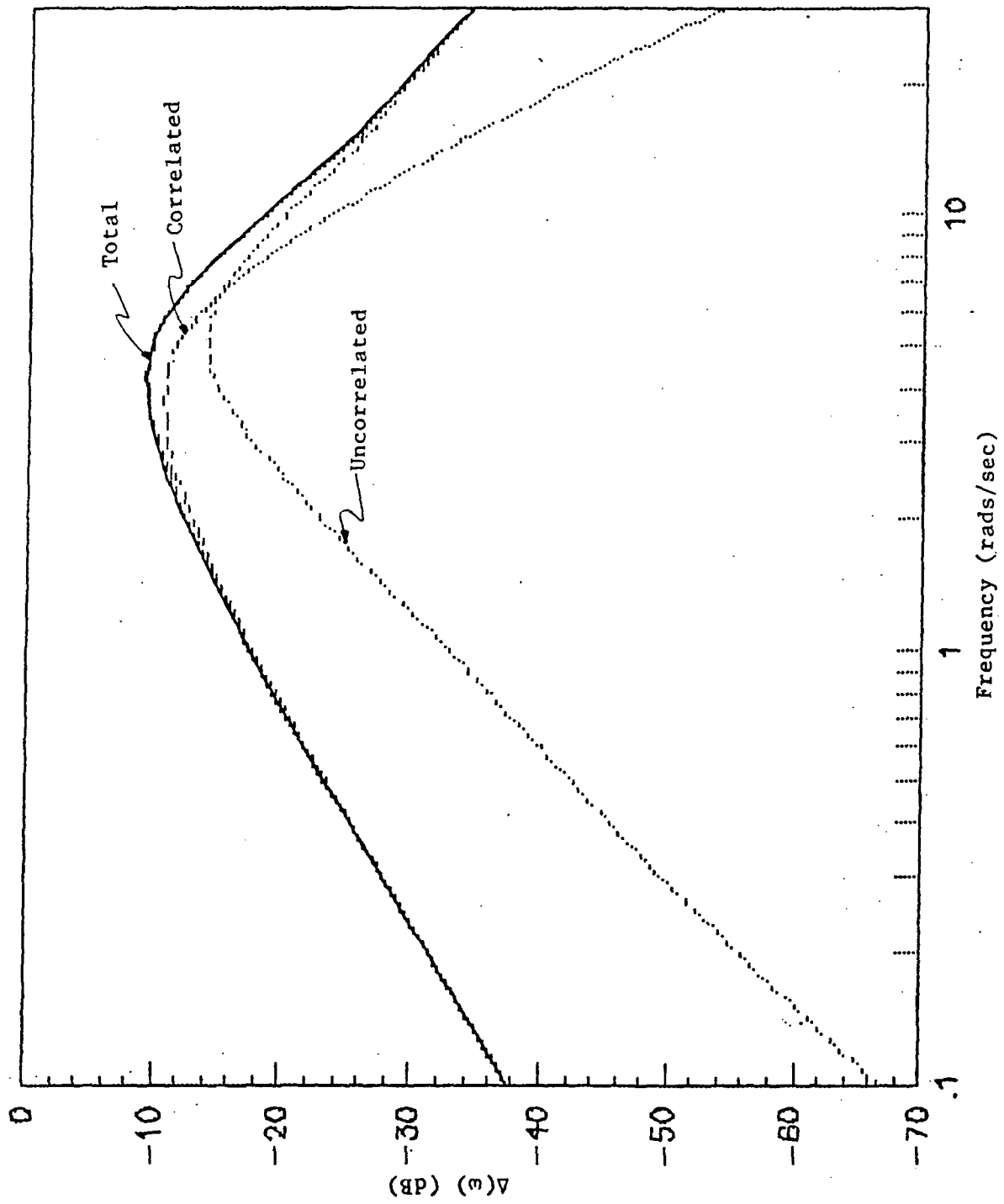


Figure C.6 Control Spectrum for Display 5

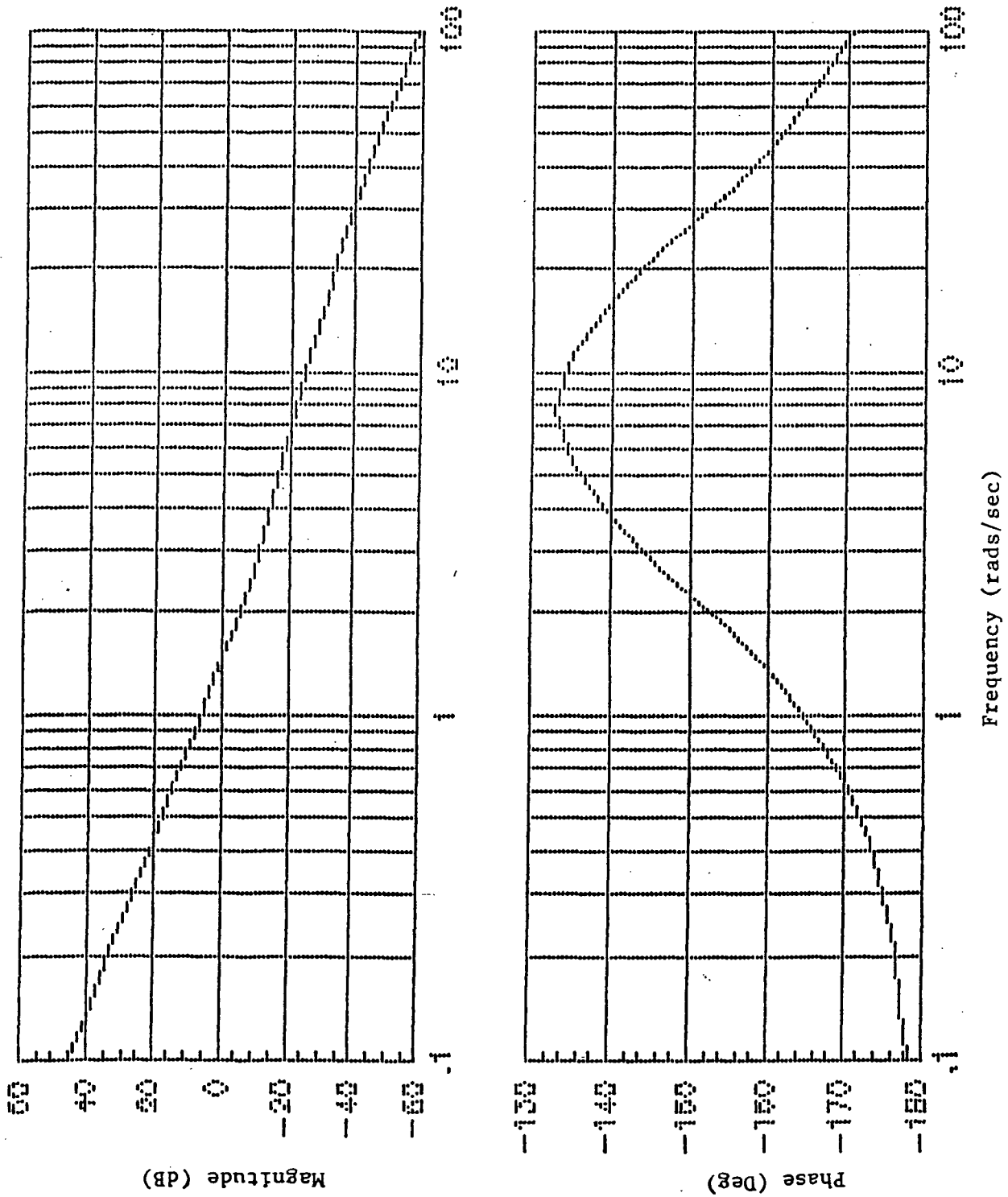
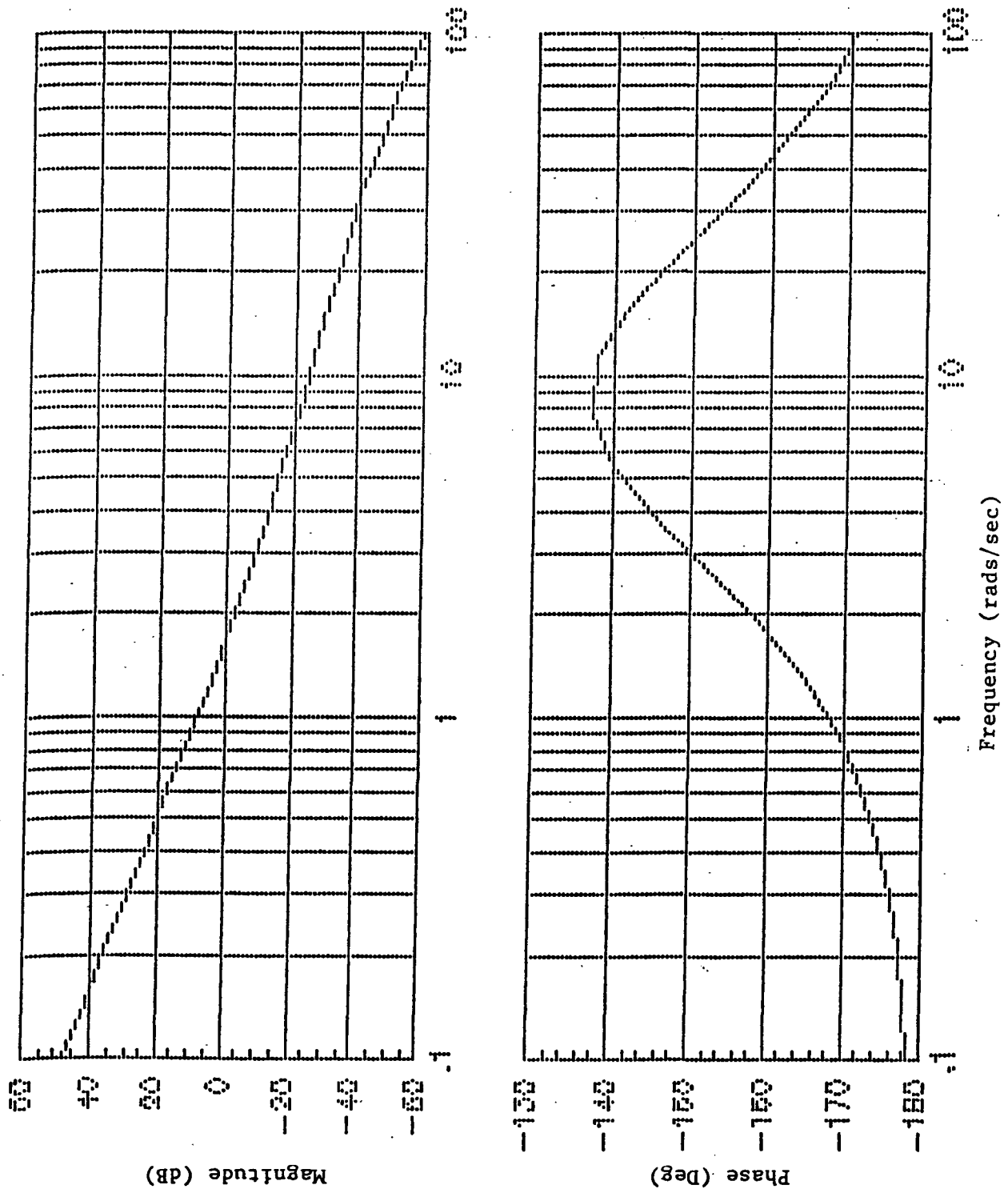


Figure C.7 Bode-plots of  $K/s^2$  Plant Plus Display 1

Figure C.8 Bode-plots of  $K/s^2$  Plant Plus Display 2

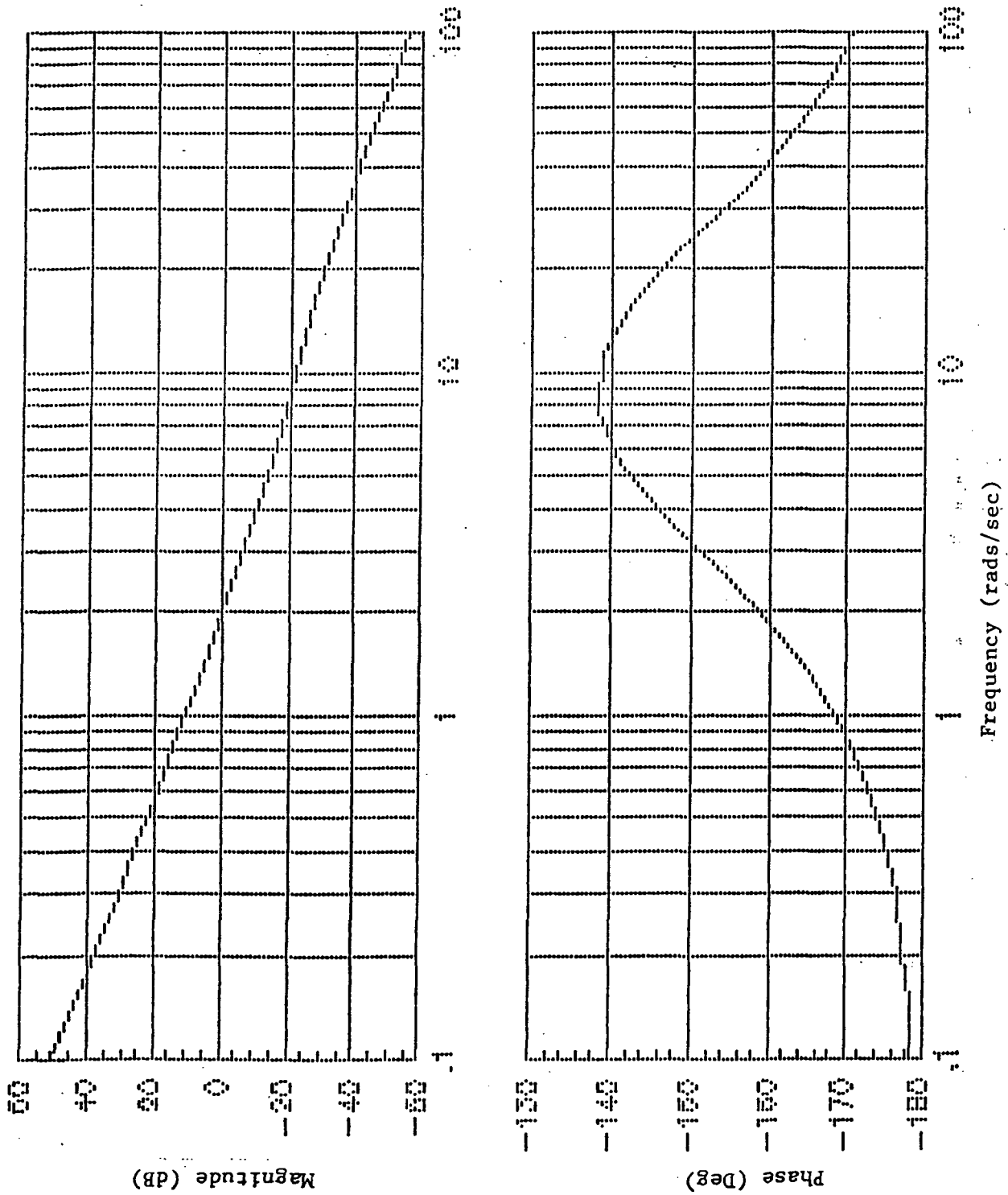


Figure C.9 Bode-plots of  $K/s^2$  Plant Plus Display 3

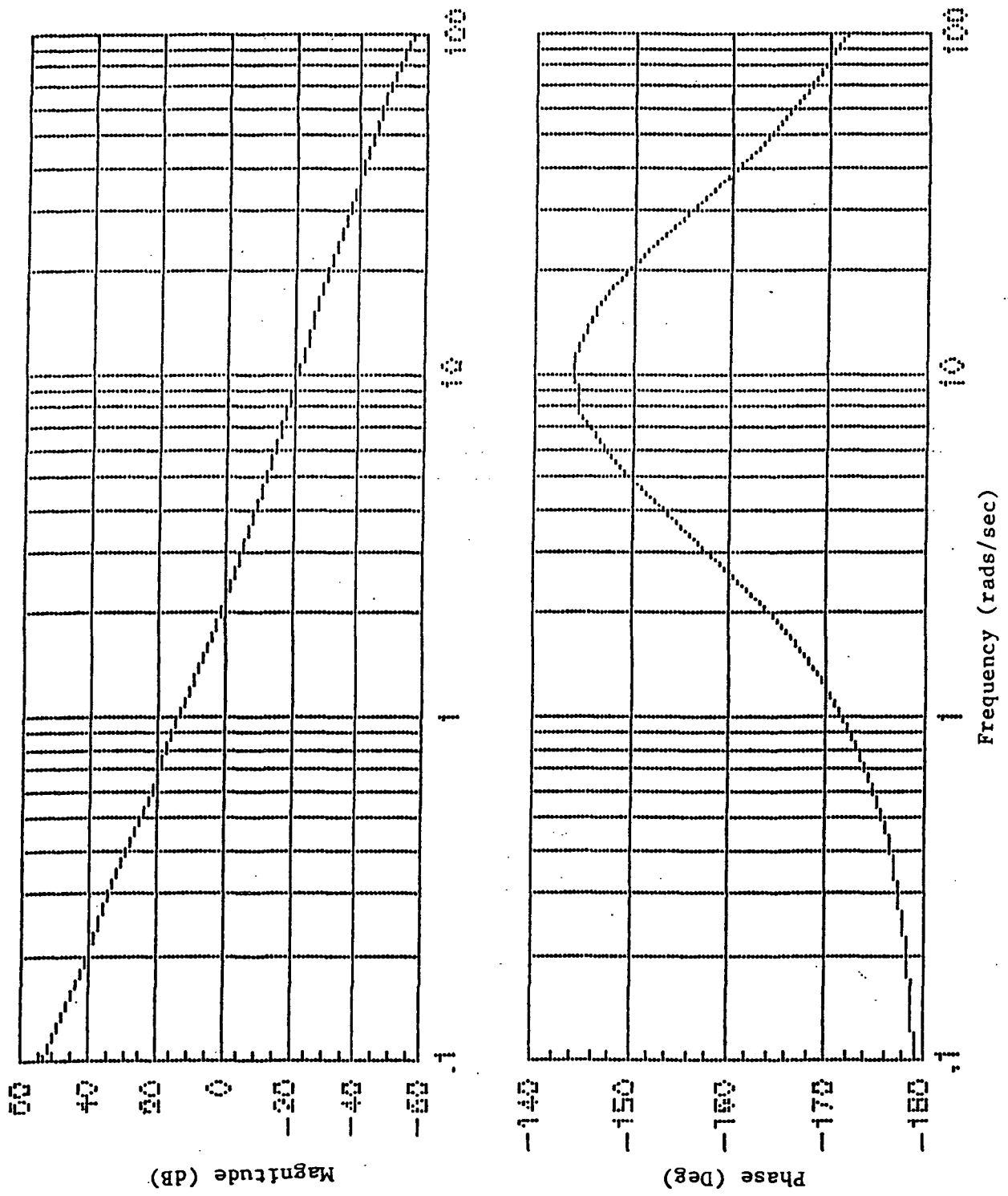


Figure C.10 Bode-plots of  $K/s^2$  Plant Plus Display 4

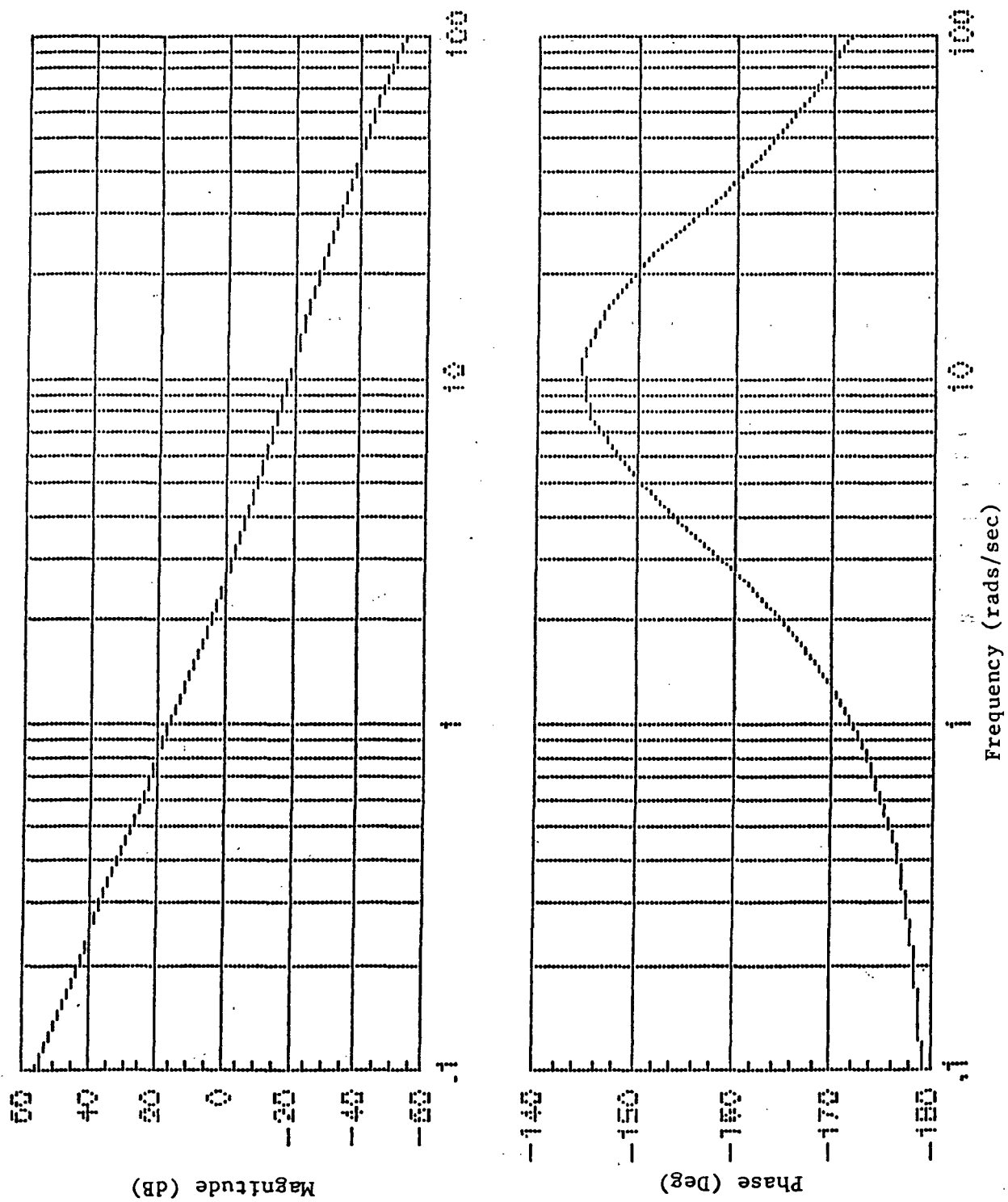


Figure C.11 Bode-plots of  $K/s^2$  Plant Plus Display 5



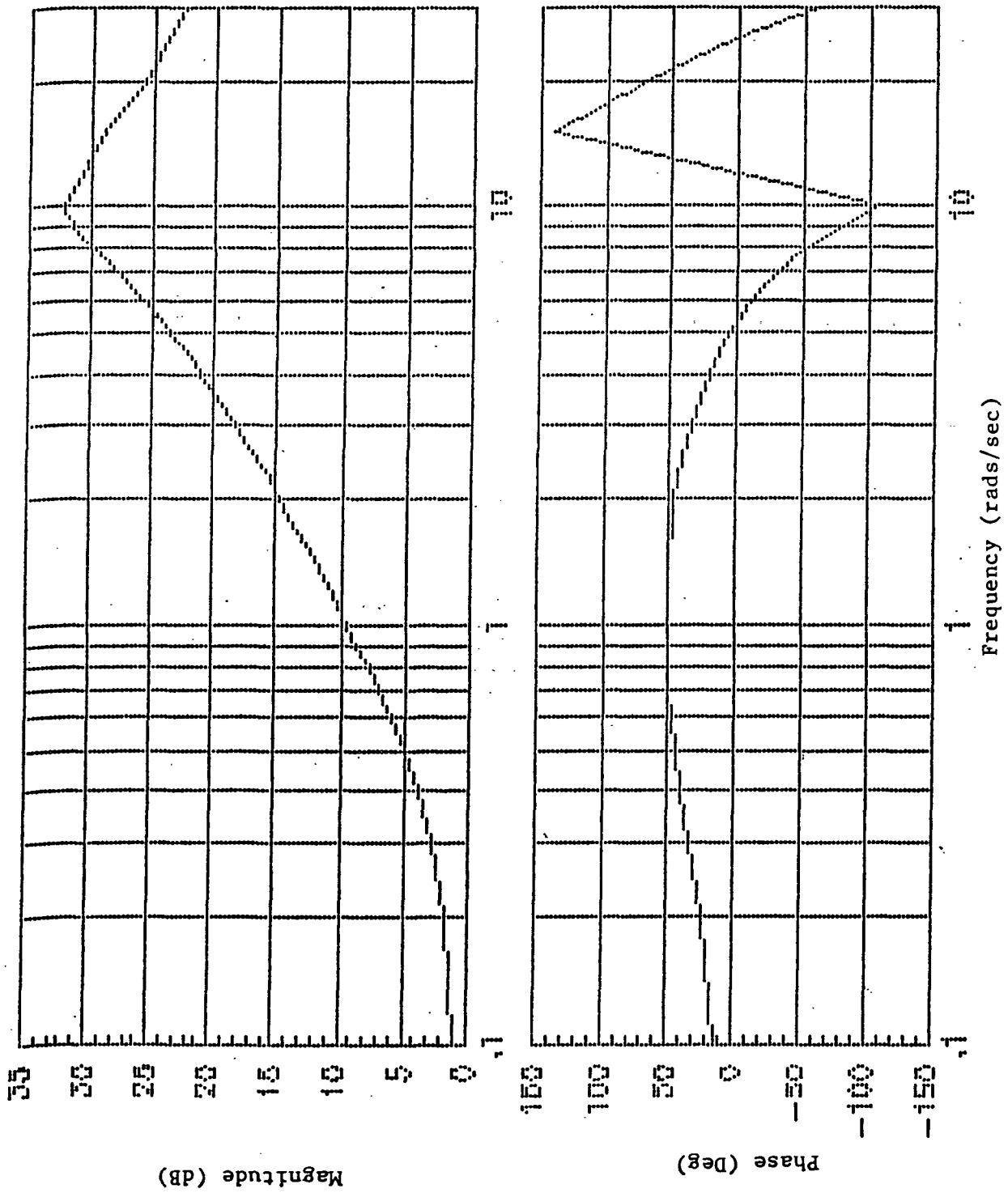


Figure C.12 Pilot Describing Function for Limiting Case - A

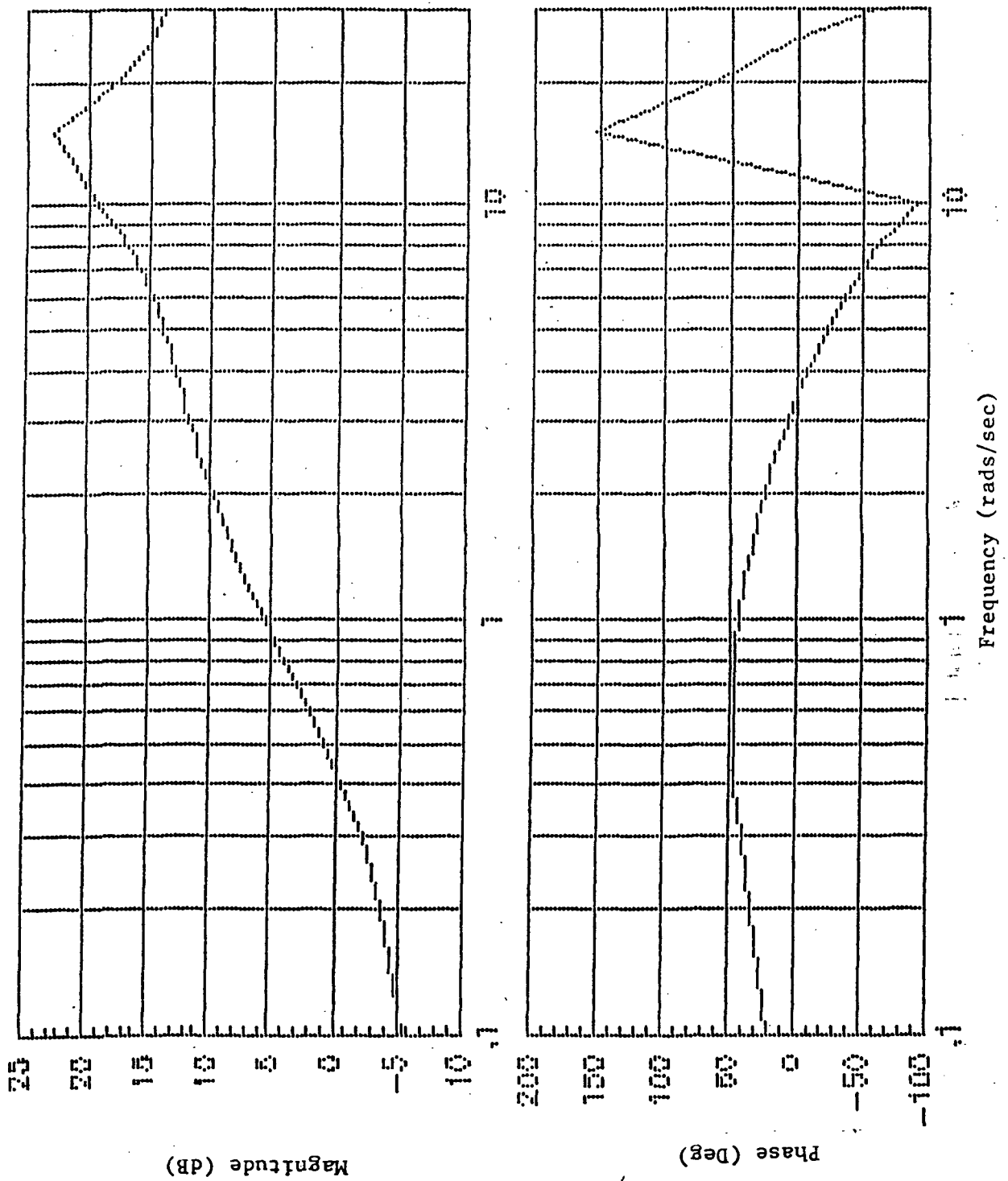


Figure C.13 Pilot Describing Function for Display 1

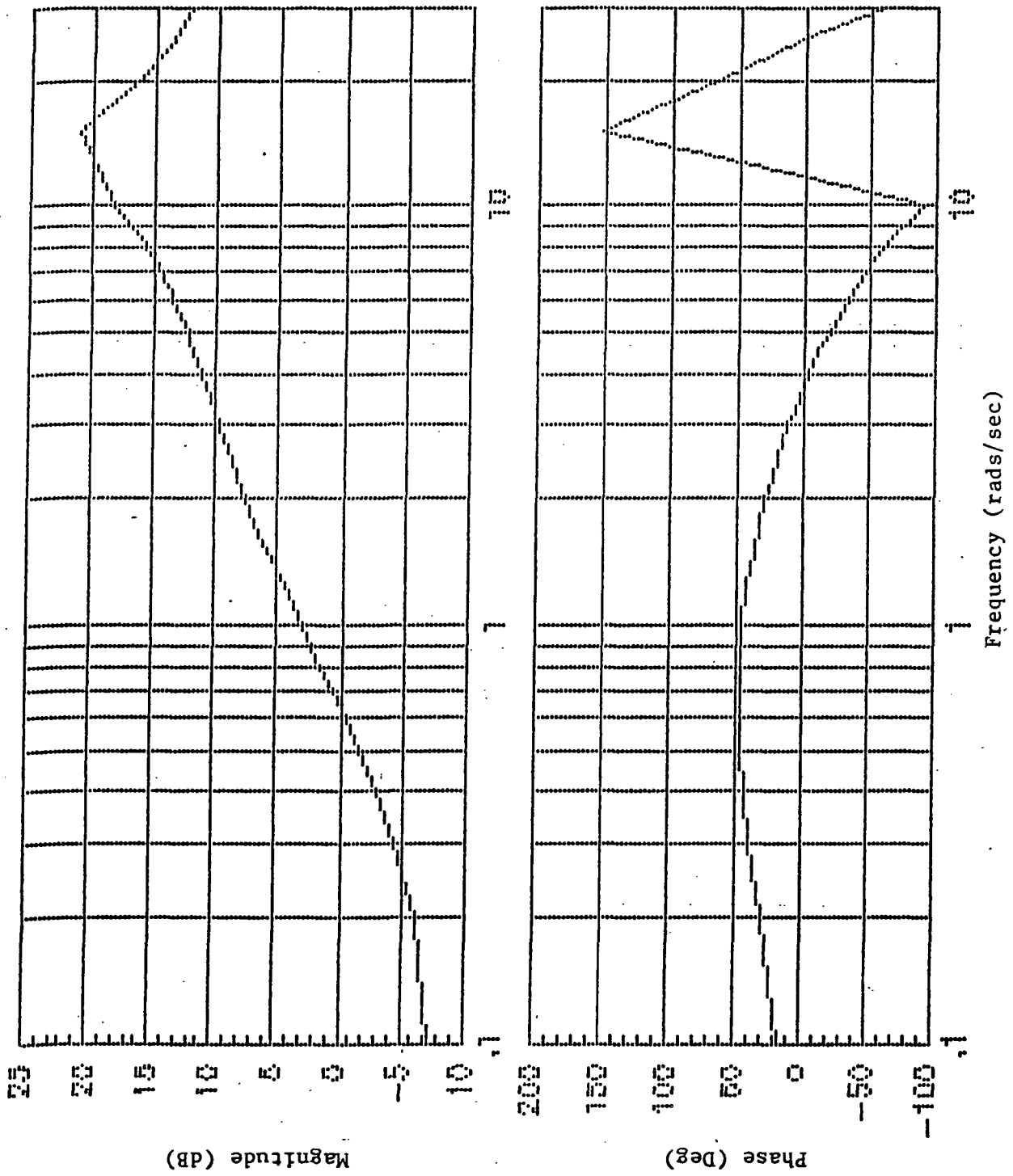


Figure C.14 Pilot Describing Function for Display 2

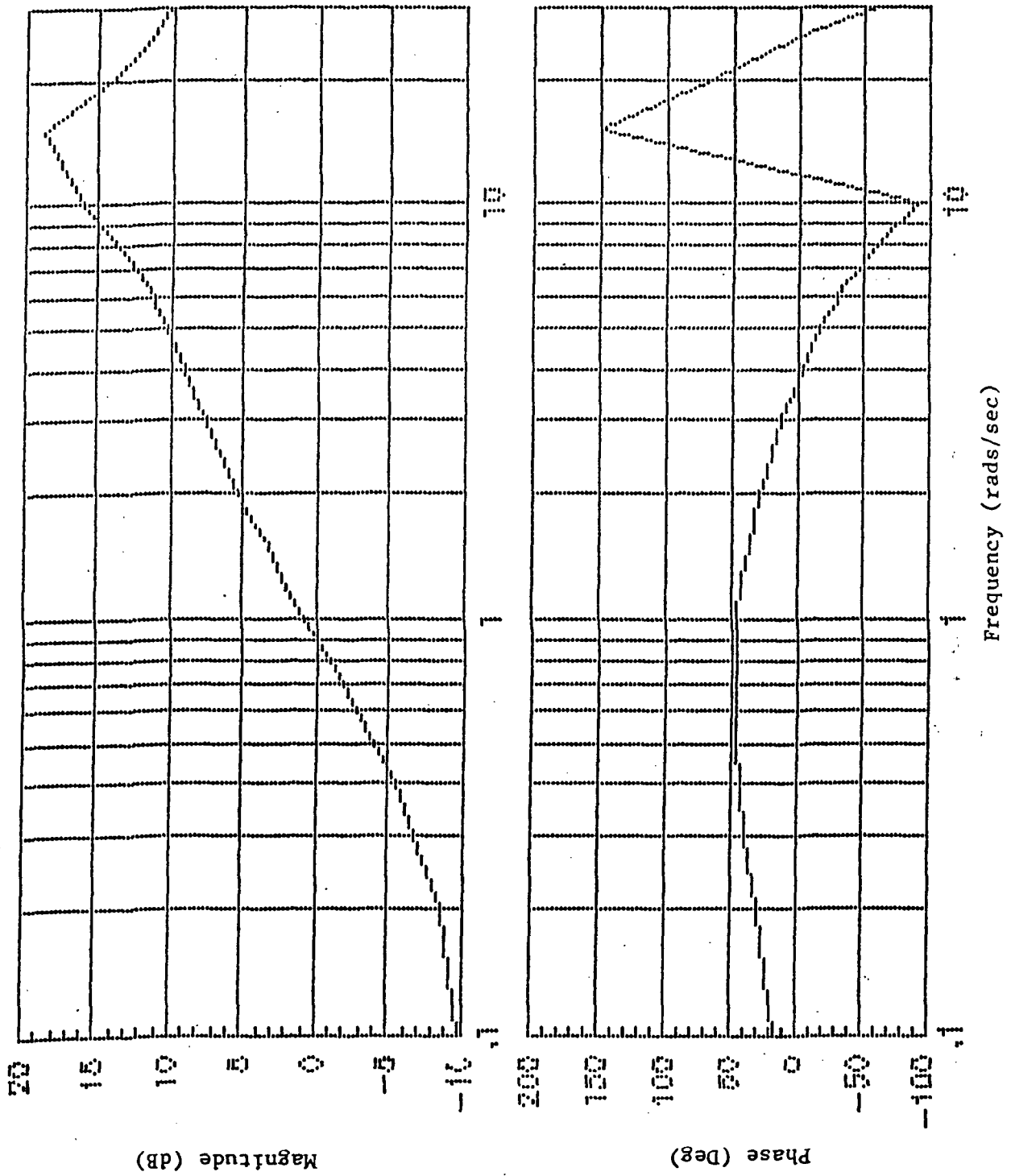


Figure C.15 Pilot Describing Function for Display 3

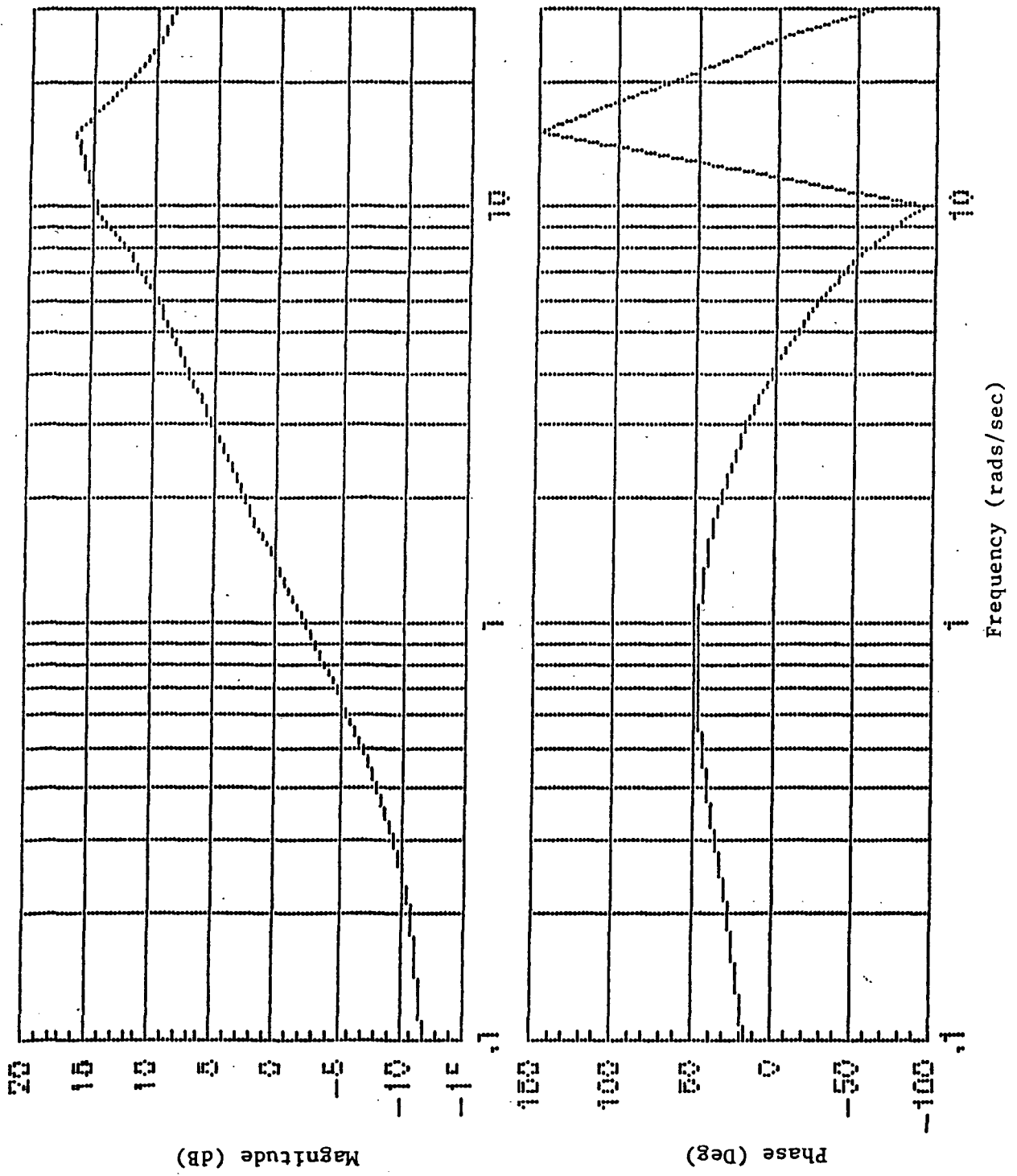


Figure C.16 Pilot Describing Function for Display 4

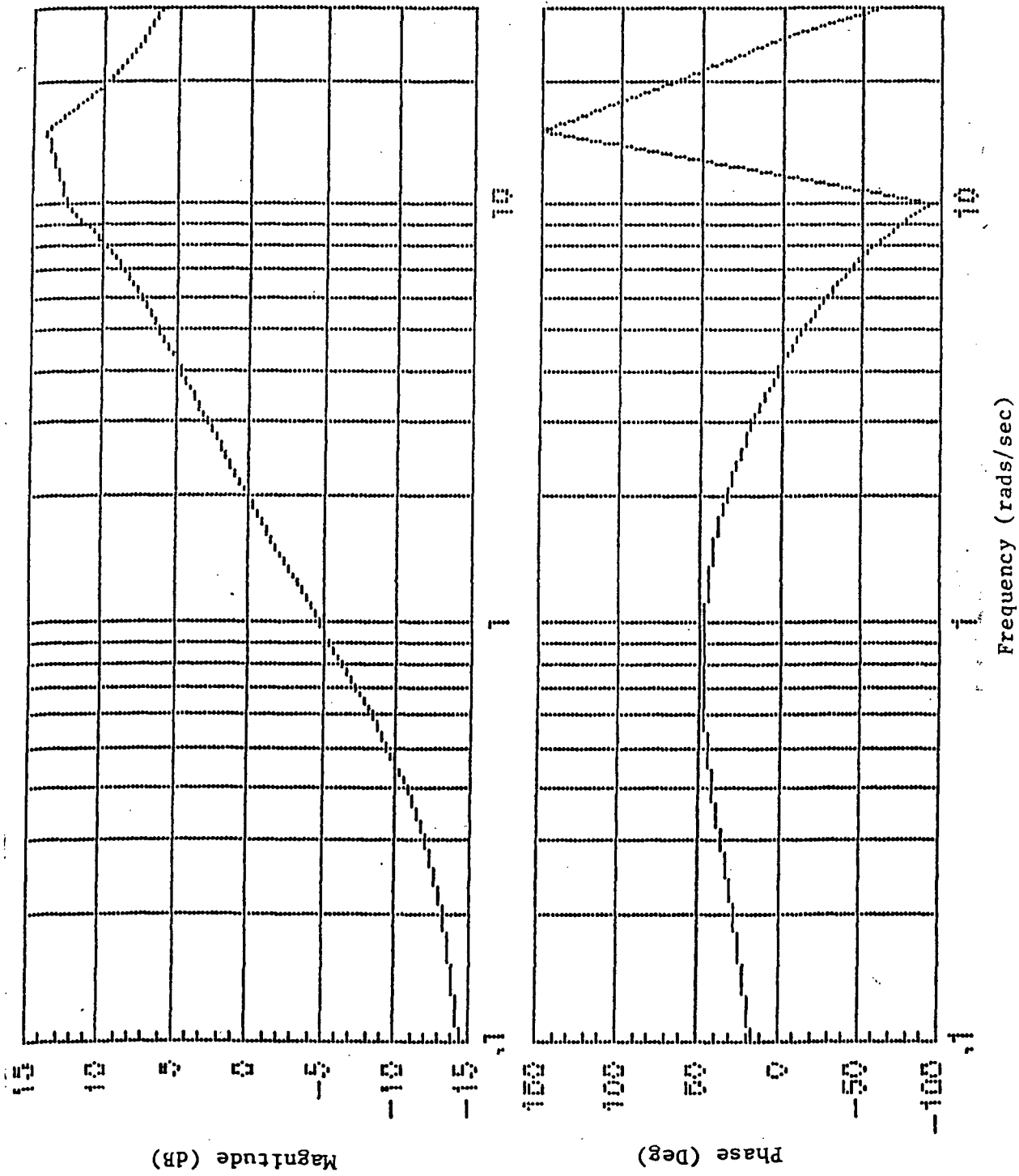


Figure C.17 Pilot Describing Function for Display 5

APPENDIX D

DATA AND ANALYSIS RESULTS FOR F-15 AIRCRAFT

TABLE D.1: TRIM CONTIIONS FOR F-15 MODEL

Altitude	$h_o$	32,000 ft.
Angle of Attack	$\alpha_o$	$11^\circ$
Pitch Angle	$\theta_o$	$11^\circ$
Mach Number	$M_o$	.4775
Velocity	$V_o$	470.9 ft/sec
Thrust	$T_o$	6270 $lb_f$
Weight	$W_o$	40,700 $lb_f$
Elevator	$\delta e_o$	$-4.76^\circ$
Dynamic Force	$\bar{q}_s$	55,821.1 $lb_f$



TABLE D.2: MATRICES  $A_v$  AND  $B_v$  FOR F-15 MODEL

$$A_v = \begin{bmatrix} -0.0019 & -0.3072 & 0. & -0.1222 & 0. & 0.9816 \\ -0.0009 & -0.3420 & 1.0000 & -0.0541 & 0. & 0.0019 \\ 0.0235 & -1.5480 & -0.9870 & -3.8000 & 0. & -0.0001 \\ 0. & 0. & 1.0000 & 0. & 0. & 0. \\ 0. & 0. & 0. & -20.0000 & 0. & 0. \\ 0.1014 & 0. & 0. & 0. & -0.1000 & 0. \\ 0. & 0. & 0. & 0. & 0. & -0.1050 \end{bmatrix}$$

$$B_v = \begin{bmatrix} 0. & 0. & 0. & 0. & 0. & 0. \\ 0. & 0. & 0. & 0. & 0. & 0. \\ 0. & 0. & 0. & 0. & 0. & 0. \\ 20.0000 & 0. & 0. & 0. & 0. & 0. \\ 0. & 0. & 0. & 0. & 0. & 0. \\ 0. & 0. & 0. & 0. & 0. & 0.1050 \end{bmatrix}$$

TABLE D.3: PILOT OBSERVATION MATRICES FOR STATUS DISPLAY

$$C_o = \begin{bmatrix} \text{COLUMNS 1 THRU 7} \\ 1.0000 & 0. & 0. & 0. & 0. & 0. & 0. \\ 0. & 1.0000 & 0. & 0. & 0. & 0. & 0. \\ 1.0000 & 0. & 0.0041 & 1.6105 & 0. & 0. & 0.2548 \\ 0. & 1.0000 & -0.0015 & -0.5521 & 1.6105 & -0.0013 & -5.1840 \\ 0. & 0. & 0. & 0. & 0. & 0. & 0. \\ 0. & 0. & 0. & 0. & 0. & 0. & 0. \\ 0. & 0. & 0. & 0. & 0. & 0. & 0. \\ 0. & 0. & 0. & 0. & 0. & 1.0000 & 0. \\ 0. & 0. & 0. & 0. & 1.0000 & 0. & 0. \end{bmatrix}$$

$$\begin{bmatrix} \text{COLUMNS 8 THRU 9} \\ 0. & 0. \\ 0. & 0. \\ 0. & 0. \\ 0. & 0. \\ 1.0000 & 0. \\ -0.1000 & 0. \\ 0. & 0. \\ 0. & 0. \end{bmatrix}$$

$$E_o = \begin{bmatrix} 0. & 0. & 0. & 0. & 0. & 0. & 0. & 0. & 0. \\ 0. & 0. & 0. & 0. & 0. & 0. & 0. & 0. & 0. \\ 0. & 0. & 0. & 0. & 0. & 0. & 0. & 0. & 0. \\ 5.0960 & 0. & 0. & 0. & 0. & 0. & 0. & 0. & 0. \\ 0. & 0. & 0. & 0. & 0. & 0. & 0. & 0. & 0. \end{bmatrix}$$

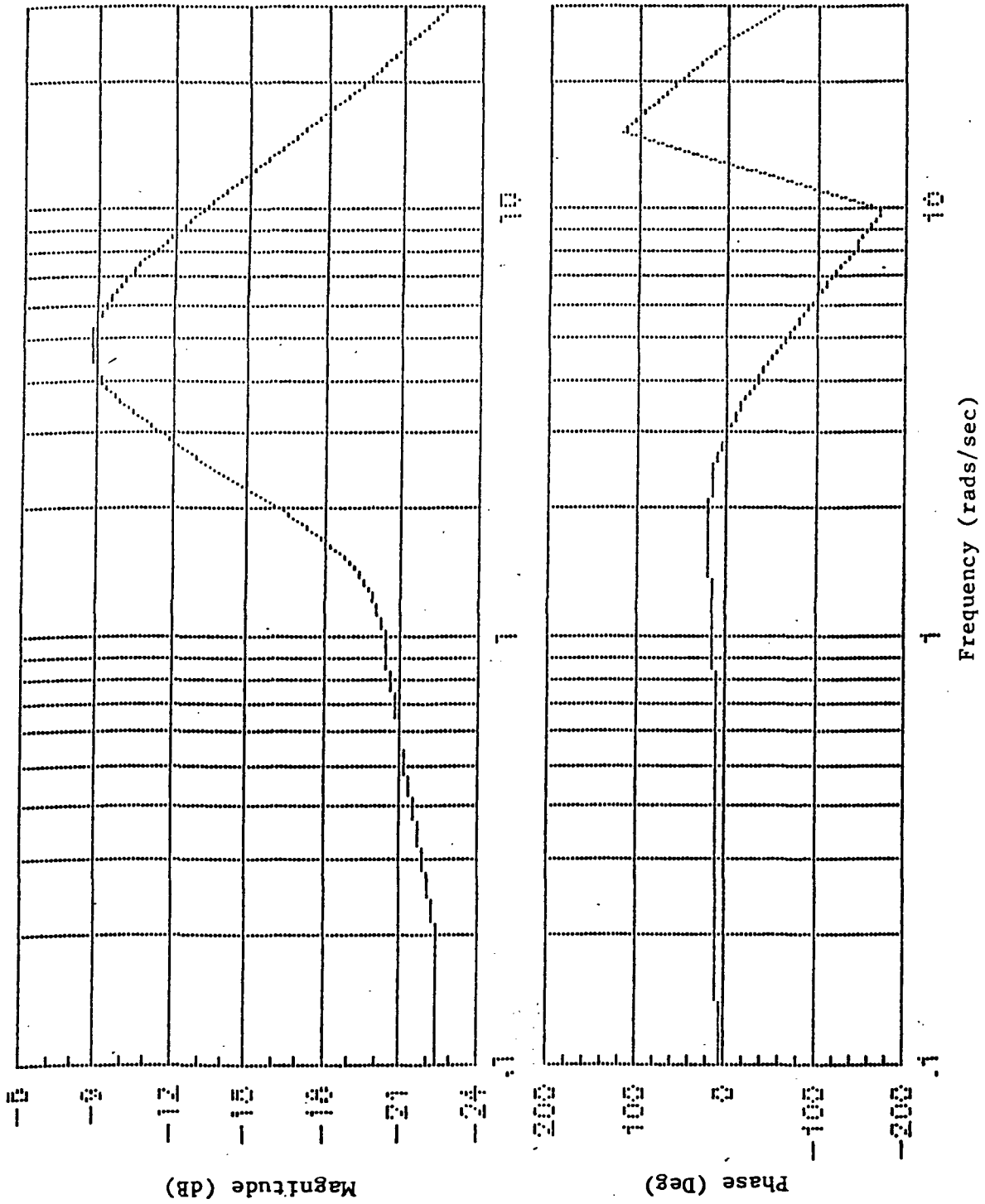


Figure D.1 Pilot Describing Function  $P_{\frac{\delta e}{a_{zc}}}$   
for Status Display

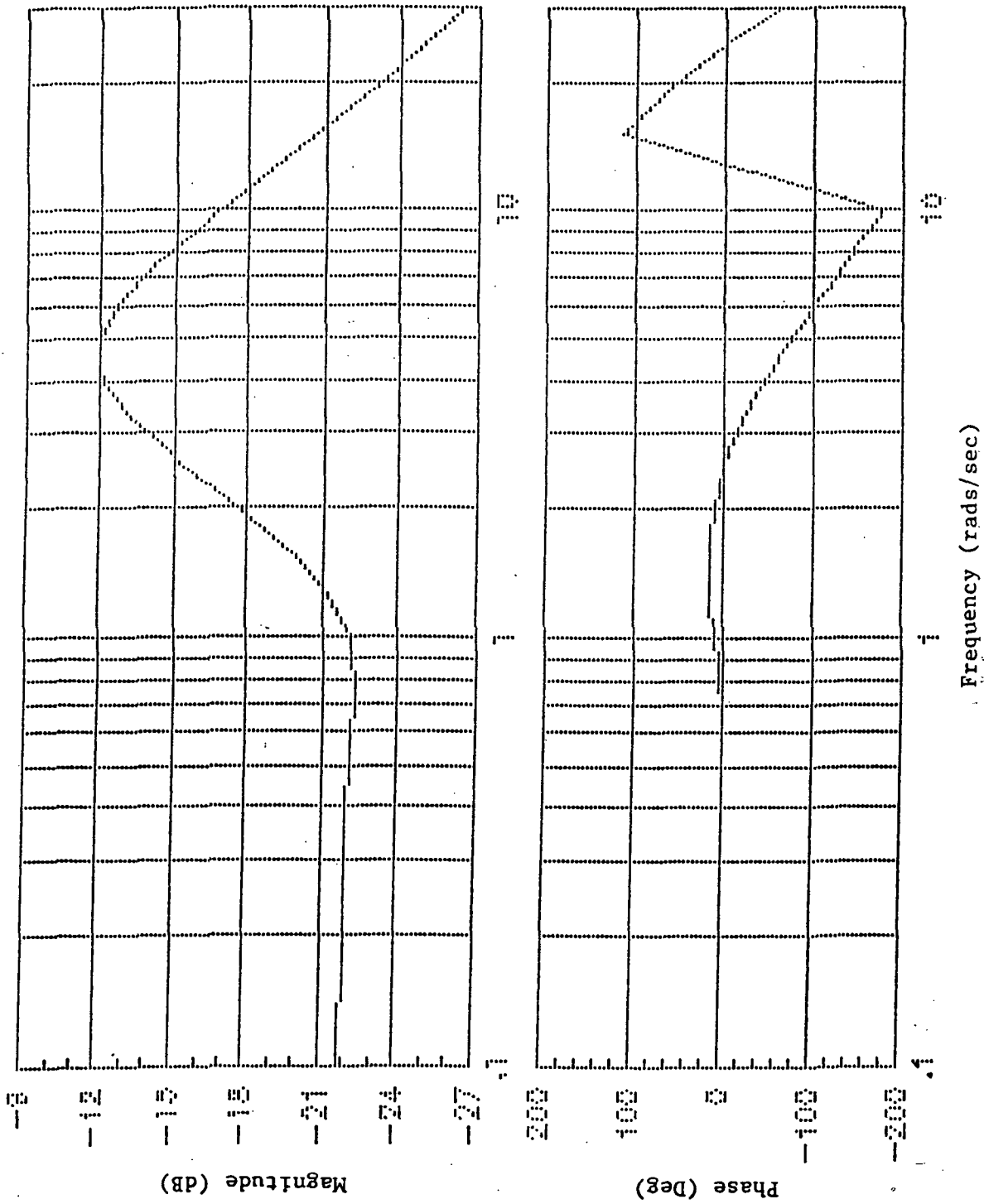


Figure D.2 Pilot Describing Function  $P_{\frac{\delta e}{e_{az}}}$   
for Status Display

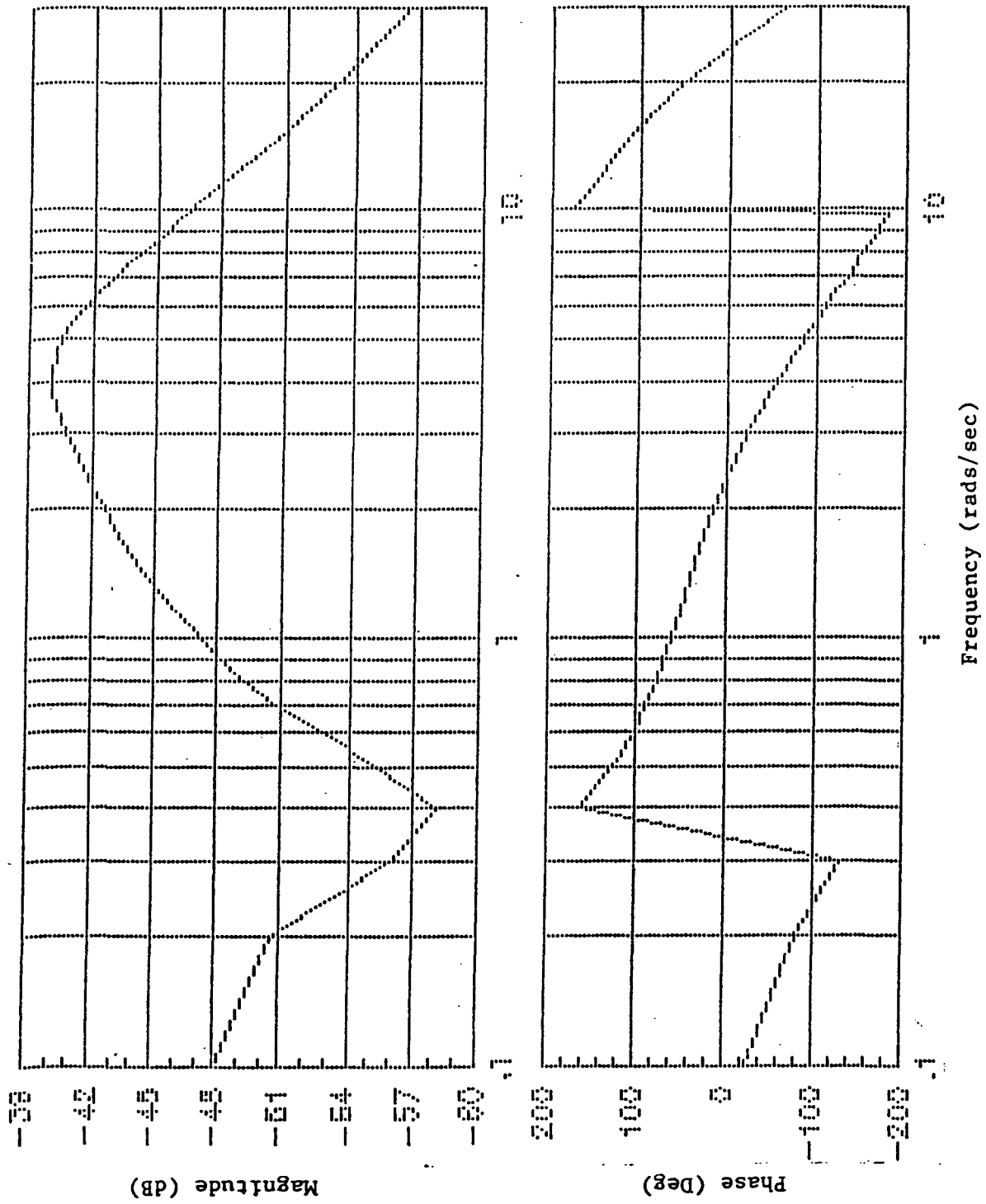


Figure D.3 Pilot Describing Function  $P_{\delta e} / M$   
for Status Display

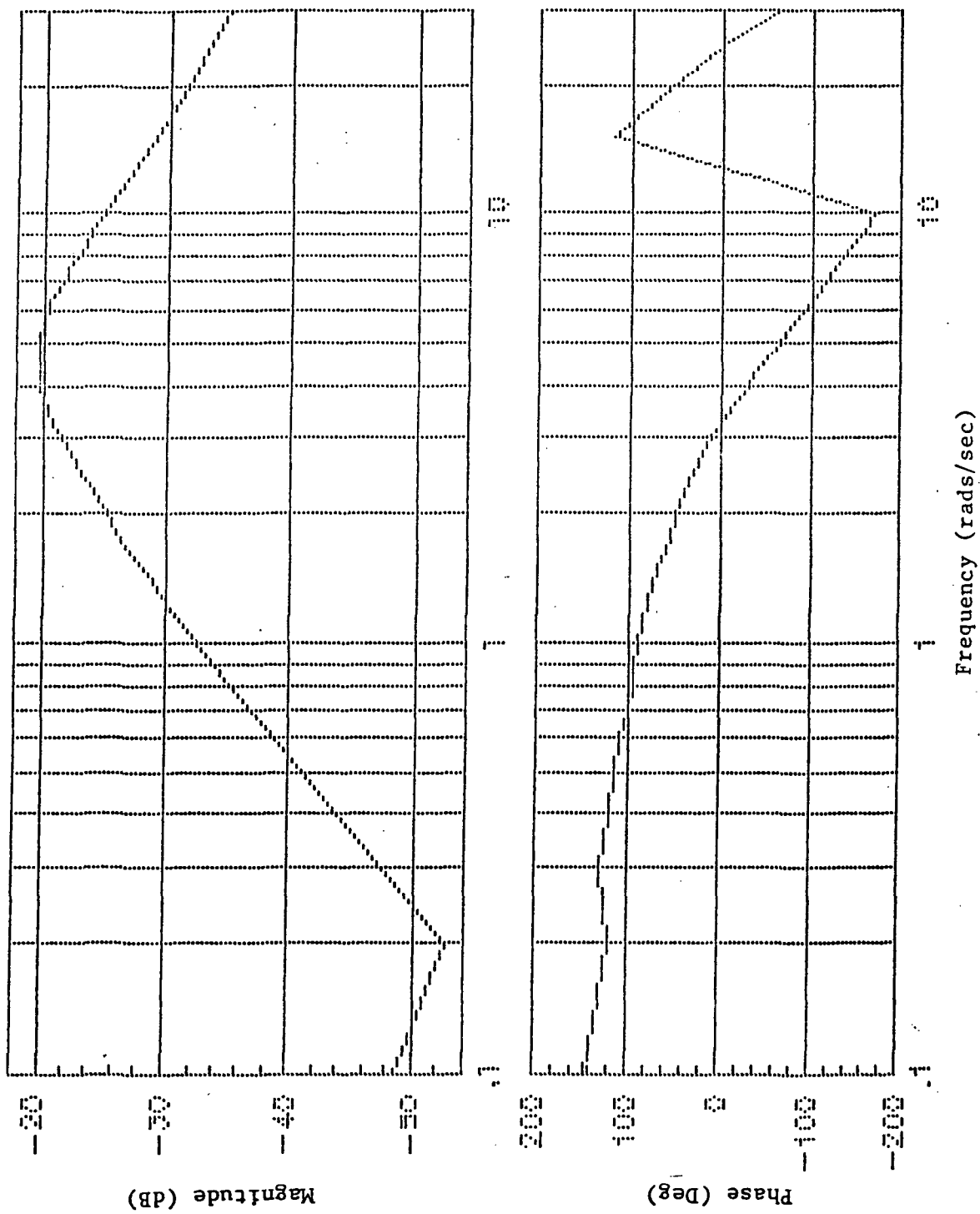


Figure D.4 Pilot Describing Function  $P_{\frac{\delta e}{\theta}}$   
for Status Display

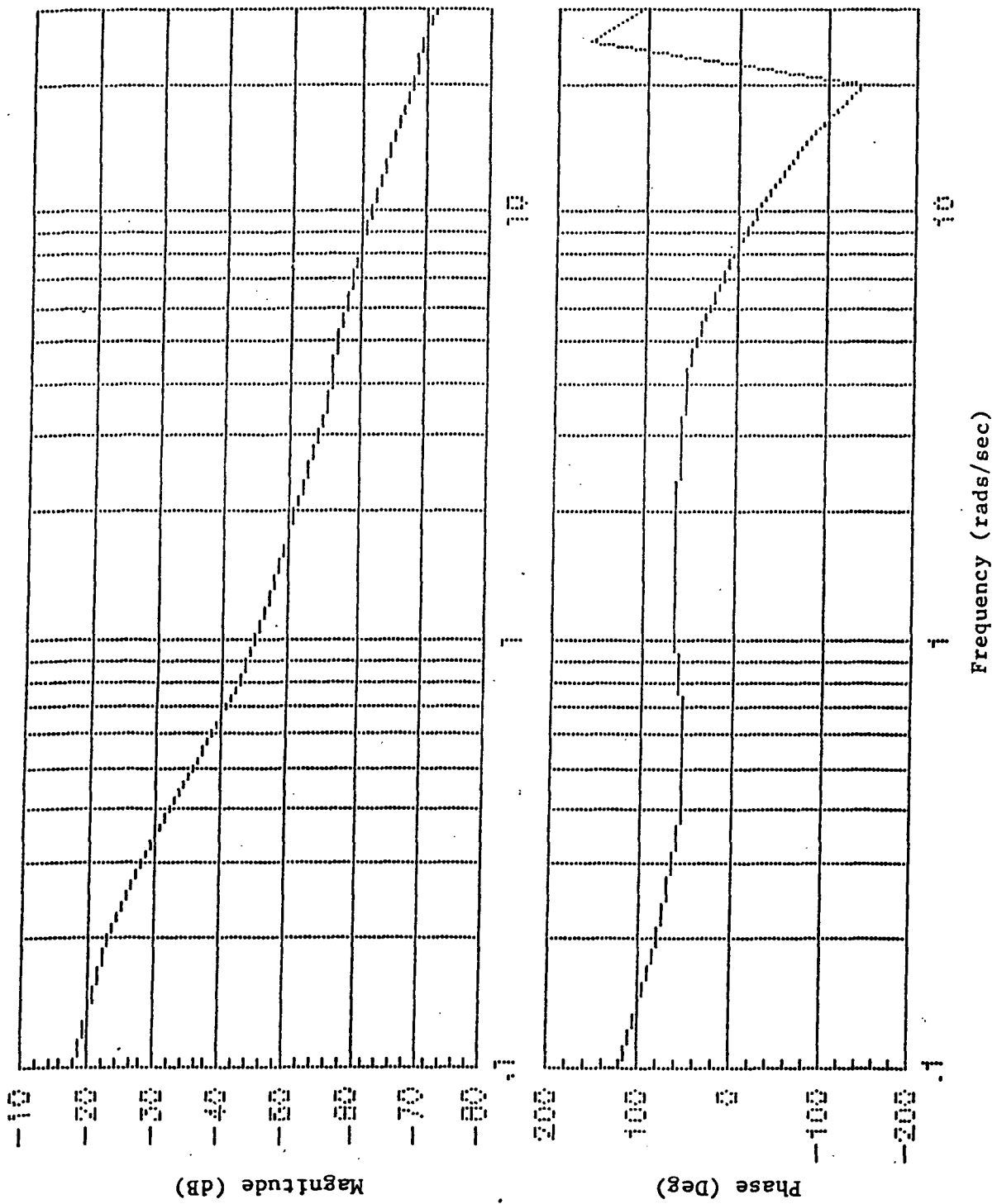


Figure D.5 Pilot Describing Function  $P \frac{\delta T}{a_{zc}}$   
for Status Display

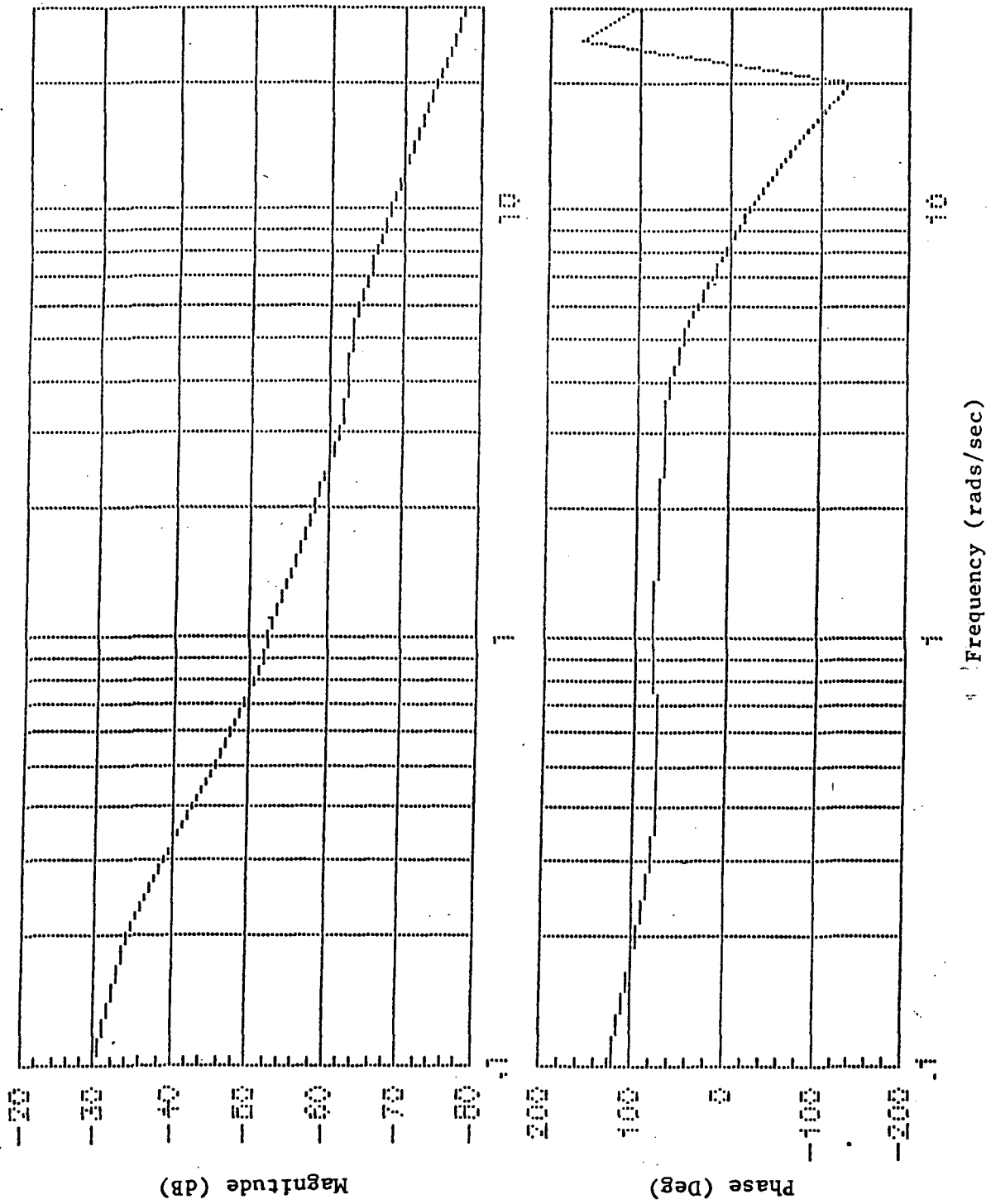


Figure D.6 Pilot Describing Function  $P \frac{\delta T}{e_{az}}$   
for Status Display



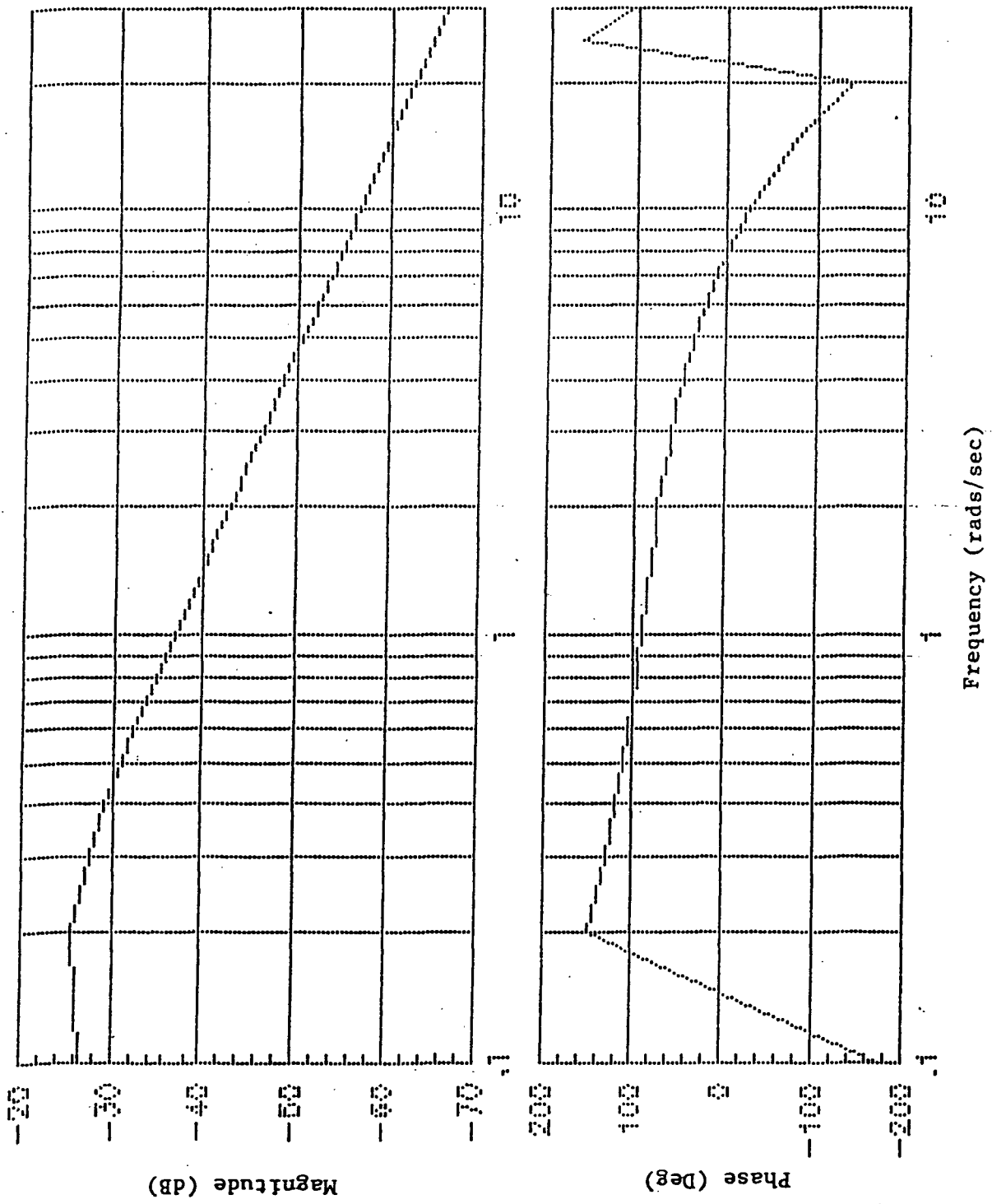


Figure D.7 Pilot Describing Function  $P_{\frac{\delta T}{M}}$   
for Status Display

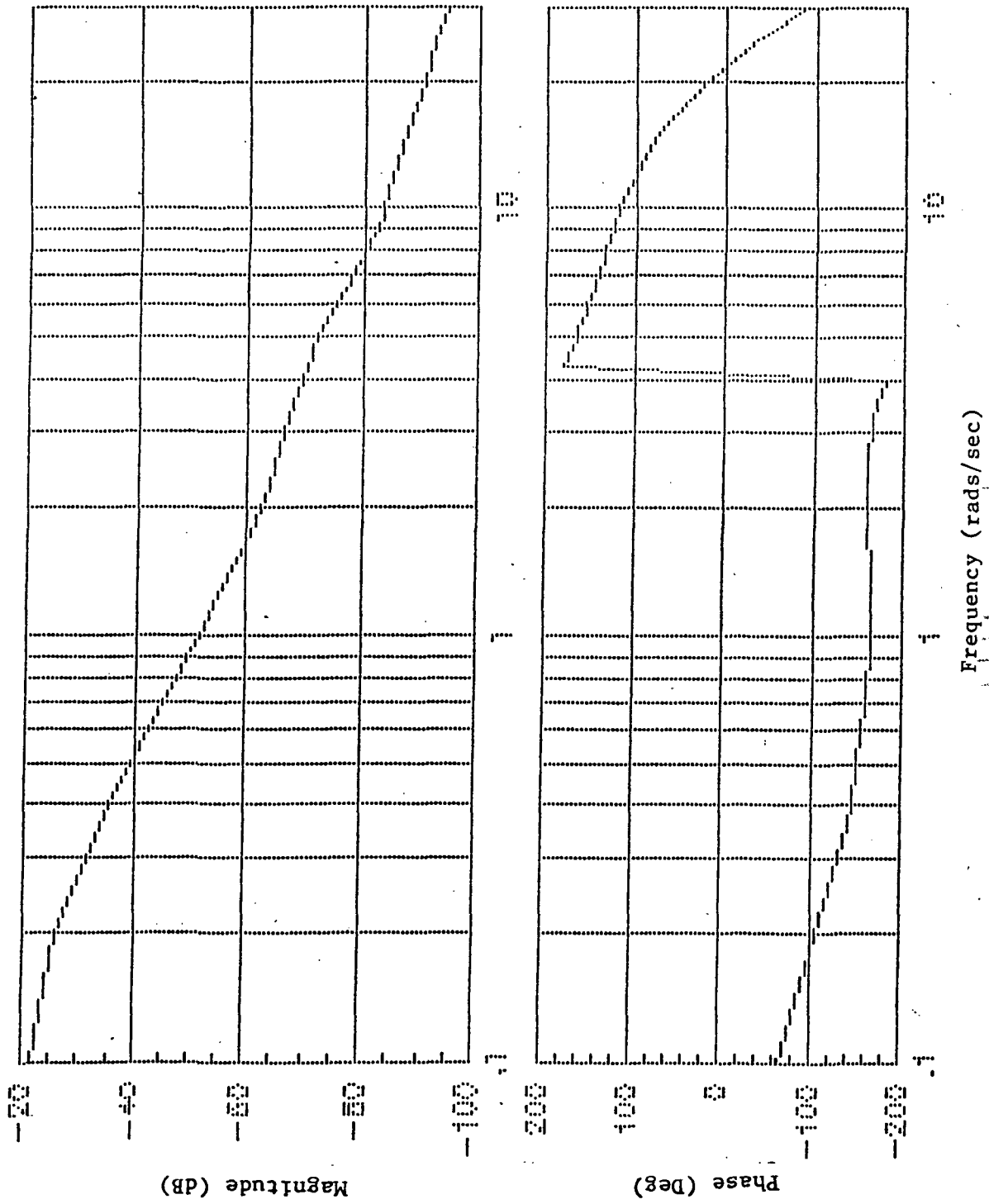


Figure D.8 Pilot Describing Function  $P_{\frac{\delta T}{\theta}}$   
for Status Display

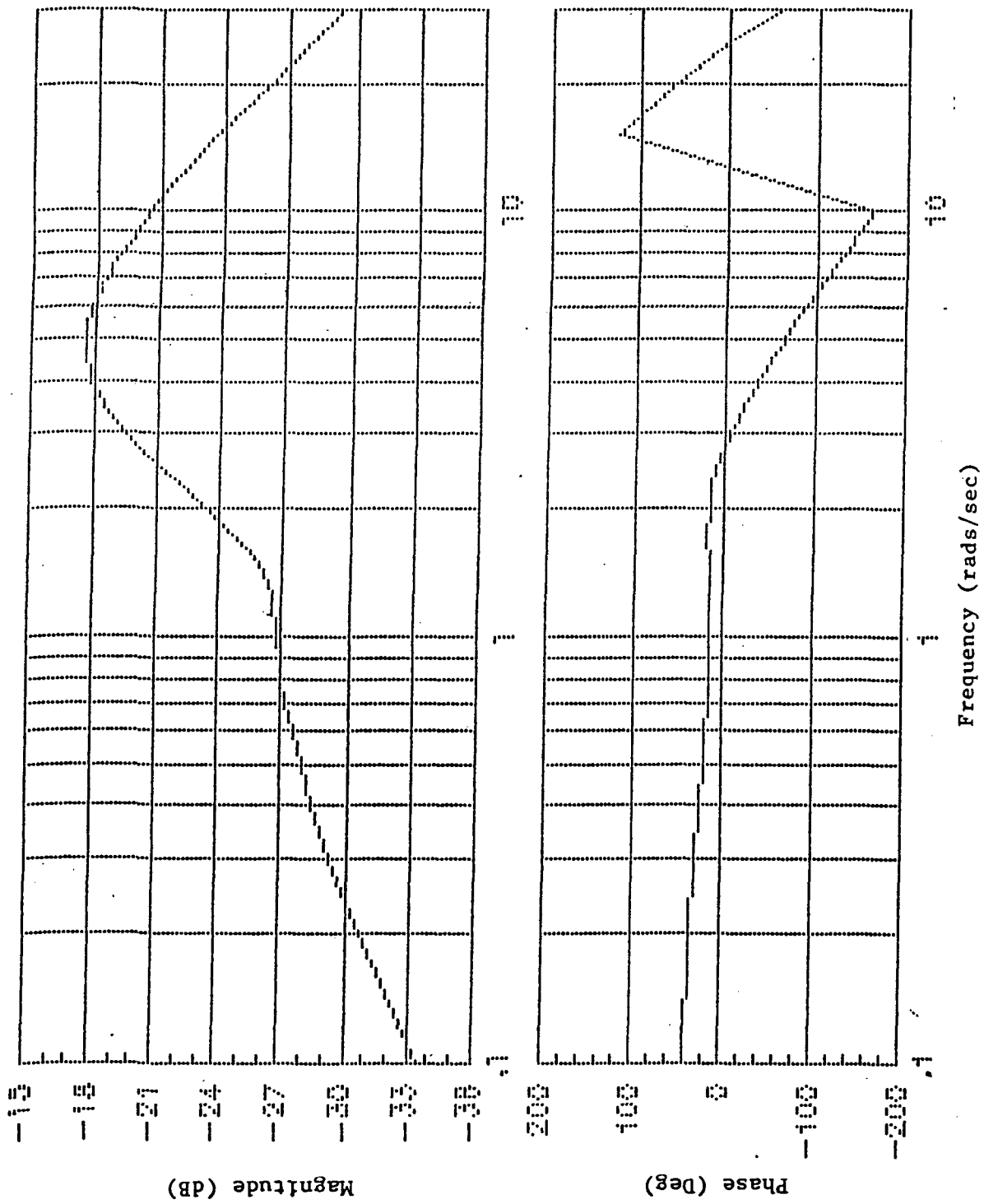


Figure D.9 Pilot Describing Function  $P_{\frac{\delta e}{a_{zc}}}$   
for Augmented Display

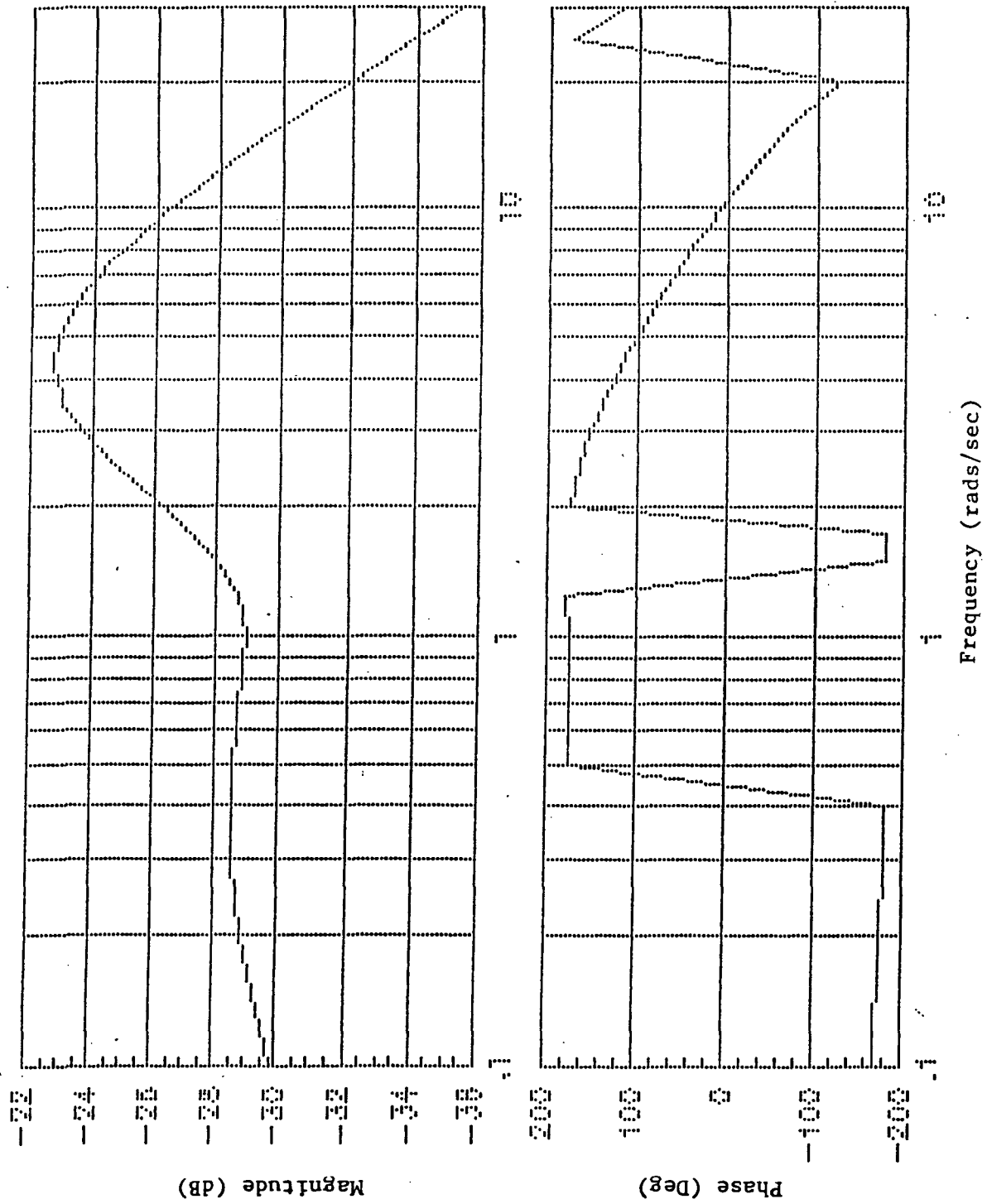


Figure D.10 Pilot Describing Function  $P_{\frac{\delta e}{x_{d1}}}$   
for Augmented Display

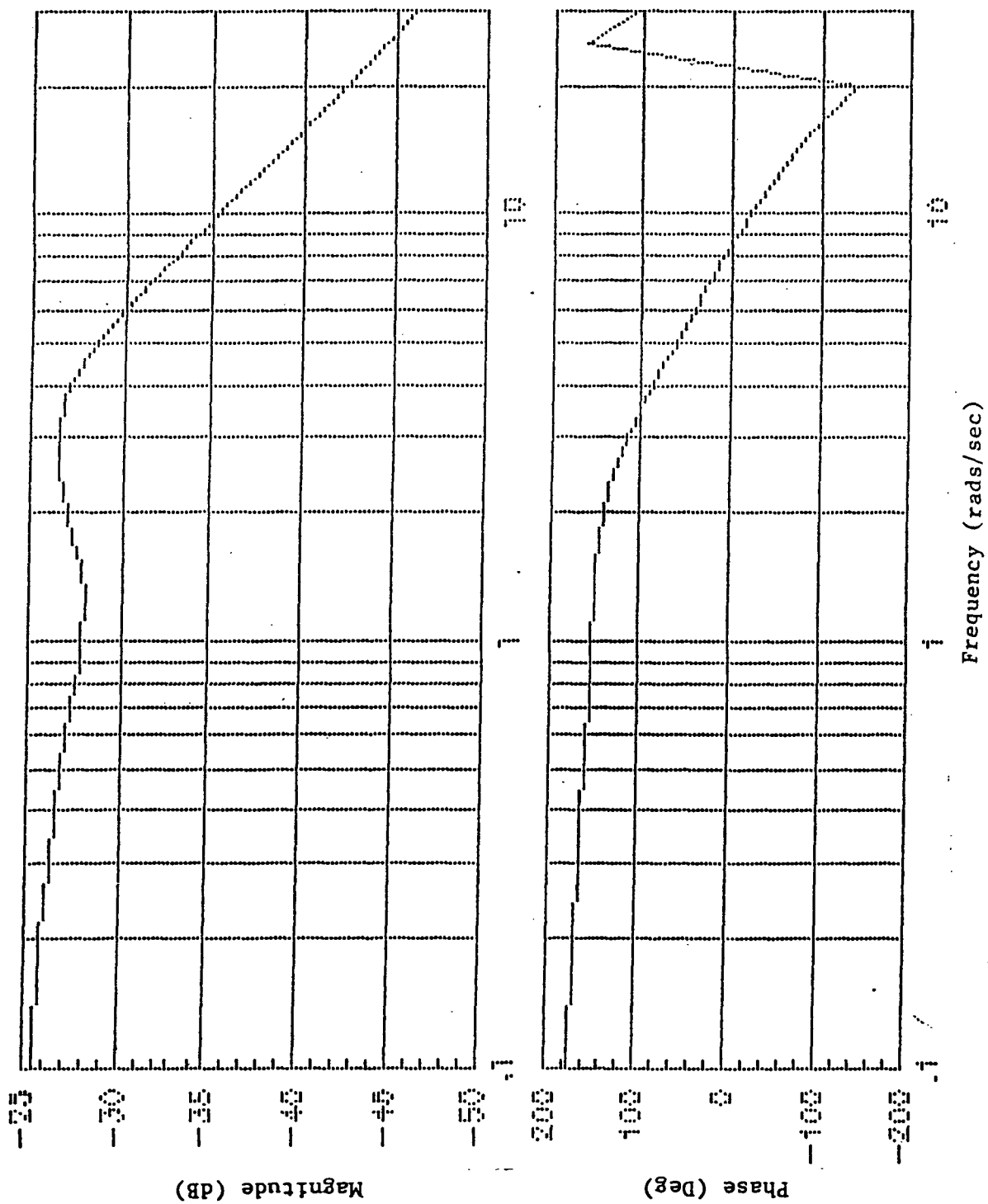


Figure D.11 Pilot Describing Function  $P_{\frac{\delta e}{x_{d2}}}$   
for Augmented Display

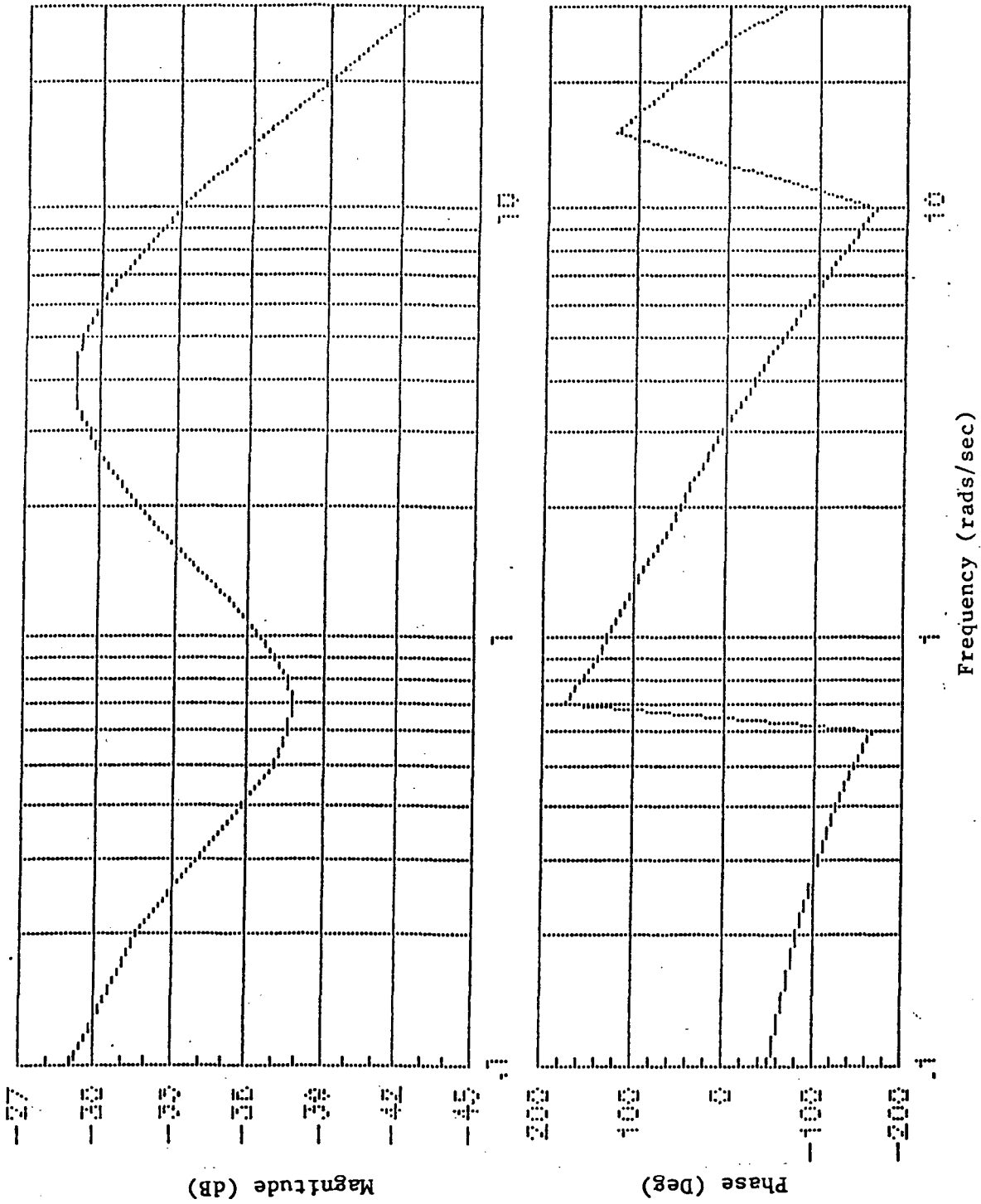


Figure D.12 Pilot Describing Function  $P_{\delta e} / \theta$   
for Augmented Display

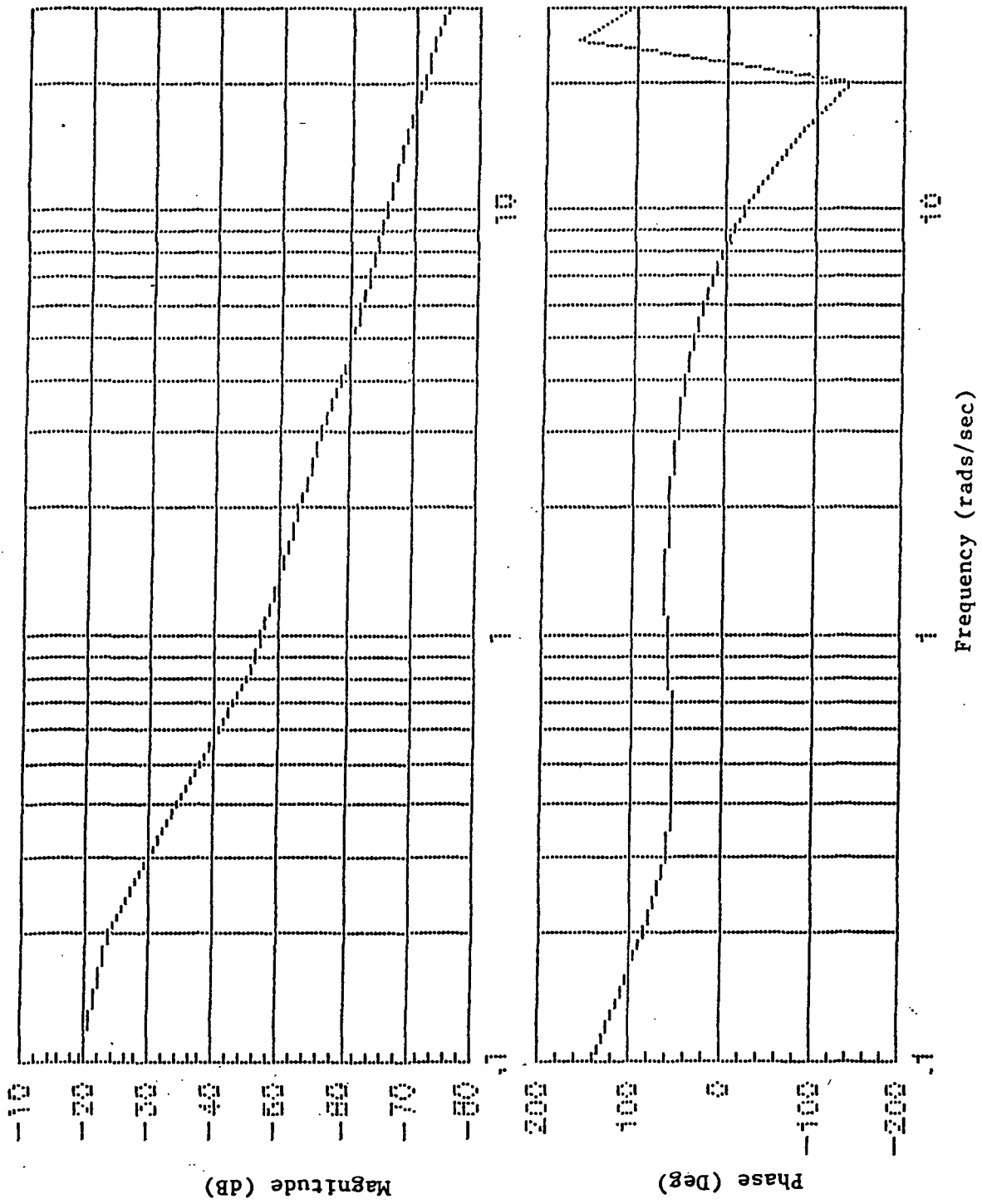


Figure D.13 Pilot Describing Function  $P_{\frac{\delta T}{a_{zc}}}$   
for Augmented Display

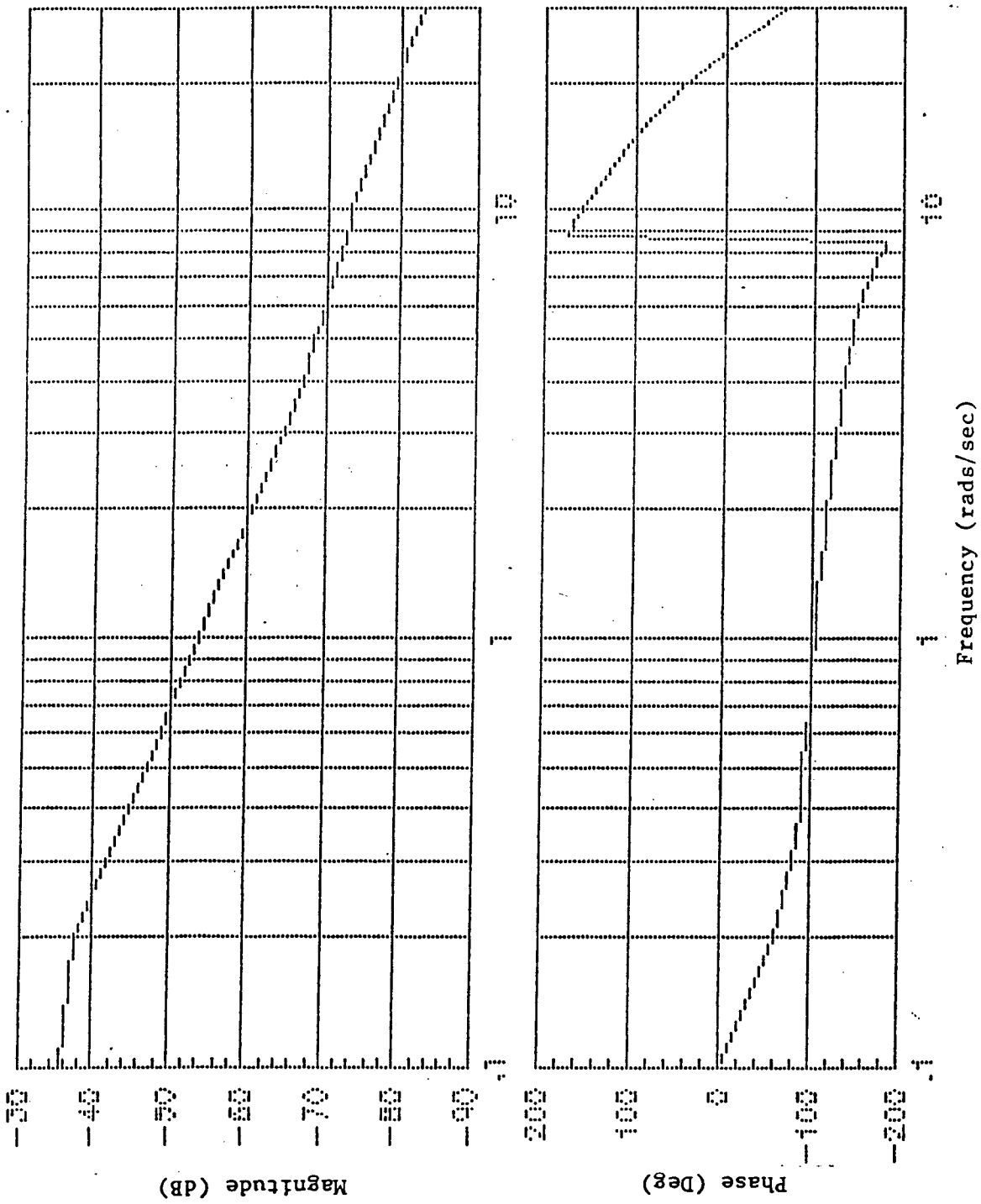


Figure D.14 Pilot Describing Function  $P \frac{\delta T}{x_{d1}}$   
for Augmented Display



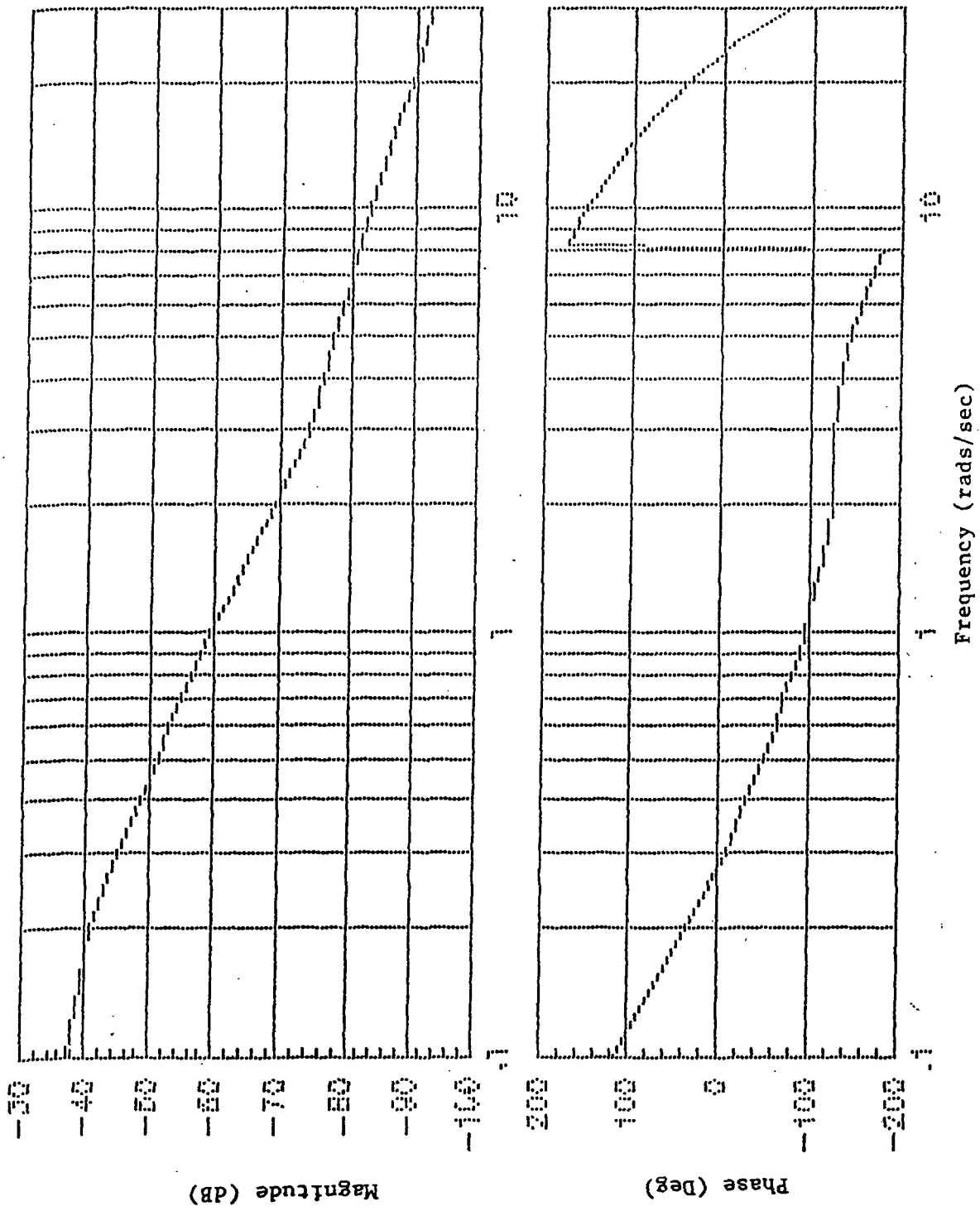


Figure D.15 Pilot Describing Function  $P \frac{\delta T}{x^{1/2}}$   
for Augmented Display

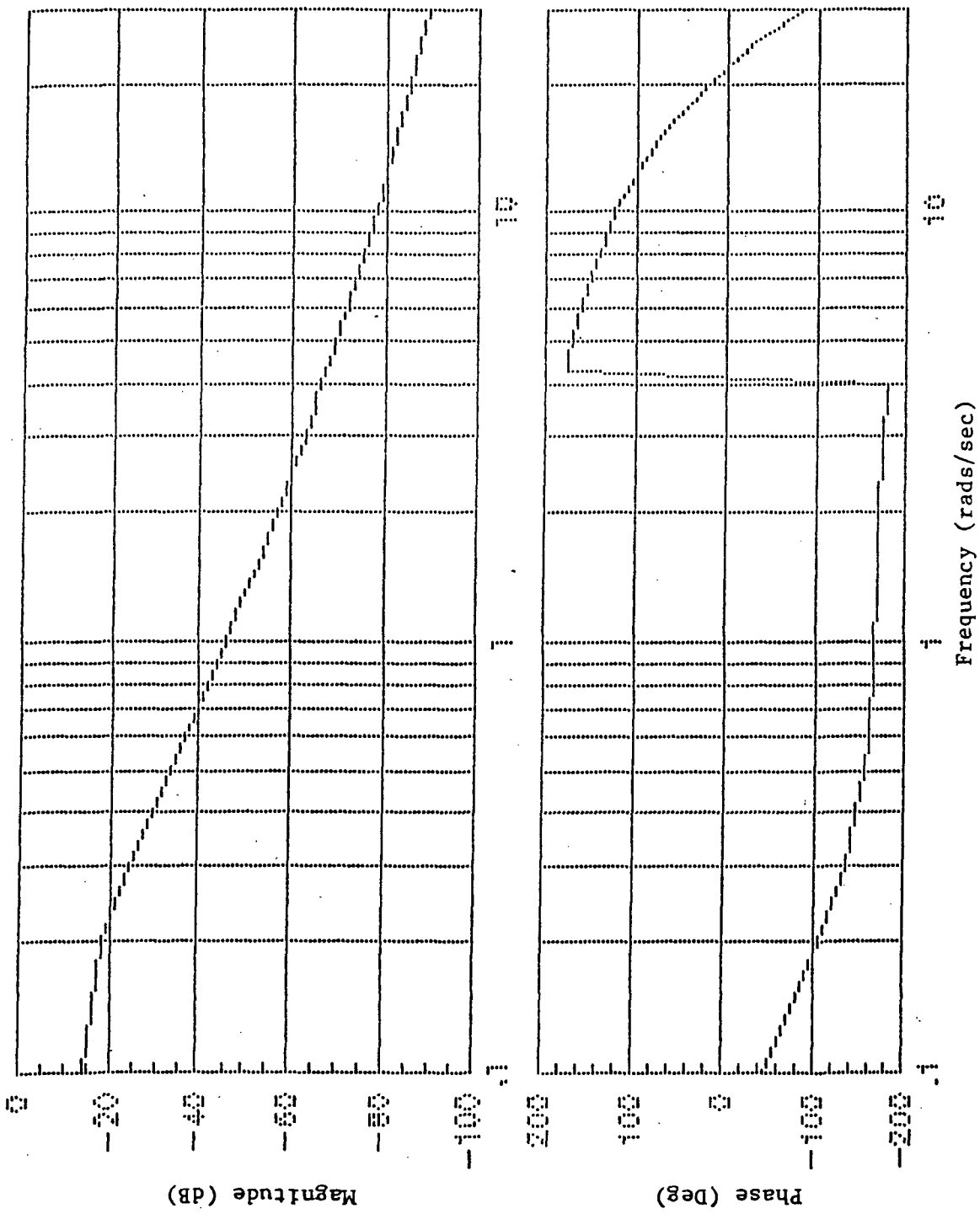


Figure D.16 Pilot Describing Function  $P_{\frac{\delta T}{\theta}}$   
for Augmented Display

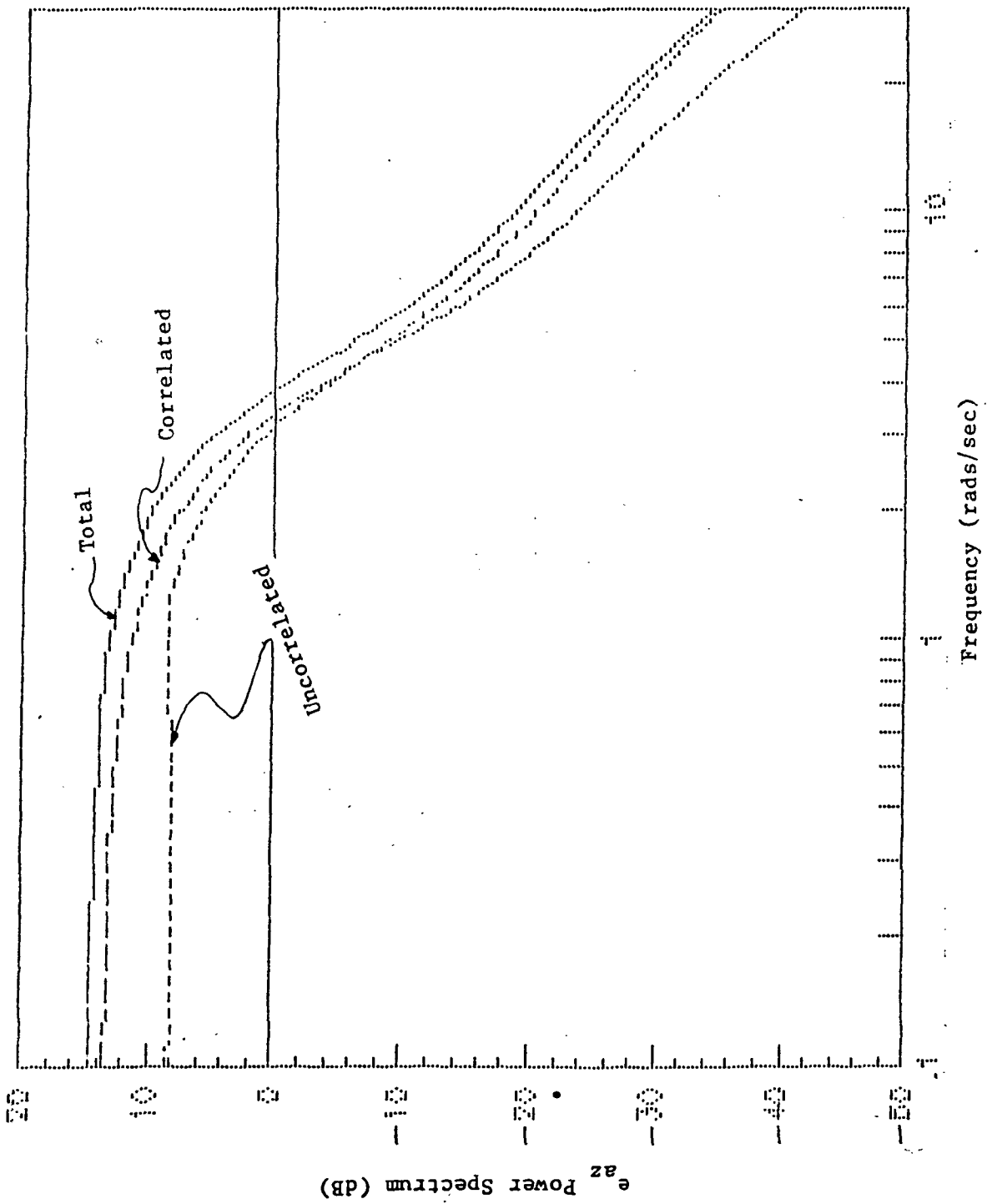


Figure D.17  $e_{az}$  Power Spectrum for Status Display

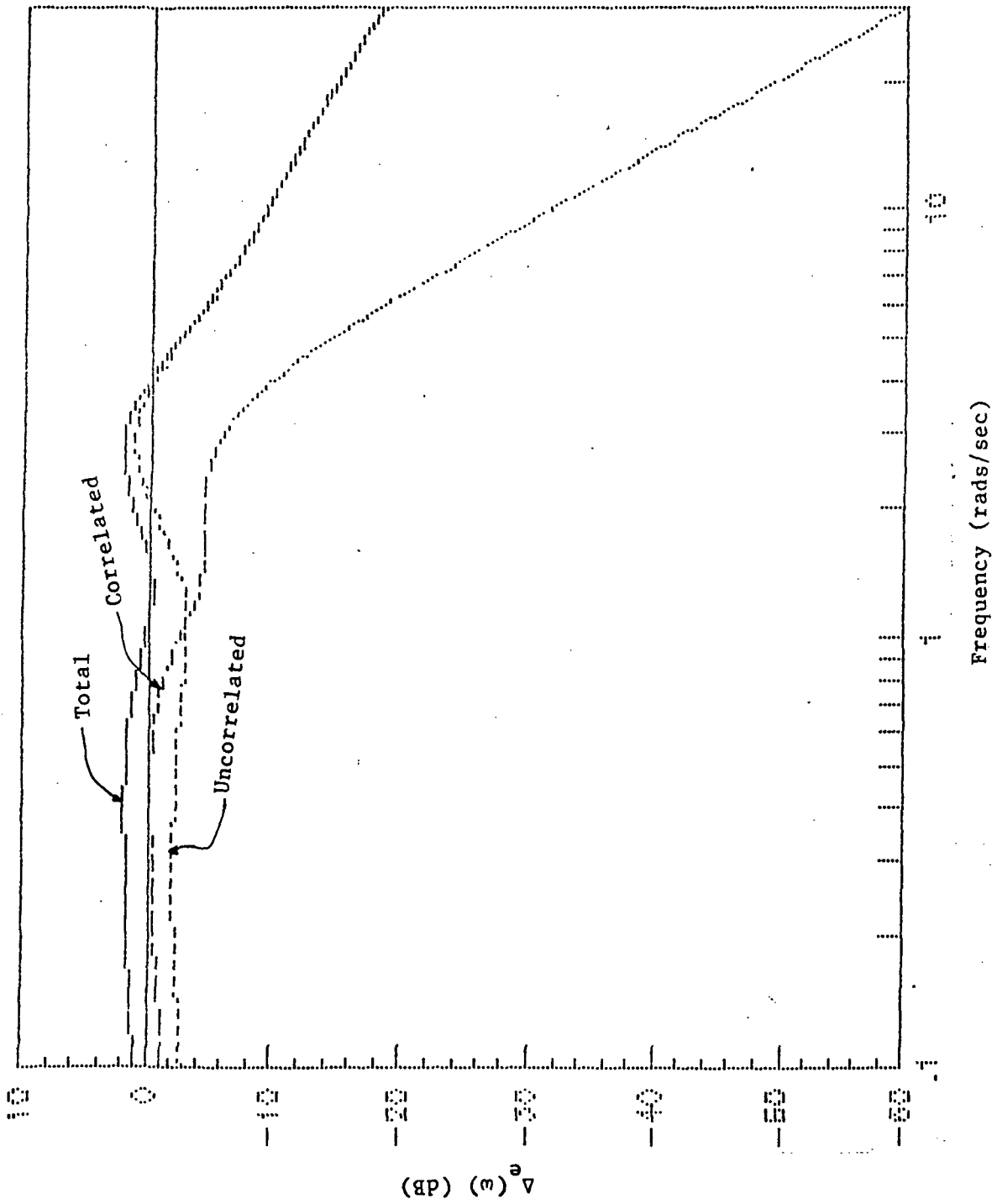


Figure D.18 Pilot Commanded Elevator Spectrum for Status Display

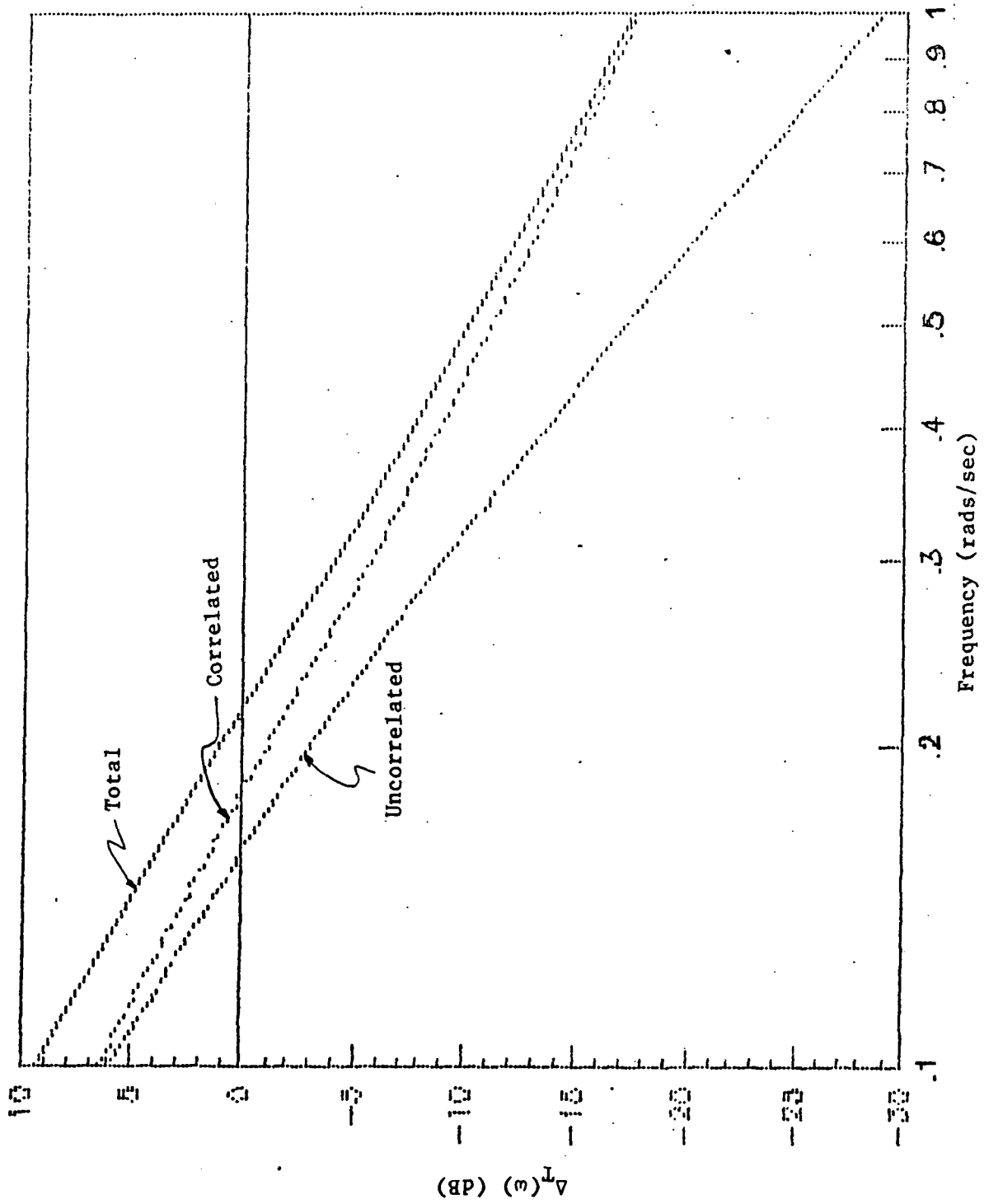


Figure D.19 Pilot Commanded Throttle Spectrum for Status Display

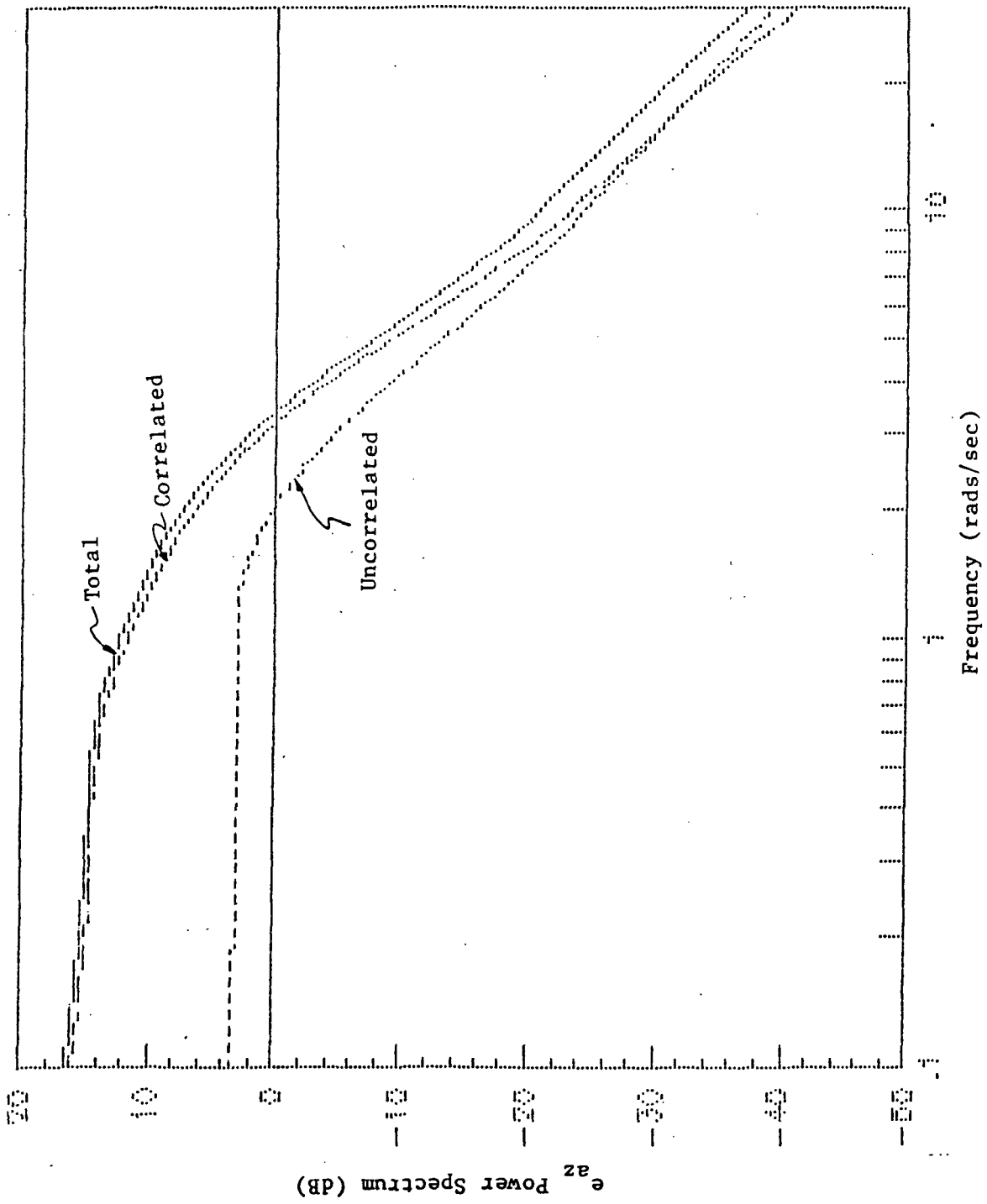


Figure D.20  $e_{az}$  Power Spectrum for Augmented Display

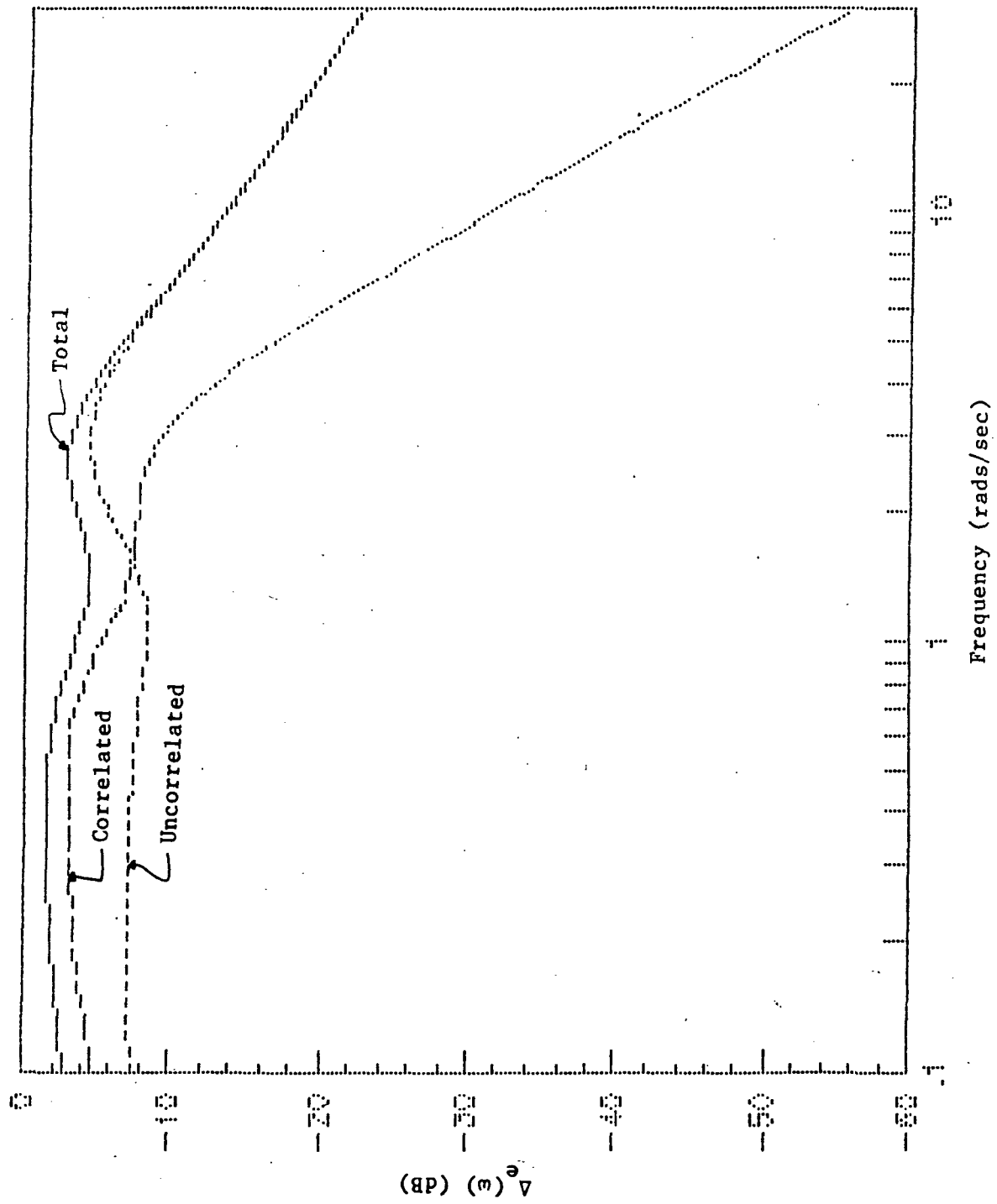


Figure D.21 Pilot Commanded Elevator Spectrum for Augmented Display

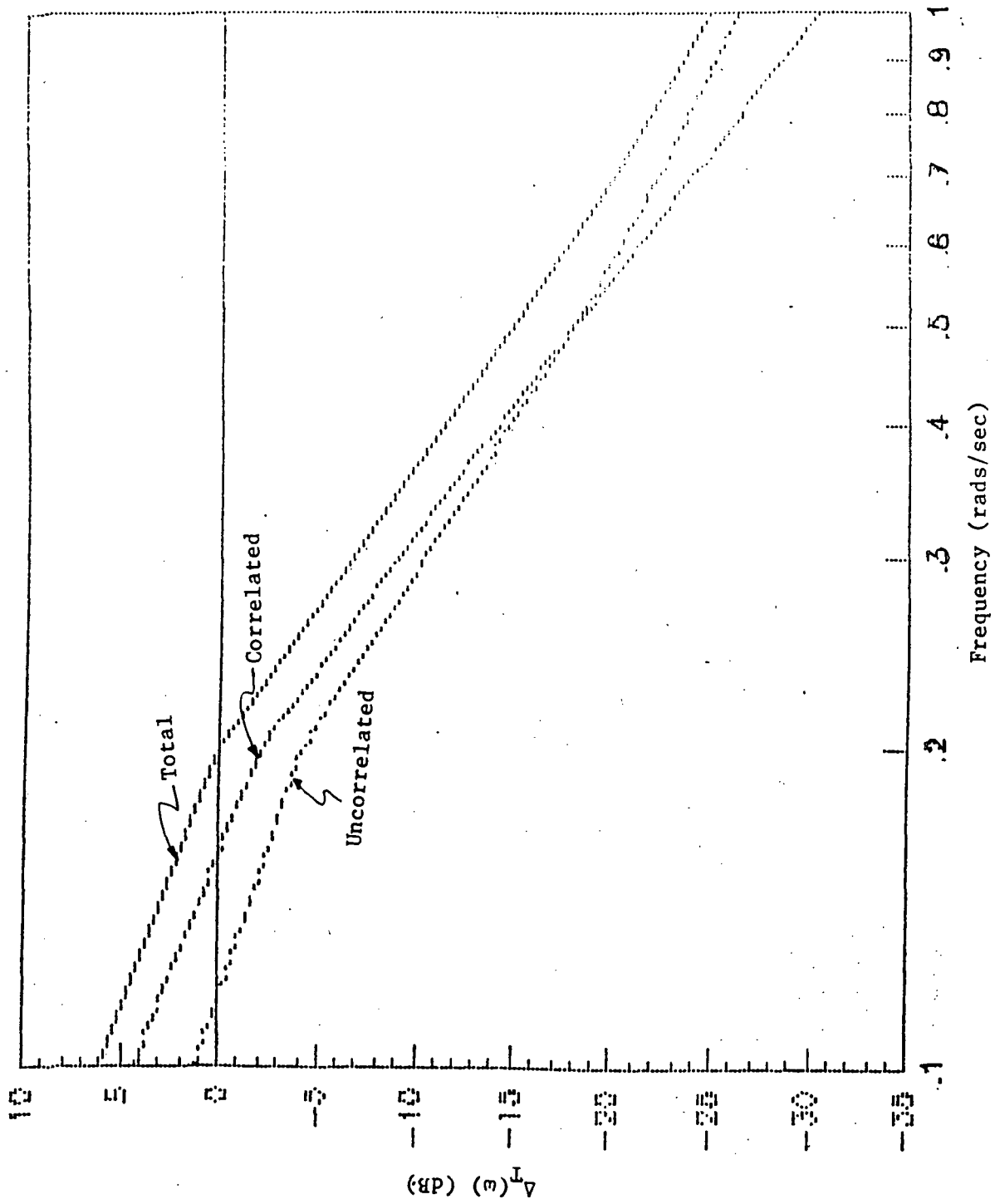


Figure D.22 Pilot Commanded Throttle Spectrum for Augmented Display